Aerodynamics of the curve-ball: An investigation of the effects of angular velocity on baseball trajectories

Article · January 1998

CITATIONS
36

READS
6,260

1 author:

Leroy W. Alaways

18 PUBLICATIONS **294** CITATIONS

SEE PROFILE

Aerodynamics of the Curve-Ball: An Investigation of the Effects of Angular Velocity on Baseball Trajectories

By

LEROY WARD ALAWAYS
B.S. (California State University, Chico) 1984
M.S. (University of California, Davis) 1987

DISSERTATION

Submitted in partial satisfaction of the requirements for the degree of

DOCTOR OF PHILOSOPHY

in

Engineering

in the

OFFICE OF GRADUATE STUDIES

of the

UNIVERSITY OF CALIFORNIA

DAVIS

Approved:

Mont Hubbard

_____

C.P. van Dam

_____

Bruce White

_____

Committee in Charge

1998

To Dad

CONTENTS

CONTENTS (Cont.)

CONTENTS (Cont.)

CONTENTS (Cont.)

CONTENTS (Cont.)

ILLUSTRATIONS

ILLUSTRATIONS (Cont.)

ILLUSTRATIONS (Cont.)

ILLUSTRATIONS (Cont.)

TABLES

TABLES (Cont.)

ACKNOWLEDGMENTS

I would like to thank my major advisor, Professor Mont Hubbard, dissertation committee members, Professors Bruce White and Case Van Dam, and the supporting staff in the mechanical, civil, and agricultural engineering departments at the University of California, Davis campus for all their help and support over the years, and I also would like to thank the following people and organizations for the support and expertise that made this dissertation not only possible but also lot of fun in the process:

Dennis Hefling at Rawling Sporting Goods Company for supplying Major League baseballs and technical information on the construction of the ball; Jim Gates, librarian at the National Baseball Hall of Fame and Museum, for all the great information and leads on the history of the curve in baseball; John Whitehead and Lawrence Livermore National Laboratory for the loan of a three-dimensional MotionAnalysis system for my preliminary investigation and for the great information on how to obtain patent files; Tom Whitaker, Pat Miller and John Greaves at MotionAnalysis Corporation for the use of their ten camera HiRes Motion Analysis system, their 240 Hz. VCR and the lab space when I realized I needed more power and room; Igor I. Sikorsky, Jr., Ralph Lightfoot and the folks at the Sikorsky Archives for helping me obtain the Sikorsky lift data on spinning baseballs; Professors Neil Schwertman and Gene Meyer at California State University, Chico for all the great statistics help; Major League hopeful, Anthony "Tony" Dellamano for pitching and his roommate, Tim Sloan, for catching; UC Davis head baseball coach, Phil Swimley, and his staff for all their support in supplying pitchers, pitching machines and technical advice whenever I asked; Antonia Tsobanoudis and Lisa Schultz for their help in building the calibration device and determining the detailed mass properties of baseballs; Terry Evans and Paul Hopper for the loan of equipment and the extra muscle during my experiments; my friends and family for supporting me over the last five years, in particular,

Cara “Kybelle” Barker for being such a great friend whenever I needed one (like right now) and Mogie for all the dog kisses, the long white hairs on my notes and the look of “is it time to throw a ball”; and last, my laboratory mates, especially Sean Mish and Mike Hendry, for supplying the extra hands, advice and the throwing arms when I couldn’t do it all myself.

I would especially like to thank UC Davis Professor Emeritus John Brewer and Professors Fidelis Eke and Mel Ramey for being on my qualification exam committee, for the great debates in baseball and softball, for their faith in me and always for the encouragement along the way. I wouldn’t have gone this far without it.

I end this by saying, this was my project and because of all the people mentioned above and many more along the way — I finished it and it feels good!

ABBREVIATIONS

The following is a list of abbreviations and symbols used throughout this dissertation. In general, **bold face** are used to denote vectors, *italics* are used to denote scalars or vector magnitude, and though not listed below the use of subscripts x, y, and z denote vector components in those directions.

A	Cross-sectional area; (6.446 in^2 [41.59 cm^2] for Major League baseballs).
C_D	Coefficient of drag; (non-dimensional).
C_L	Coefficient of lift; (non-dimensional).
C_Y	Coefficient of cross-force; (non-dimensional).
$\mathbf{D}$	Drag component of aerodynamic force; (N).
D	Magnitude of drag component of aerodynamic force; (N).
d	Diameter of the ball; (2.864 inches [7.26 cm] for Major League baseballs).
$\mathbf{F}$	Total force vector acting on the ball; $\mathbf{F} = \mathbf{F}_A + \mathbf{F}_G$. (N).
$\mathbf{F}_A$	Aerodynamic force acting on the ball; $\mathbf{F}_A = \mathbf{L} + \mathbf{D} + \mathbf{Y}$ (N).
$\mathbf{F}_G$	Force due to gravity; (N).
G	Center of mass of the ball; (m).
$\mathbf{g}$	Gravitational field strength; (m/s^2).
$\mathbf{H}_G$	Angular momentum with respect to the center of mass of the ball; (kg-m^2/s).
$\mathbf{I}_G$	Inertia with respect to the center of mass of the ball; (kg-m^2).
k	Proportionality constant for lift coefficient. (non-dimensional).
$\mathbf{L}$	Lift component of aerodynamic force; (N).
L	Magnitude of lift component of aerodynamic force; (N).
$\mathbf{M}_G$	Aerodynamic moment with respect to the center of mass of the ball; (N-m).
n.d.	No date.
$\mathbf{P}$	Linear momentum; (kg-m/s).
Re	Reynolds number; (non-dimensional).

ABBREVIATIONS (Cont.)

r	Radius of the ball; (1.432 inches [3.63 cm] for Major League baseballs).
S	Spin parameter; $S = U / V$ (non-dimensional).
SRD	Spin Rate Decay parameter; (non-dimensional).
t	Time; (sec).
U	Tangential velocity of the ball ($r\omega$); (m/s).
$\mathbf{V}$	Velocity of the ball or free stream velocity in a wind-tunnel; (m/s).
V	Magnitude of $\mathbf{V}$; (m/s).
$\mathbf{Y}$	Cross-force component of aerodynamic force; (N).
Y	Magnitude of cross-force component of aerodynamic force; (N).
ε	Surface roughness; (m).
μ	Dynamic viscosity; (N-s/m^2).
ν	Kinematic viscosity; (m^2/s).
ρ	Fluid density; (kg/m^3).
$\boldsymbol{\omega}$	Angular velocity vector; (rad/s).
ω	Magnitude of $\boldsymbol{\omega}$; (rad/s).
κ	Dimensionless surface roughness; (non-dimensional).
ζ	Angle between $\mathbf{V}$ and $\boldsymbol{\omega}$; (rad).

ABSTRACT

In this dissertation the aerodynamic force and initial conditions of pitched baseballs are estimated from high-speed video data. Fifteen parameters are estimated including the lift coefficient, drag coefficient and the angular velocity vector using a parameter estimation technique that minimizes the residual error between measured and estimated trajectories of markers on the ball's surface and the center of mass of pitched baseballs. Studies are carried out using trajectory data acquired from human pitchers and, in a more controlled environment, with a pitching machine. In all 58 pitch trajectories from human pitchers and 20 pitching machine pitches with spin information are analyzed. In the pitching machine trials four markers on the ball are tracked over the first 4 ft (1.22 m) and the center of mass of the ball is tracked over the last 13 ft (3.96 m) of flight.

The estimated lift coefficients are compared to previous measured lift coefficients of Sikorsky (Alaways & Lightfoot, 1998) and Watts & Ferrer (1987) and show that significant differences exists in the lift coefficients of two- and four-seam curve balls at lower values of spin parameter, S. As S increased the two- and four-seam lift coefficients merge becoming statistically insignificant. The estimated drag coefficients are compared to drag coefficients of smooth spheres and golf-balls and show that these data sets bound the drag-coefficient of the baseball. Finally, it is shown that asymmetries of the ball associated with the knuckleball can influence the trajectory of the more common curve and fastball.

CHAPTER 1 – BACKGROUND

> Now *I'll* tell *you* something, boy. *No man alive, nor no man that ever lived, has ever thrown a curve ball.* It can't be done.
>
> R.W. Madden (1941), *New Yorker*

1.1 Introduction

In May 1941, when Madden wrote those words to the editor of the *New Yorker,* he rekindled the flames of one of the great debates in baseball. The dispute probably had been argued since the game began and continues to this day in sandlots and bar rooms across the nation. It is a simple argument that stirs up a lot of passion and brings out the folklore that legends are made of. The question is simply, does a baseball curve? For months, in the *New Yorker,* the discussion raged on in letters to the editor. Then in September of that year, *Life* magazine added fuel to the flames by publishing a photographic investigation concluding that "a baseball is so heavy an object … that the pitcher's spinning action appears to be insufficiently strong appreciably to change its course" (Baseball's Curve Balls: Are They Optical Illusions, 1941). A few months later a note appeared in the *American Journal of Physics* describing an experimental study by Verwiebe (1942). Verwiebe constructed five wooden frames containing screens of fine cotton thread and placed them between home-plate and pitcher's mound. Using collegiate pitchers, a series of pitches were then thrown through the screens, thus breaking threads and allowing Verwiebe to crudely reconstruct the trajectories. Verwiebe reported curves in the horizontal plane between 2.5 and 6.5 inches (6.35 and 16.51 cm) and that "the ball dropped more sharply than would be the case for free fall alone". The debate continued.

In 1949, *Look* magazine brought the discussion back to the nation's attention with "Visual Proof that a Baseball Curves" (Cohane, 1949). Using multiflash pictures, Cohane concluded that "there is no such thing as a 'straight' ball". Not to be outdone, *Life*

magazine, with the aid of strobe photography, changed its opinion and reported that a baseball does curve but not suddenly — or in baseball lingo 'break' (Camera and Science Settle the Old Rhubarb About Baseball's Curve Ball, 1953). Along with the photographic evidence, *Life* reported that Joseph Bricknell of MIT with the aid of a wind tunnel, had shown that with the 43 mph (19.22 m/s) velocity and rotation rate (23 rps) reported in their article, a baseball could curve as much as six inches (15.2 cm). Later findings would show that a curve ball can curve as much as 18 inches (45.7 cm) (Briggs, 1959; Selin, 1957).

In almost all of the previous work concerning the aerodynamics of sport balls the definition of the terms "curve", "curve ball", and "break" are omitted or ambiguous. For the benefit of the reader the following three definitions are included here as they will be used throughout this dissertation:

Curve: The "curve" of a pitch is the total deviation that occurs in the trajectory due to the lift and cross force components of the aerodynamic force acting on the ball in flight and is measured when the ball passes through the y-z plane in the local coordinate frame defined in section 2.5.1.

Curve ball: In baseball a "curve ball" is a ball released with top-spin resulting with the ball dropping faster than a normal gravitational parabolic arc. However, in this dissertation a curve ball is any ball that has a curved trajectory.

Break: A "break" is a sudden movement in the trajectory of the ball. Though this phenomenon is highly unlikely it is a common term used in baseball folklore and is sometimes confused with the curve.

Today, the consensus in the scientific community is that baseball flight paths do curve. The question now is, how much and to what degree does the spin or angular velocity influence the deflection? This question is the primary focus of this dissertation.

1.2 Motivations for the Curve-ball

In Major League Baseball the pitcher stands 60.5 feet (18.44 m) from the back end of home-plate and attempts to throw the ball past the awaiting batter. A 90 mile-per-hour

(40.2 m/s) pitch completes its journey to the plate in less than a half-second. Hitting the pitch is not an easy task. To make it all the more difficult, the pitcher, by introducing spin, alters the trajectory from the simple parabolic to one in which the aerodynamic force plays a significant role.

There is essentially only one type of pitch in baseball. All pitches — the fastball, curve, slider, fade-away, change-up, screwball, drop-ball, fork-ball, split-finger fastball, knuckleball and others — are uncontrolled spinning projectiles once they leave the pitcher's hand. The only differences are the initial release conditions (i.e., position, ball orientation, translational velocity vector, and angular velocity vector); the unifying principle is that they all follow the same dynamic laws. The knuckleball, however, is unique since it is thrown with very little rotation which can produce asymmetric configurations resulting in force imbalances and extraordinary deviations in the trajectory (Adair, 1990; Hollenberg, 1986). Because of the unpredictability of those force imbalances, the knuckleball was not a primary focus of this dissertation though results pertaining to the knuckleball are also included.

The baseball's path can be predicted given the set of initial release conditions and a complete knowledge of the atmosphere and ball aerodynamics. Conversely, the initial conditions for a trajectory also can be estimated given the path of the ball. Knowing how the initial conditions affect the curve can lead to different and interesting possibilities. These range from determining the characteristics of a certain pitching style and grip, to designing a pitching machine that throws various trajectories by altering the appropriate initial condition.

Understanding how angular velocity and seam orientation influences the most important half-second of "America's pastime" is the initial motivation for this work. The challenge, on the other hand, to accurately capture not only the baseball's trajectory but to determine the angular velocity in flight is the "primary" motivation that makes this dissertation all the more challenging.

1.3 Previous Work

Curves in flight are now well recognized in almost every sport in which a round ball is either struck or thrown. In the following sections a brief history of the curve ball in baseball is given along with a more extensive examination of the past scientific work on the aerodynamics of spinning spheres and the development of video-data-acquisition systems. Though this dissertation is on the curve in baseball, no explanation on how to throw a curve will be given here.

1.3.1 Curve-ball Facts and Folklore

For years, in the general public's mind, there were arguments on the curve in baseball. In spite of that, in baseball's own eyes there was no debate and the Baseball Hall of Fame in Cooperstown, New York, credits William "Candy" Cummings as the first pitcher to throw a curve[1] (Adair, 1990; Mercurio, 1990; Spalding, 1992). Cummings (*n.d.*) claims that in 1863 the idea for the curve came to him as he and a number of boys were amusing themselves by "throwing clam shells and watching them sail along through the air, turning now to the right, and now to the left". Cummings thought it would be a great joke to play if he could make a baseball curve the same way and began to experiment with different grips and releases to consistently throw a curve. It wasn't until 1867, as a junior member of the Excelsior Club, that he "perfected the curve" while pitching against the Harvard Club. Cummings noted that "the batters were missing a lot of balls; I began to watch the flight of the ball through the air, and distinctly saw it curve".

In 1870, National League pitcher, Fred Goldsmith, demonstrated his mastery of the curve ball by placing three poles along a straight chalk line (Adair, 1990; Allman, 1981). Goldsmith then threw a ball whose trajectory started on the right of the first pole, traveled to the left of the second, and then to the right of the third. Not everyone was convinced, however; some thought it was an optical illusion.

---

[1] For his baffling "new" pitch, Cummings was inducted into the hall of fame in 1939 (Mercurio 1990).

The principal organizer of the National League, A.G. Spalding, wrote in his 1911 classic *America's National Game*, that in 1877 Cincinnati had its own little dispute on the subject of the curve (Spalding, 1992). Spalding quoted two *Cincinnati Enquirer* letters to the editor, one for and one against the curve. In the first letter, Prof. Swift of Rochester University is quoted as saying, "Suppose the pitcher, at the instant the ball leaves his hand, should impart to it a rotation whose axis would lie in the zenith and nadir like a spinning top, such a ball, because the friction is greater against the compressed than the rarified air, will 'curve' either to the right or left, depending in which direction it rotates". In the other letter, Prof. Stoddard of Wooster University wrote: "It is not only theoretically but practically impossible for any such impetus to be conveyed to a moving body as would be required to perform the action supposed…". The Cincinnati debate carried over into the ball park and on October 20, 1877, at the end of the second inning of the Cincinnati – Boston game, Goldsmith's demonstration was duplicated using the two starting pitchers of the day[2].

In the 1877 Cincinnati experiment, the chalk line that runs parallel with the line from home-plate to first base, in a north-south direction, was used as the base of operation[3]. Figure 1–1 shows the layout for the experiment and symbols used in the figure are defined below. The pitcher was placed at the south end of the line. A barrier was placed on the west side of the line at the half point along of the line, with one end resting on the line. This was to compel the pitcher, who also stood on the west side of the line, to throw the ball across to the east side. An additional barrier was placed on the east side of the line opposite first base. This was to stop the ball unless it's path described a curved trajectory that would carry back to the west. Down where the pitcher stood, a board was set on one end of the line and held in position to insure that the pitcher did not reach over and release the ball on the wrong side of the line. Bond, the Boston pitcher, then took his place on the

---

2 "Curved Balls," *Cincinnati Daily Gazette*, October 22, 1877.

3 Ibid.

west side of the line and tried the experiment. After a few attempts he was successful with the ball landing two feet west of the line. Mitchell, the Cincinnati pitcher, was then called up, and, being a lefty, took his position on the east side of the chalk line. The barriers were moved accordingly, and after a few tries Mitchell also was successful with the demonstration. In figure 1–1, B indicates the position of Bond and M marks the position of Mitchell. In both cases the starting point of the ball is indicated by the letter b. The ball's position as it passed the first barrier is indicated by c, and when it reached the last, by d. The dashed line through these points approximates the course pursued by the ball. The ball was curved in opposite directions by these two pitchers, thus disposing of the theory that the wind helped divert the ball from its course. The tests were "regarded as entirely satisfactory, and created great interest"[4], yet did not create enough sustained awareness to prevent the *New Yorker*/*Life*/*Look* debate more than 60 years later.

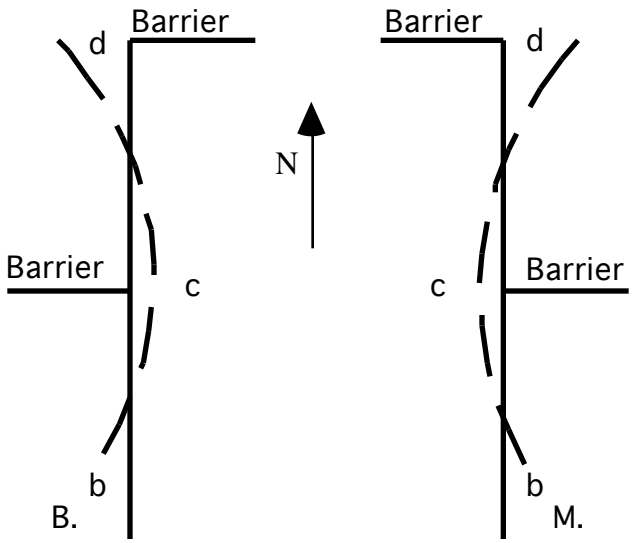

Figure 1–1: Layout of October 20, 1877 curve ball demonstration.

Throwing a curve ball became almost an obsession among baseball players after the pitch was developed and demonstrated. Besides players, authors and inventors alike became fixated with the pitch. An 1888 book titled *The Art of Curve Pitching* was so successful that author Edward J. Prindle found enough material for a sequel, *The Art of*

---

4 "Curved Balls," *Cincinnati Daily Gazette*, October 22, 1877.

Zigzag Curve Pitching (Gutman, 1995). Prindle (1888) showed insight into the pitch dynamics by noting in the opening paragraph of the first book that; “The science of curved pitching is governed by two very important conditions. The conditions are: First, the resistance offered to the ball by the air and, second, a revolving motion of the ball.”

For pitchers who lacked the skill necessary to throw the curve on their own, a number of inventors dreamed up devices that would lend them a hand. One of these, the “base ball curver”, was invented by McKenna and Baker (1888) of St. Louis. It was a piece of rubber with a loop that was slipped around the second finger as shown in figure 1–2. The body of the curver was roughened in order to put added spin on the ball when it was released. In figure 1–2, “Fig. 3” shows the correct position for an “out-curve”, “Fig. 4” for an “up-shoot,” and “Fig. 5” for a “down-shoot.”

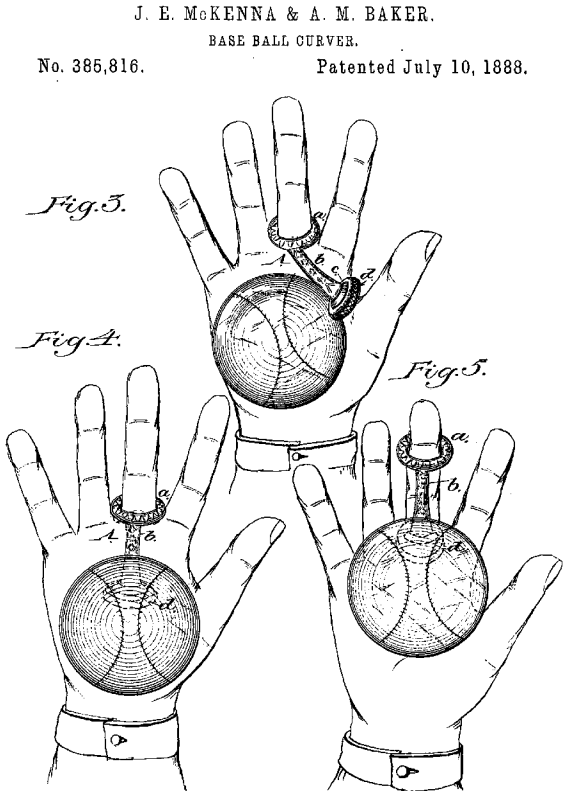

Figure 1–2: Base Ball Curver (Taken from McKenna and Baker, 1888).

One of the strangest inventions in baseball was submitted to the U.S. Patent Office in 1890 by Emile Kinst of Chicago and is shown in figure 1–3 (Kinst, 1890). Kinst wrote

"the object of my invention is to provide a ball-bat which shall produce a rotary or spinning motion of the ball in its flight … and thus to make it more difficult to catch the ball, or, if caught, to hold it." The Major League Rules Committee, needless to say, nixed the "banana bat" (Gutman, 1995).

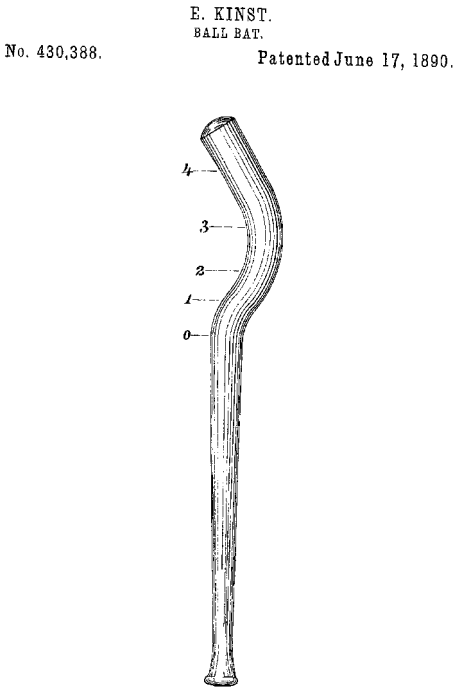

Figure 1–3: Kinst's Ball Bat (Taken from Kinst, 1890).

The demonstrations of the 1880's quieted most of the critics of the curve until, as mentioned in the previous sections, Madden (1941) wrote his letter to the editor of the *New Yorker*. Though during the *New Yorker*/*Life*/*Look* debate it was pointed out that some 30 years earlier the mystery of the curve had been examined even in the world of fiction. For in another letter to the editor of the *New Yorker*, Houston (1941) described a scene from a *Rover Boys*[5] book. Houston details how in the story Dick Rover built a number of wooden frames over which he pasted dampened tissue paper. He then placed them in a straight line between home-plate and pitcher's mound and threw his best "Sunday curve" through the paper covered frames. When the frames were collected and carefully placed

---

5 The *Rover Boys* was a book serial written from 1899 to 1926 by Arthur M. Winfield and published by various publishers.

face-to-face a clear curve was shown in the frames as the ball neared home-plate. It is interesting to note that Houston's letter appeared during the *New Yorker*/*Life*/*Look* dispute and shortly thereafter Verwiebe (1942) published his research where he essentially duplicated the fictional Dick Rover experiment. Verwiebe, on the other hand, improved upon the experiment by including a ballistic pendulum to measured the velocity of the ball while it crossed home-plate.

One of the results of the *New Yorker*/*Life*/*Look* discussion was an increased interest in the curve at a time when wind tunnels and photographic techniques were becoming more routinely available to scientist and researchers. The fact that the general public was agreeing that the baseball did curve, nevertheless, did not slow the scientific curiosity of the researcher and many scientific publications were written concerning the aerodynamics of the ball in flight. These papers are covered more thoroughly in the following sections.

1.3.2 Aerodynamics

Any ballistic spinning object in flight is acted upon by forces and moments that uniquely determine its trajectory. These forces and moments include the gravitational force, aerodynamic force, and an aerodynamic moment which acts to slow the spinning motion. The following sections review the previous research concerning the aerodynamic kinetics of spinning spheres. Note that these forces and moment, in the ballpark, can be greatly influenced by wind gusts and other changes in atmospheric conditions. However, for this research all experiments were conducted in a controlled environment to minimize the effect of unseen atmospheric anomalies.

The models used for this dissertation will be covered in greater detail in chapter 2; however, the following definitions are given here for the benefit of the reader[6].

---

6 In this dissertation, bold face will be used to signify **matrix** and **vector** quantities and italic text will signify a *scalar* or the *magnitude* of a vector.

Aerodynamic Force: The aerodynamic force, $\mathbf{F}_A$, is the total force produced from atmospheric interaction with the ball in flight. This force is the combination of the three mutually perpendicular drag, lift and cross force components defined below.

Drag: The drag, **D**, is a retarding force characterized in terms of a dimensionless number, the drag coefficient, C_D. The magnitude of **D** is a function of ρ, A, V, μ, ω, and ε where, ρ is the fluid density of air, A is the cross-sectional area of the ball, V is the velocity of the ball, μ is the dynamic viscosity of air, ω is the angular velocity of the ball and ε is the surface roughness. The drag coefficient is a function of the Reynolds number, spin parameter and roughness ratio all of which are defined below.

Lift: The lift, **L**, is a spin induced force perpendicular to the translational and angular velocity vectors characterized in terms of a dimensionless number, the lift coefficient, C_L. The magnitude and direction of **L** is strongly dependent upon translational velocity vector **V** and the angular velocity vector, ω. The magnitude of **L** is also a function of ρ, A, μ, and ε in the same manner as the drag. The lift coefficient is a function of the Reynolds number, spin parameter and roughness ratio all of which are defined below.

Cross Force: The cross force, **Y**, is a shape induced force perpendicular to the lift and drag and is generated by surface and shape asymmetries. The magnitude of **Y** is also a function of ρ, A, V, μ, ω, and ε . No previous work on this force for sport balls was found during the literature review of this dissertation. This component of the aerodynamic force will, however, be included in this dissertation.

Reynolds Number: The Reynolds number, Re, is a dimensionless variable proportional to the ratio of the inertia force/unit area to viscous force/unit area that acts on the ball.

Spin Parameter: The spin parameter, S, is a dimensionless variable equal to the ratio of the tangential velocity, U, (of the ball due to spin) to the magnitude of the velocity vector. The tangential velocity is given by the product $r\omega$, where r is the radius of the ball and ω is the spin rate.

Roughness Ratio: The roughness ratio, κ, is a dimensionless quantity equal to the ratio of the surface roughness, ε, to the diameter of the ball, *d*.

1.3.2.1 Lift

In 1671 Newton (1671) noted how the flight of a tennis ball was affected by spin and gave the following explanation: "For, a circular as well as a progressive motion…, it parts on that side, where the motions conspire, must press and beat the contiguous air more violently than on the other, and there excite a reluctancy and reaction of the air proportionably greater." In 1742, Robins (Barkla and Auchterlonie, 1971) noted that ballistic shot curved when angular velocity was imparted to it. Robins succeeded in showing that a lateral aerodynamic force on a spinning sphere could be detected by suspending it as a pendulum. However in 1777, Euler (Barkla and Auchterlonie, 1971) completely rejected the possibility of an aerodynamic force resulting from spin. It was Lord Rayleigh (1877), in his paper on the irregular flight of a tennis ball, who credited Magnus with the first "true explanation" of the effect. Magnus (Barkla and Auchterlonie, 1971), like Robins, noted that ballistic shot curved when spinning, though Magnus was only successful in demonstrating this effect with rotating cylinders. This curve is obtained by rotating the ball about an axis non-collinear with the line of flight. The rotation and the translational velocity combine to produce a pressure difference on the sides of the ball and thus create a lateral aerodynamic force commonly known as the "Magnus Effect" (Roberson and Crowe, 1980).

Figure 1–4 shows a graphical definition of this lateral aerodynamic force (lift) with respect to the velocity vectors. The explanation of the Magnus Effect is a relatively simple exercise in aerodynamics and conservation of momentum. When any object is moving through a fluid, such as air, its surface interacts with a thin layer of air known as the boundary layer. In the case of the sphere or ball, the boundary layer separates from the surface, creating a wake or low-pressure region behind ball. The front-to-back pressure

difference creates a backward force on the ball, which slows the forward motion of the ball. This is the normal air resistance, or aerodynamic drag, that acts on every object. However, if the ball is spinning as it moves, the boundary layers separates at different points on opposite sides of the ball — further upstream on the side of the ball that is turning into the airflow, and further downstream on the side turning with the airflow.

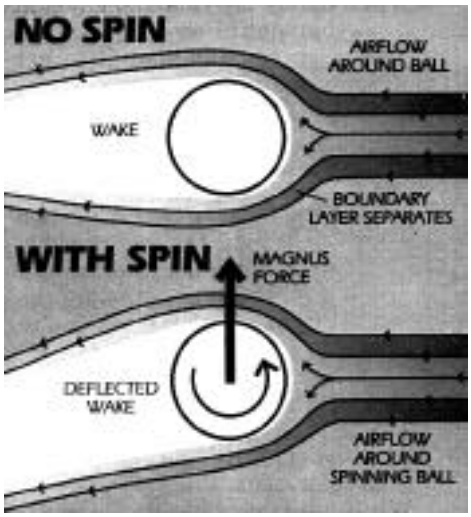

Figure 1–4: Definition of Magnus force with respect to translational and angular velocity vectors (After Brancazio, 1997).

Consequently, the air flowing around the ball is deflected slightly sideways, resulting in an asymmetrical wake behind the ball as shown in figure 1–4. If it is assumed that the air in the wake has downward (as seen in the figure) or negative momentum, for momentum to be conserved the ball must possess an equal but opposite or upwards momentum. Hence a sideways deflection in the trajectory occurs. The magnitude and direction of this resulting momentum vector and its corresponding Magnus force is directly dependent on the velocity vector, angular velocity vector, surface roughness, cross-sectional ball area and air density.

In 1896, Tait (1896) presented his work on the path of a different rotating spherical projectile, namely the golf-ball. Tait derived a set of differential equations based on Robins' work and included a model for a "gradual diminution" of spin during flight. Tait determined the initial velocity by means of a ballistic pendulum. The rotation rate was

measured by attaching an untwisted tape to the ball and counting the twists found in the tape after a four-foot (1.219 m) flight. The grueling task of integrating the differential equations by hand fell upon a graduate student even though Tait was not completely satisfied with the lift coefficients. These integrated results clearly show the golf ball curving in flight as shown in figure 1–5.

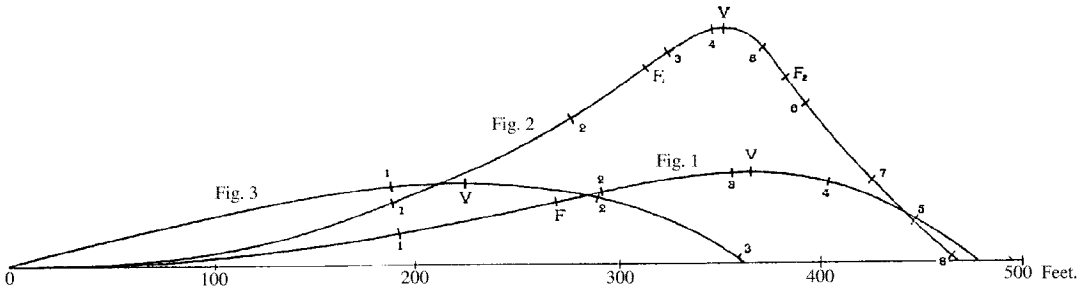

Figure 1–5: Predicted paths of rotating spherical projectiles. (Taken from Tait, 1896).

The first experimental determination of the forces experienced by a spinning sphere in an air stream was conducted by Maccoll (1928). Maccoll used a spherical, six-inch (15.24 cm) diameter, *smooth* wooden sphere gauge and force balance to measure the lift and drag forces at various rotation rates and free-stream velocities. Maccoll's calculated results for the lift and drag coefficients are shown in figure 1–6. In this figure there is an interesting feature in the lift-coefficient data; the appearance of negative lift coefficients at low values of spin parameter, $S = U / V$, where U is the tangential velocity and V is the

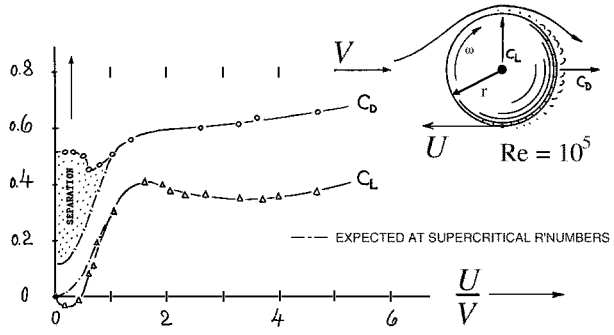

Figure 1–6: Maccoll's lift and drag coefficients for a rotating sphere. (After Hoerner, 1965)

free-stream velocity. Maccoll postulated that the negative lift might be due to turbulent flow at small rotations or some other type of flow that may develop.

Davies (1949) calculated the lift and drag coefficients from the drift of golf-balls by dropping spinning balls through the horizontal stream of a wind tunnel. *Smooth* and dimpled balls were tested at rotational velocities up to 8000 rpm while falling through a wind stream having a translational velocity of 105 ft/sec (32 m/s). Davies measured negative lift for the *smooth* ball at rotational speeds less than 5000 rpm. The negative lift results were consistent with Maccoll's, and Davies attributed the negative lift to unknown changes in the boundary layer.

Sikorsky and Lightfoot became the first investigators to measure the lift on the baseball using a wind tunnel in 1949 (Alaways and Lightfoot, 1998; Drury Jr., 1953). Major league baseballs were mounted to a small electric motor and rotated from 0 to 1200 rpm, clockwise and counter-clockwise, at wind-stream speeds of 80, 95, and 110 mph (35.76, 42.47 and 49.17 m/s). The lift was measured and recorded for the four-seam and two-seam[7] orientations as shown in figure 1–7. These measurements show that seam orientation does play a major role in the lift and thus in the trajectory. Sikorsky and Lightfoot also theoretically showed that the baseball could curve as much as 2.0 ft (60.96 cm) in a 60.5 ft (18.44 m) trajectory from the mound to home-plate.

Briggs (1959) essentially repeated Davies' experiment but with baseballs at spin rates up to 1800 rpm and wind speeds of 150 ft/sec (54.72 m/s). Briggs also used balls that were spinning about a vertical axis and thus gave the maximum lateral deflection, whereas in Davies' measurements the axis of rotation was horizontal and normal to the wind stream. Briggs concluded that the lateral deflection was proportional to ωV^2 . Briggs also measured

---

7 Four- and two- seam curve-ball are defined by the number of seams on the ball that trip the boundary layer at the ball's surface during rotation. These types of pitches are made possible due to the "hour-glass" design of the two pieces of leather that are stitched together forming the baseball's cover.

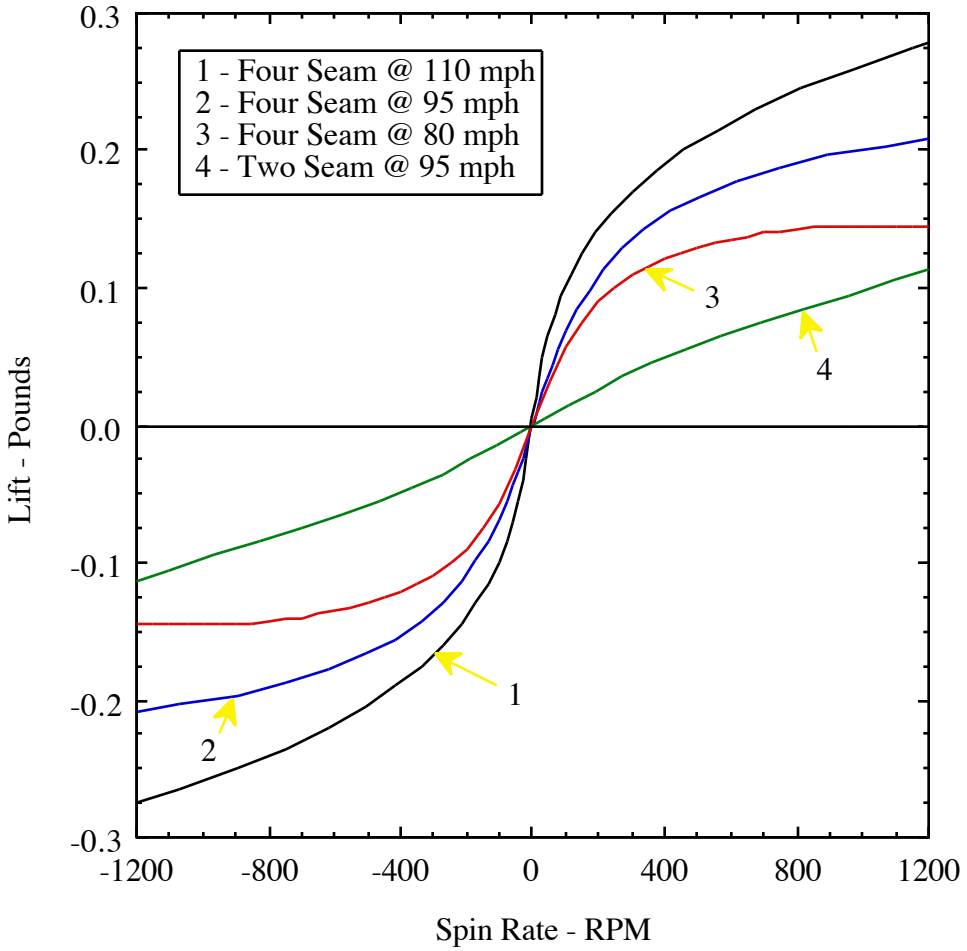

Figure 1–7: Sikorsky/Lightfoot's lift versus spin rate for four- and two-seam curve balls. Negative values of spin represent counter-clockwise rotation of the ball. (Taken from Alaways & Lightfoot, 1998).

the lateral deflection of a "smooth" rubber ball, using the same setup employed with baseballs. The ball was "practically" the same in diameter but slightly heavier and deflected laterally in the opposite direction of baseballs.

The first high-speed "three-dimensional" analysis of baseball trajectories was completed by Selin (1957). Selin use two high-speed (64 and 128 Hz) film cameras to capture the complete trajectory of over 200 pitches made by 14 collegiate pitchers from teams in the Big Ten Conference. All pitches were analyzed for velocity and spin rate. Selected pitches were further analyzed in terms of direction of rotation, rotation angle, vertical deviation, horizontal deviation, vertical forces and horizontal forces. Horizontal

deviations for the curves ranged up to 18 inches (45.72 cm) and the direction was consistent with the lift direction found for non-smooth balls by Maccoll, Davies and subsequently by Briggs. Selin noted that "none of the pitches followed the course which would be followed by a free-falling object".

Another high-speed three-dimensional analysis was conducted by Miller, Walton and Watts (Allman, 1982), this time using 120 Hz strobe photography. Miller, Walton and Watts also used surveyed markers to calibrate a three-dimensional control volume and with algorithms developed by Walton (1981) theoretically tracked the ball to within 0.1 inches (0.254 cm). Their study concluded that a pitch follows a smooth arc and does not have a sharp break as the folklore of baseball might suggest. Their finding is consistent with that of the second *Life*[8] magazine photo investigation.

Additional aerodynamic data on spinning spheres was measured on golf-balls by Bearman and Harvey (1976) and on baseballs by Watts and Ferrer (1987). Bearman and Harvey measured the aerodynamic forces on model (dimpled) balls over a wide range of Reynolds numbers ($0.4 \times 10^5 - 2.4 \times 10^5$) and rotation rates (0 – 6000 rpm). The variation of lift and drag coefficients obtained by Bearman and Harvey has the same overall trends as the data obtained by Davies. The Bearman and Harvey data also show that the lift on a rotating sphere is directly proportional to ωV rather than to ωV^2 as Briggs suggested. This is consistent with the Kutta-Joukowski theorem which implies that the lift is directly proportional to the circulation and linear velocity (Houghton and Carruthers, 1982).

Watts and Ferrer (1987) used strain gauges to measure the lateral force on spinning baseballs in a wind tunnel for three different seam orientations at various Reynolds numbers and rotation rates. Watts and Ferrer's force results show that the force on a spinning ball does not depend strongly on the orientation of the seams with respect to the angular velocity vector in contrast to the Sikorsky/Lightfoot measurements. Watts and

---

8 Camera and Science Settle the Old Rhubarb About Baseball's Curve Ball (1953)

Bahill (1990), nevertheless, question these observations concerning the lack of noticeable changes in lift due to seam orientation because of the low maximum speed (40 mph [17.88 m/s]) of the wind tunnel used.

The latest reported work on non-*smooth* spheres was presented by Smits and Smith (1994). Smits and Smith measured the lift, drag and spin decay rate of golf balls using a wind tunnel by mounting actual golf balls on thin metal spindles. Data was collected for the spin parameter, S, in the range $0.08 < S < 1.3$ at various values of Reynolds number. Six different ball types were tested. Results for only one were presented, though the results presented were typical of all six. Smits and Smith proposed the following model for the lift coefficient, C_L, if the Reynolds number lies between 7.0×10^4 and 2.1×10^5, and with S ranging between 0.08 and 0.20;

$$C_L = 0.54 S^{0.4} . \qquad (1–1)$$

The graph generated by equation 1–1 seems to be a natural extension of the four-seam data measured by Sikorsky and Lightfoot (Alaways and Lightfoot, 1998) and will be presented in chapter 2.

1.3.2.2 Drag

The aerodynamic drag on a non-spinning sphere is fairly well understood and reviewed in most undergraduate engineering texts on fluid dynamics (for example, see Roberson and Crowe, 1980). Figure 1–8 shows a typical plot of the drag coefficient versus the Reynolds number for *smooth* non-spinning spheres.

There are three things to note about figure 1–8; first that the sphere was not spinning, second the sphere was *smooth*, and finally the large drop-off in C_D at "critical" Reynolds numbers between 10^5 and 10^6. This last phenomenon is commonly known as the "drag crisis". Each of these items will be discussed in the following sections and more thoroughly in chapter 2.

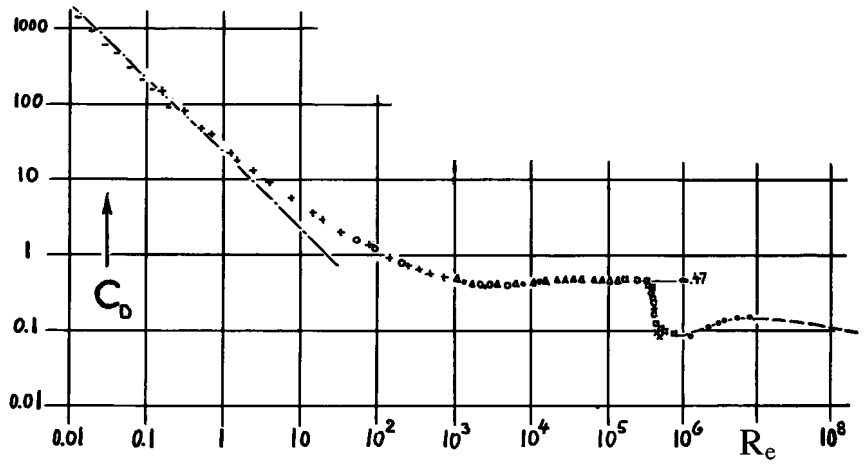

Figure 1–8: Coefficient of drag versus Reynolds number for a non-spinning sphere (Taken from Hoerner, 1965).

1.3.2.2.1 Drag Crisis

In the plot of the drag coefficient versus Reynolds number for an ideal (*smooth*) non-spinning sphere (see figure 1–8), a sharp drop-off in drag coefficient occurs when the Reynolds number exceeds about 2×10^5. This feature is called the "drag crisis" (Frohlich, 1984). Frohlich claims that this may explain several features of the game of baseball which previously have been unexplained or attributed to other cases.

The fluid mechanical explanation of the "drag crisis" is the appearance of turbulent flow in the downstream areas of the boundary layer and a consequential readjustment of the wake. The wake contracts and this leads to a temporary reduction of the drag (Cole, 1962). The value of Reynolds number at which the crisis occurs is termed the critical Reynolds number and in wind-tunnel experiments is found to lie between 1.0×10^5 and 3.0×10^5 for *smooth* non-spinning spheres as seen in figure 1–9. Figure 1–9 is a compilation of lift coefficient results for *smooth* spheres found in eight different wind tunnels. Kaufman (1963) explains that this large spread is due to variation in the turbulence level in wind-tunnels and indeed this drag crisis onset, for smooth spheres, is now used as a measure of the free stream turbulence level in wind-tunnel calibration.

Achenbach (1974) showed that the roughness ratio also has a major role on the "drag crisis". Interestingly, no experimental results pertaining to the crisis occurring with spinning spheres could be found and thus it is not known whether the spin affects the "drag crisis" directly.

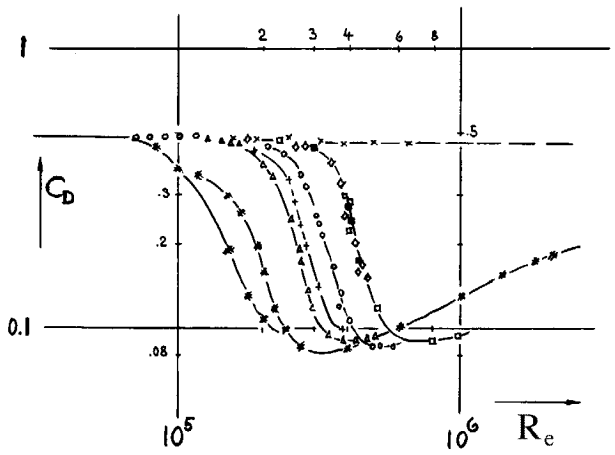

Figure 1–9: Typical experimental results for the drag coefficient of the sphere in the critical range of Reynolds number (Taken from Hoerner, 1965).

1.3.2.2.2 Spinning Spheres

As mentioned in the previous sections, Maccoll (1928) was the first person to publish experimentally measured drag on spinning *smooth* spheres. Maccoll's results for drag coefficient also are plotted in figure 1–6. Notice that figure 1–6 was taken from Hoerner (1965) and shows the measured lift and drag coefficients of Maccoll at $Re = 10^5$. However, figure 1–6 also shows values of C_D for a region of separation and at supercritical *Re*. These results were not in the original paper of Maccoll and are believed to be speculated by Hoerner to account for the drag crisis. Interestingly, in figure 1–6 Maccoll's measured drag coefficients range between 0.4 and 0.6 and are nearly constant when *S* is less than 0.5. However, Hoerner's hypothesized separation region anticipates drag coefficients as low as 0.1.

As in the case of lift, the majority of the past research on spinning non-*smooth* spheres has been in the area of golf. Davies (1949), Bearman & Harvey (1976) and Smits

& Smith (1994) all published experimental wind-tunnel results concerning the golf-ball. The latter two are more consistent and are thus of most interest. Both studies exhibit drag coefficients between 0.25 and 0.35 for Reynolds numbers in the range of $1.45 \times 10^5 < Re < 2.24 \times 10^5$ corresponding to baseball velocities of 66.9 to 103.3 mph (29.89 to 46.17 m/s).

The one interesting published result on a baseball's drag coefficient was made by Briggs (1959). Briggs reported that Dryden measured the "terminal velocity" of a baseball using the National Advisory Committee for Aeronautics vertical wind tunnel. The terminal velocity found was about 140 ft/sec (42.67 m/s) corresponding to an estimated drag coefficient of 0.31 at an estimated Reynolds number of 2.07×10^5, assuming an ambient air temperature of 70 ˚F (21.1 ˚C).

The models used for the drag component of the aerodynamic force in this dissertation will be explained in more detail in chapter 2.

1.3.2.3 Moment

In a recent review, de Mestre (1990) noted that the sum of the moments due to shear forces on the ball is generally negative after release and consequently the angular velocity of a spinning sphere is continuously diminished. This moment is rarely mentioned in literature but Rubinow and Keller (1961) noted that in 1876, Kirchhoff obtained the following equation for the moment vector, **M**

$$\mathbf{M} = -\pi\mu d^3\omega \tag{1–2}$$

where, μ is the dynamic viscosity, d the diameter of the ball and ω the angular velocity vector. However, this equation is valid only for vanishingly small Reynolds number.

Maccoll (1928) while determining the lift and drag coefficients on *smooth* spheres also calculated a value for the air torque on the sphere (2 oz.-in. [0.0141 N-m] at 4,000 rpm) and indicated that the difference in the air torque for the wind on and for the wind off was very slight. Maccoll noted this by the fact that when the wind was put on the spinning sphere, the "rate of spin was but very slightly affected".

Selin (1957) also noticed that aerodynamic moment has little effect on spinning baseballs. In his study, Selin determined rotation rates between 19 and 39 revolutions per second (rps) with a mean of 30 rps and that "the rotation rate for each pitch remained constant."

Smits and Smith (1994) measured the spin rate decay rate for golf-balls and determined an algebraic expression for spin rate decay as a function of spin parameter by determining the best fit line through their data. The expression is valid for Reynolds numbers between 7.0×10^4 and 2.1×10^5 and spin parameters between 0.08 and 0.20. Their equation is given by:

$$SRD = \left(\frac{d\omega}{dt} \right) \frac{r^2}{V^2} = -0.00002S \qquad (1\text{–}3)$$

where; *SRD* is the dimensionless spin rate decay and *t* is time.

Ranger (1996) found an exact solution of the Navier-Stokes equations for the motion representing exponentially time-dependent decay of a solid sphere translating and rotating in a viscous fluid relative to a uniform stream. In his solution the angular velocity decays exponentially with a time constant inversely proportional to ν, the kinematic viscosity.

The model and assumptions used for the aerodynamic moment in this dissertation will be explained in more detail in chapter 2.

1.3.2.4 Closing Comment

A literature review on the past work into the aerodynamics of sports balls would not be complete without the mentioning the review of Mehta (1985). Mehta's paper is a complete literature summary covering the past aerodynamic research on non-*smooth* spheres in the areas of baseball, golf and cricket. Many of the publications previously cited are mentioned by Mehta, but also included in Mehta's review are the topics of the knuckleball and the circumferential stitching pattern found on the cricket ball. Mehta (1985) was used as a starter document for this research and is the best review known at this time.

1.3.3 Data Acquisition

Attempts at acquiring accurate aerodynamic and trajectory data have always gone hand-in-hand with trying to understand the dynamics of the curve. Robins (Barkla and Auchterlonie, 1971) spun a sphere and cylinder on a pendulum, while Maccoll (1928), Sikorsky & Lightfoot (Alaways and Lightfoot, 1998), Davies (1949), Briggs (1959), Bearman & Harvey (1976), and Watts & Ferrer (1987) all used various forms of wind-tunnel tests to obtain information about the "Magnus Effect". Lord Rayleigh (1877) and Verwiebe (1942) used ballistic pendulums to obtain velocity information. Lord Rayleigh also used an untwisted tape while *Life*[9] magazine and Selin used painted balls to measure rotation rates. Verwiebe and the fictitious *Rover Boys* (Houston, 1941) found position data by throwing balls through fixed frames; Briggs looked at the lateral deviations at impact with the ground, and *Life*[10], *Look* (Cohane, 1949), and Selin used various forms of high-speed/strobe photography to capture trajectory information. All of these were experimental attempts to understand the aerodynamic nature of spinning spheres.

The most interesting and sophisticated study was done by Miller, Walton and Watts (Allman, 1982) in acquiring accurate baseball trajectory information. This study will be explained in more detail in the following paragraphs.

High-speed photography has been used to make kinematic measurements for more than 120 years since Eadweard Muybridge began his investigation of the trotting horse for Leland Stanford (Mozley, Haas, and Forster-Hahn, 1972), but only in the last 25 years have significant advances been made in data capture techniques (Walton, 1994). In the past, high-speed and strobe photography had been used to perform qualitative assessments of rapid events, but it failed to become a regular means of quantitative measurement. The Miller, Walton and Watts study was the first quantitative study to "accurately" measure a baseball trajectory.

---

9 Camera and Science Settle the Old Rhubarb About Baseball's Curve Ball (1953).

10 Ibid.; Baseball's Curve Balls: Are They Optical Illusions (1941).

In the 1970's new algorithms were developed and a software package was created to solve the calibration and intersection problems associated with reconstructing two- and three-dimensional trajectories from two or more synchronous views (Walton, 1981). Miller, Walton and Watts (Allman, 1982) constructed a "tunnel" eight feet (2.44 m) wide and eight feet (2.44 m) high, stretching from the mound to the plate. The walls of the tunnel were marked with calibrated Ping-Pong balls, allowing the baseball trajectory to be reconstructed to within 0.1 inches (0.254 cm). The equations used to reconstruct the three-dimensional trajectory are based on the "collinearity condition", a fundamental principle of photogrammetry, in which an object point, its ideal image and the perspective center fall on a straight line (Walton, 1994). This mapping has become known as the Direct Linear Transformation (DLT), a name given to it by Abdel-Aziz and Karara (1971), who worked with it extensively at the University of Illinois.

With the advent of consumer electronics and desktop computing the processing speed and accuracy of "real-time" high-speed video analysis has reached the point where fast feedback quantitative systems are now available. In fact such systems are now the standard in motion analysis research. For example, Hubbard and Alaways (1989) used a high-speed motion analysis system based on the DLT and Walton's (1981) algorithm to accurately estimate in under two minutes, from the time of release, the release conditions of a javelin throw. Additionally, Koff (1990) reported that such a system can have a dynamic accuracy in position as high as one part in 2000 of the field-of-view[11], though great care is needed in calibrating the system and in the data acquisition to achieve that level of accuracy (Alaways et al., 1996).

During the 1997 Major League season the first successful attempt at revealing more information to the general television audience concerning the pitch was made. Both, NBC and FOX utilized SuperVision in their national baseball broadcasts. SuperVision records

---

11 The latest 1997 MotionAnalysis Corporation system specifications reports the 3D dynamic accuracy to be one part in 35,000 of the field-of-view.

images of the pitch at 16 three-dimensional positions using stadium-mounted cameras, computers, special-effects generators and trigonometric triangulation (Kaat, 1997). The system can replay a graphic trajectory of the pitch within one second after the balls hits the catcher's mitt. SuperVision claims to show the ball's actual path of travel from the mound to home-plate and the breaking movement of the ball inside the strike zone.

1.4 Components of the Problem and Strategy of Investigation

As pointed out in the previous sections, the "Magnus Effect" is the principle mechanism in the curve-ball. The trajectory of the ball is determined by the initial conditions at the moment of release and the forces acting on the ball during flight. The initial conditions include the three Cartesian positions, the translational velocity vector, the angular velocity vector, and the initial orientation of the ball. The forces acting on the ball include the gravitational force along with the aerodynamic force and moment. To show how the spin or angular velocity affects the curve of a pitch, it is necessary to know the initial conditions, along with some form of model for the above forces and moment.

Utilizing an accurate and fast high-speed video motion analysis system, one can reconstruct or "track" the trajectory of an object. Hubbard and Alaways (1989) showed that with the appropriate model and with "good" trajectory data the release conditions for a javelin could rapidly be determined. The problem, therefore, in understanding the effect that angular velocity has on the trajectory of a baseball is twofold. First, models for the aerodynamic forces and moments need to be established. Second, accurate trajectory data needs to be obtained.

The aerodynamic models that determine the forces and moment will be based on the past research described in the previous sections and will be thoroughly explained in the next chapter. The models will be based on the lift coefficients from the wind-tunnel results of Sikorsky & Lightfoot (Alaways and Lightfoot, 1998), Smits & Smiths (1994) and Davies (1949); the drag coefficients based on the work of Dryden (Briggs, 1959) and Smits & Smith (1994); and the moment from the solution of Smits & Smith. Limited as

they are, these models are still the best results available in describing the aerodynamic forces acting on the ball.

1.5 Equipment and Software Used

To obtain accurate trajectory data, a MotionAnalysis ExpertVision 3D EVa HiRES system was used for the data acquisition. This system was based on ten 240-Hz MotionAnalysis FALCON cameras with red LED synchronized strobe lighting. The cameras were arranged so that six or seven cameras were used to track points on the ball during the first four feet (1.22 m) of flight and the remaining three or four cameras tracked the entire ball as a single point for the last 13 to 46 ft (3.96 to 14.01 m) of the trajectory as the ball crossed over the plate. The MotionAnalysis EVa software version 4.64 was used to synchronize the video cameras, and to perform calibration, tracking and editing of the acquired data sets. The software was hosted on a SUN/SPARC workstation operating under the Solaris common desktop environment.

A Major League hopeful was used to pitch and his comments on the pitch were recorded for comparison. Additionally, two non-experienced throwers also were used and pitching machine tests utilizing an Athletic Training Equipment Company (ATEC) pitching machine were conducted.

Finally, estimation software was written to analyze the three-dimensional trajectory information based on the method developed by Hubbard and Alaways (1989). The software was used to process the data and determine the initial conditions. Though multiple pitches were collected, only selected pitching machine throws were analyzed for spin information along with cross force and aerodynamic coefficient estimation. The remaining trajectories were analyzed to obtain more information on the drag-coefficient. The analysis was confined to pitches, with initial velocities near 70 mph (31.29 m/s) and spin rates between 20 and 70 rps. Although, it was not planned, nevertheless results for three knuckleballs are also included. The estimated initial conditions and trajectory profiles are presented with concluding remarks.

CHAPTER 2 – BASEBALL DYNAMICS

> It can't be done. You cannot throw or bat a baseball that does not curve or change directions, if it is in the air long enough for its spin, or lack of spin, to take effect. If it spins, it will curve.
>
> Martin Quigley (1984), *The Crooked Pitch*

2.1 General Comments

Once a ball becomes ballistic, that is once it becomes detached from its launching mechanism, only gravitational and aerodynamic forces act on the ball. It is for this reason that the trajectory of baseballs can be modeled. The general equations of motion that model the trajectory are represented by the following vector equations,

$$\sum \mathbf{F} = \frac{d\mathbf{P}}{dt}, \tag{2–1}$$

and

$$\sum \mathbf{M}_G = \frac{d\mathbf{H}_G}{dt}, \tag{2–2}$$

where, $\mathbf{F}$ is the vector of external forces (gravitational and aerodynamic), $\mathbf{P}$ is the linear momentum vector, $\mathbf{M}_G$ is the vector of external (aerodynamic) moments about the center of mass, G, of the ball and $\mathbf{H}_G$ is the angular momentum vector referenced to the center of mass of the ball.

These equations can be expanded to show more qualitatively how the forces, moments and velocities play a role in the trajectory dynamics. First, equation 2–1 is simplified by exploiting the definition of linear momentum. Linear momentum is defined as the product of the mass, m, with the translational velocity of the center of mass, $\mathbf{V}$, and noting that the mass of the ball remains constant when pitched transforms equation 2–1 into,

$$\sum \mathbf{F} = m\frac{d\mathbf{V}}{dt}. \tag{2–3}$$

This equation is expanded further by noting that the only forces acting on the ball are the gravitational force, $\mathbf{F}_G$, and the aerodynamic force, $\mathbf{F}_A$. Substituting these forces for the summation in equation 2–3 results in,

$$\mathbf{F}_G + \mathbf{F}_A = m\frac{d\mathbf{V}}{dt}. \tag{2–4}$$

Equation 2–2 also is expanded by exploiting the definition of angular momentum and assuming that the inertia matrix, $\mathbf{I}_G$, is diagonal (i.e. the ball is spherical and mass uniformly distributed) and constant. In this case equation 2–2 can be rewritten as,

$$\sum \mathbf{M}_G = \mathbf{I}_G\frac{d\omega}{dt}. \tag{2–5}$$

In the following sections these forces and moments will be examined in more detail and the final set of equations of motion is presented.

2.2 Gravitational Force

The gravitational force $\mathbf{F}_G$ is calculated by,

$$\mathbf{F}_G = m\mathbf{g} \tag{2–6}$$

where, $\mathbf{g}$ is the *gravitational field strength* or acceleration due to gravity. Resnick and Halliday (1977) give an excellent example detailing how the magnitude of the acceleration has a local value depending on earth latitude and elevation; representative values are shown in table 2–1. Using table 2–1 and knowing that the local latitude and elevation for Santa Rosa, California (experiment site) is 38° 32’ 42” North and 50 ft (15.24 m), respectively, the local gravitational acceleration was determined to be 32.156 ft/s^2 (9.801 m/s^2). Therefore, the downward (negative) gravitational force used in this dissertation is given by[1],

$$F_G = -9.801m. \tag{2–7}$$

---

[1] The primary units of this dissertation are based on the units of feet and miles per hour, because these are the historical units of baseball. However, metric units were used in the simulation and therefore equation 2–7 is presented here in metric units.

Table 2–1: Acceleration due to gravity for sea level at various latitudes. (After Weast, 1982)

Latitude	Acceleration due to gravity	
•	cm/sec^2	ft/sec^2
0	978.039	32.0878
5	978.078	32.0891
10	978.195	32.0929
15	978.384	32.0991
20	978.641	32.1076
…		
35	979.737	32.1435
36	979.822	32.1463
37	979.908	32.1491
38	979.995	32.1520
39	980.083	32.1549
…		
70	982.608	32.2377
75	982.868	32.2463
80	983.059	32.2525
85	983.178	32.2564
90	983.217	32.2577

Correction for Altitude.

-0.000003086 $ft/sec^2/ft$ for altitude in feet.

-0.0003086 $cm/sec^2/m$ for altitude in meters.

2.3 Aerodynamic Forces

Any body immersed in a flowing fluid is acted upon by both pressure and shear viscous forces from the flow (Roberson and Crowe, 1980). The sum of the force components that act parallel and opposed to the translational velocity vector is defined as drag, **D**, and the sum of the force components that act perpendicular to the translational velocity vector is typically defined as lift, **L**. However, in this case with a spinning sphere, the direction of the lift component is defined as being mutually perpendicular to both the translational velocity vector and the angular velocity vector. With this being the case, a third

component of the aerodynamic force that is mutually perpendicular to the lift and drag components is needed to completely define the aerodynamic force vector. This third force component is usually called the side force, but since the lift component can act entirely in the horizontal plane or sideways direction it was decided to label this force component the "cross-force", **Y**, in this dissertation. Figure 2–1 shows the aerodynamic force components with respect to the translational and angular velocity vectors. The assumptions and equations used to model these force components are given in the following sections.

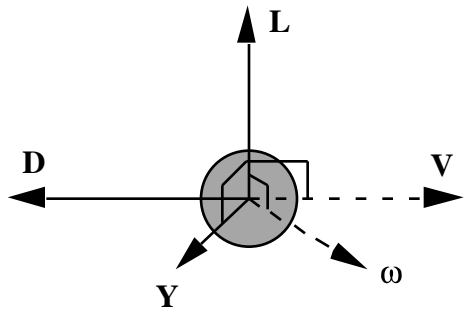

Figure 2–1: Aerodynamic force components. (Note that the four vectors **V**, **D**, **Y** and ω lie in the plane perpendicular to **L**.)

2.3.1 Lift

Generally, the lift, **L**, is characterized in terms of a dimensionless number, in this case the lift coefficient, C_L,

$$\mathbf{L} = \frac{\rho C_L A V^2}{2} \frac{\omega \times \mathbf{V}}{|\omega \times \mathbf{V}|}. \tag{2–8}$$

where, ρ is the fluid density of air, A is the cross-sectional area of the ball, and **V** is the translational velocity of the ball[2]. C_L is also a function of the Reynolds number, Re, the spin parameter, S, and the roughness ratio, κ, of the ball. The Reynolds number is defined as,

$$Re = \frac{Vd}{\nu} \tag{2–9}$$

---

[2] In many areas of aerodynamics the aerodynamic force is written with respect to the relative wind and therefore the cross product term of equation 2–8 is $\mathbf{V} \times \omega$. In this dissertation, however, the aerodynamic force is derived with respect to the translational velocity of the ball and therefore the lift component is in the $\omega \times \mathbf{V}$ direction as indicated.

where d is the diameter of the ball and ν is the kinematic viscosity of air. The lift component has two interesting features, the first being the strong dependence of C_L on S for spheres as figure 2–2 indicates. The second is the cross product term in equation 2–8 that defines the direction of the lift force.

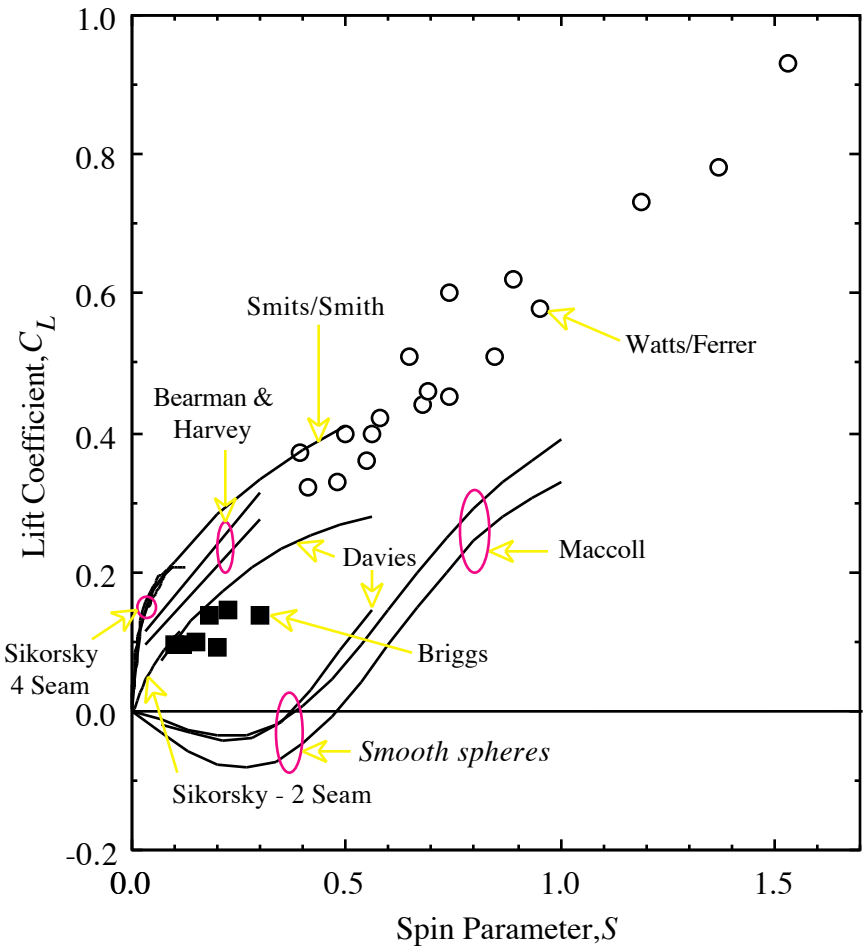

Figure 2–2: Coefficient of lift versus spin parameter for spinning spheres at various values of Reynolds number. (After Alaways & Lightfoot, 1998).

Figure 2–2 is a compilation of the determined C_L versus S plots from the data of Maccoll (1928), Sikorsky (Alaways and Lightfoot, 1998), Davies (1949), Briggs (1959), Bearman and Harvey (1976), Watts and Ferrer (1987), and from equation 1–1 (see page 17) of Smits and Smith (1994). In all of the previous work C_L was determined by either measuring the lift or lateral deviation of the ball and then calculating the lift coefficient from this information.

There are three features of figure 2–2 that require more discussion. First, note that the *smooth* sphere plots all have the same general shape and all show negative lift at the lower values of S. Though this is interesting in its own right the baseball is definitely not *smooth*. Second, the trend of the non-*smooth* data shows a dependence of C_L on S for both golf and baseballs. Lastly, the data for each ball type should be examined independently since the dimples on the golf-ball and the stitches on the baseball are ball unique quantities. The two latter points presented here are discussed more thoroughly in the following paragraphs.

In the baseball data of figure 2–2, the major item of interest is the relationship between C_L, S and seam orientation. This relationship is more clearly shown in figure 2–3 where the smooth sphere data of figure 2–2 is removed and the axes reduced to provide more detail for $S < 0.5$. Note that the Briggs data in both figures is based on Briggs' extrapolated results for total deviation of dropped balls and the validity of these results is in question. Therefore, ignoring the Briggs data and focusing only on the Sikorsky and Watts & Ferrer data yields an interesting hypothesis that will be the grounds for the aerodynamic model of this dissertation.

The Sikorsky plots show that 1) seam orientation plays a major role in the magnitude of C_L at lower values of S, 2) seam orientation may have more influence than Re on the magnitude of C_L, and 3) a possible convergence of C_L, the merging of the two- and four-seam lift coefficients, is beginning at values of S greater than 0.1. The second point is shown by noting that the 3 four-seam Sikorsky plots (data measured at 80, 95 and 110 mph [35.76, 42.47 and 49.17 m/s]) are nearly identical yet are clearly distinct from the Sikorsky two-seam plot. Seam orientation, therefore, is the deciding factor in C_L magnitude for low values of S. The latter point, the loss of seam orientation influence with increasing S, was noted by Watts and Ferrer and is shown in their data. Recall, that Watts and Ferrer measured C_L using baseballs in three different seam orientations and concluded that seam orientations did not play a major role in C_L magnitude for spin parameters greater

than 0.4. However, the decreasing slope of the Sikorsky four-seam data may be the beginning of the convergence between the Sikorsky four- and two-seam data sets. The initial hypothesis for the lift coefficient model for this dissertation is that the Sikorsky data is correct for the four- and two-seam orientations and that Watts & Ferrer are also correct in that seam orientation does not play a major role at $S > 0.4$. This hypothesis also assumes that the four- and two- seam curves of Sikorsky will slowly converge as S increases. However, before the final model is developed a look at the golf-ball data is in order.

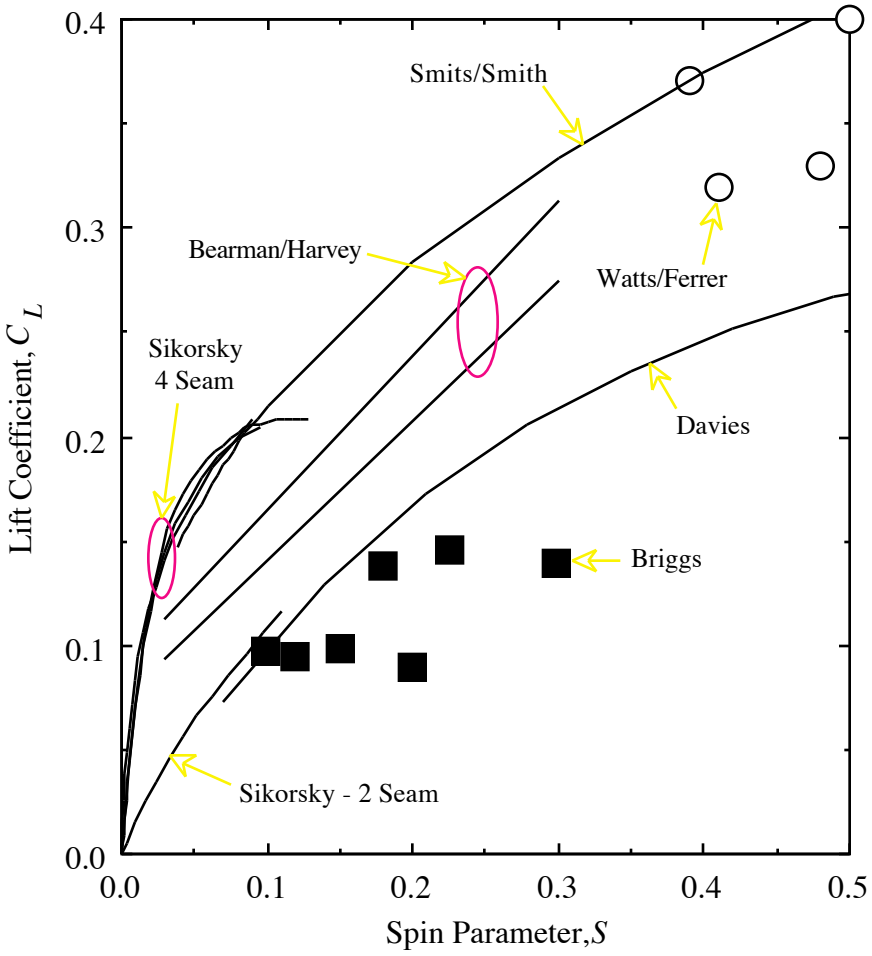

Figure 2–3: Detailed view of coefficient of lift versus spin parameter for spinning spheres. (After Alaways & Lightfoot, 1998).

Additionally, figure 2–3 shows that the majority of the data on golf-balls lies between the two extremes of the Sikorsky data. This indicates that surface roughness and dimple type may have as large an effect on the golf-ball lift as changing the spin axis

orientation does on lift of the baseball. Though it is not fully understood as to why the lift coefficient on the golf-ball has increased from study to study it is believed that changes in golf-ball design specifications have increased the effective roughness of the ball. This hypothesis is partly supported by noting that the Bearman and Harvey studied looked at different dimple types and that the hexagonal dimple was found to have a higher C_L than the less-rough semi-spherical dimple of the standard golf-ball.

Watts and Bahill (1990) suggest that a "good choice" or model of C_L is given by the straight line approximation obtained by setting $C_L = S$. This approximation fits well for the Sikorsky two-seam data but grossly underestimates the lift coefficient for the four-seam data for values of S less than 0.1 as shown in figure 2–4. However, assuming C_L is proportional to S is well founded by noting that L would be proportional to ωV as indicated by the Kutta-Joukowski theorem.

In figure 2–4 linear lines with slopes, k, of 1.0, 1.5, 2.0, and 4.0 are overlaid with the Sikorsky, Davies and Smits & Smith data. For values of spin parameter less than 0.1 it is feasible to model the lift coefficient for a baseball as a simple multiple of S if the orientation of the seams is known. However, at values of S greater than 0.1 extrapolated lines from the Sikorsky data to the Watts & Ferrer data are probably best. The lift model used for this dissertation will therefore be based upon the two Sikorsky curves for $S \leq 0.1$ and the two "extrapolated" lift coefficient lines for $0.1 < S \leq 0.5$ when values of S and the seam orientation are known. Though it was originally hypothesized above that the two- and four-seam curves would converge, this model takes the more conservative approach and attempts to bound the region of possible lift coefficients. Therefore, if only trajectory data of the center of mass is known (i.e. no direct information about the spin rate or ball orientation is available) the lift coefficient with be estimated and the Sikorsky data and the extrapolated lift coefficient lines with be used as limits for the spin parameter and thus the spin rate.

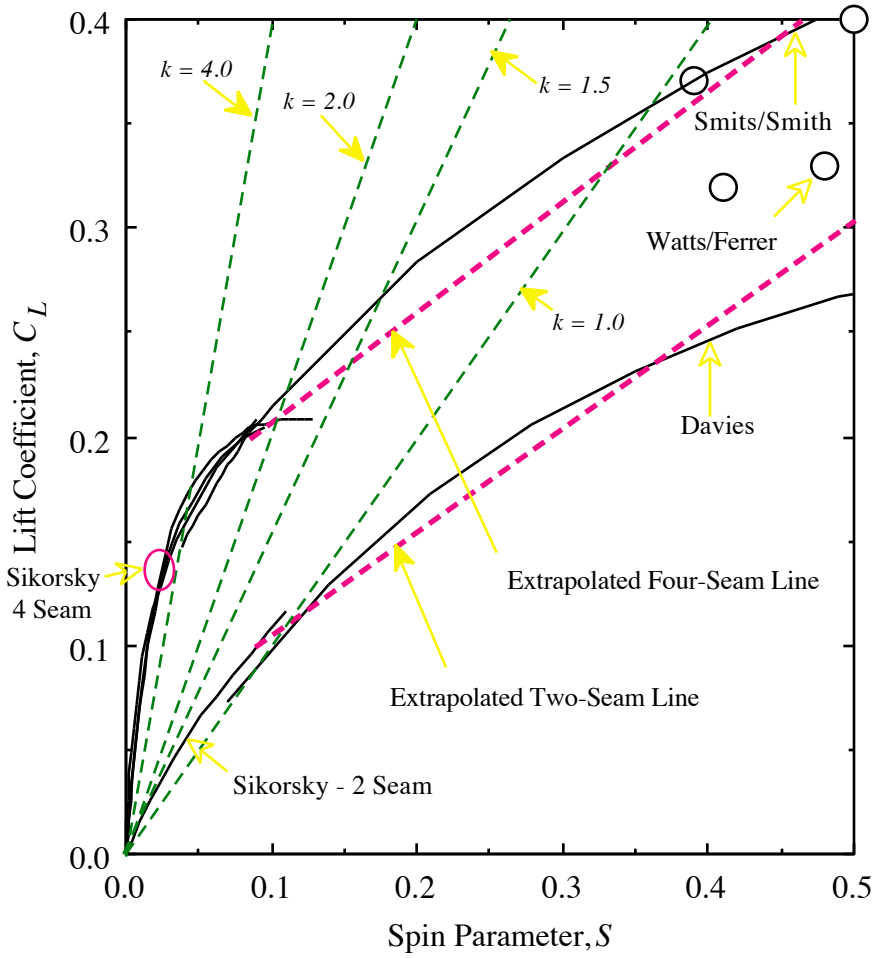

Figure 2–4: Straight-line approximations and the extrapolated lift lines for the lift coefficient.

Another interesting feature of equation 2–8 is the cross product term. Equation 2–8 assumes that the angular velocity and translational velocity vectors are perpendicular to each other. If this is not the case, the lift coefficient is diminished and the decreased values of the magnitude of the cross-product term of ω and **V** approximates it. Watts and Bahill (1990), predicted that the magnitude of the lift component will decrease approximately as the sine of the angle between the axis of rotation and the direction of motion. This possible decrease in lift also will be included in the model by incorporating the dependence of the angle between the translational and angular velocity vectors into the magnitude of C_L.

Finally, for the case when the lift coefficient is assumed to be a simple multiple of the spin parameter S (i.e. $C_L = kr\omega / V$) then letting $A = \pi r^2$ and defining ζ to be the angle between the axis of rotation and the direction of motion, equation 2–8 can be written as,

$$\mathbf{L} = \frac{\rho \pi k r^3 \omega V \sin(\zeta)}{2} \frac{\omega \times \mathbf{V}}{|\omega \times \mathbf{V}|}. \tag{2–10}$$

Equation 2–10 is further reduced by noting that $|\omega \times \mathbf{V}| = \omega V \sin(\zeta)$, resulting in,

$$\mathbf{L} = \frac{\rho \pi k r^3}{2} \omega \times \mathbf{V}. \tag{2–11}$$

Note that equation 2–11 can be used only when $C_L = kS$ and indicates that L is proportional to ω and V as predicted by the Kutta-Joukowski theorem. For this dissertation, however, the following simplified form of equation 2–8 will be used,

$$L = \frac{\rho C_L A V}{2\omega} \omega \times \mathbf{V} \tag{2–12}$$

where C_L is either estimated or determined from figure 2–3. Notice that since the entire cross product is used in equation 2–12 and not the unit vector in the $\omega \times \mathbf{V}$ direction, as in equation 2–10, this implies that $\sin(\zeta)$ is inherently included in equation 2–12. Therefore any value of C_L that is estimated using this equation must be divided by $\sin(\zeta)$ in order to compare it with the values shown in figure 2–2. Recall that the values of C_L in figure 2–2 are all from experiments where the translational and angular velocity vectors were perpendicular (i.e. ζ = 90 deg).

2.3.2 Drag

Like lift, the drag, **D**, is characterized in terms of a dimensionless number, the drag coefficient, C_D,

$$\mathbf{D} = -\tfrac{1}{2} \rho C_D A V \mathbf{V}. \tag{2–13}$$

Like C_L, C_D is also a function of the Reynolds number and the roughness ratio of the ball[3].

Typical Reynolds numbers for various balls used in sports are presented in table 2–2. For this dissertation, the typical release velocity will lie between 55 and 80 mph (25 and 36 m/s); at 60° F the corresponding range of *Re* is 1.23×10^5 to 1.78×10^5 — slightly less than the typical range of critical *Re* for non-spinning smooth spheres as shown in figure 1–8. It should be noted that the critical *Re* for baseballs in not known at this time.

Table 2–2: Representative speeds for various balls used in sports, and calculated values of Reynolds number and ratio "*D*/*g*" of aerodynamic drag force to gravitational force. For uniformity, even for balls with large *Re*, $C_D = 0.5$ was used when calculating the aerodynamic drag force. (After Frohlich, 1984).

Type of Ball	Reported speed; mph (m/s)	Diameter; inches (cm)	Mass; lb. (Kg)	Reynolds number (10^5)	*D*/*g*	Comments
Baseball	95.44 (42.67)	2.9 (7.3)	0.320 (0.145)	2.08	1.74	Terminal velocity in wind tunnel.
Basketball	16.30 (9.00)	9.6 (24.3)	1.323 (0.600)	1.46	0.21	Calculated for 25 ft (7.62 m) jump shot.
Bowling	17.36 (7.76)	8.6 (21.8)	16.0 (7.270)	1.13	0.01	Release speed of expert.
Golf	136.44 (61.00)	1.7 (4.3)	0.101 (0.046)	1.73	3.80	Moderately long drive by pro.
Shot put	31.36 (14.02)	4.3 (11.0)	16.0 (7.270)	1.03	0.01	World record performance.
Soccer	65.09 (29.10)	8.7 (22.2)	1.0 (0.454)	4.31	2.38	
Softball	98.86 (44.20)	3.8 (9.7)	0.414 (0.188)	2.86	2.53	Ball pitched by very fast professional.
Tennis	100.99 (45.15)	2.6 (6.5)	0.127 (0.058)	1.96	3.84	Serve of top professionals.
Volleyball	67.68 (30.26)	8.3 (21.0)	0.595 (0.270)	4.23	3.86	Very hard spike by male college player.

---

3 In many areas of aerodynamics the aerodynamic force is written with respect to the relative wind and therefore the drag component of the aerodynamic force is in the same direction as the velocity vector (i.e. is positive). In this dissertation, however, the aerodynamic force is derived with respect to the translational velocity of the ball and therefore the drag component is in the direction indicated.

Recall, that Maccoll (1928) was the first to publish drag coefficients for *smooth* spinning spheres (see figure 1–6) and obtained values near 0.5 for S less than unity and that Briggs (1959) reported that the terminal velocity of a baseball was 140 ft/sec (42.67 m/s) which corresponds to an estimated drag coefficient of 0.31 at an estimated Reynolds number of 2.07×10^5, assuming an ambient air temperature of 70° F (21.1 °C). Smits & Smith (1994) and Bearman & Harvey (1976) both published wind-tunnel results for golf-balls that exhibited drag coefficients ranging from 0.25 to 0.33 for *Re* applicable for the average baseball pitch as shown in figure 2–5.

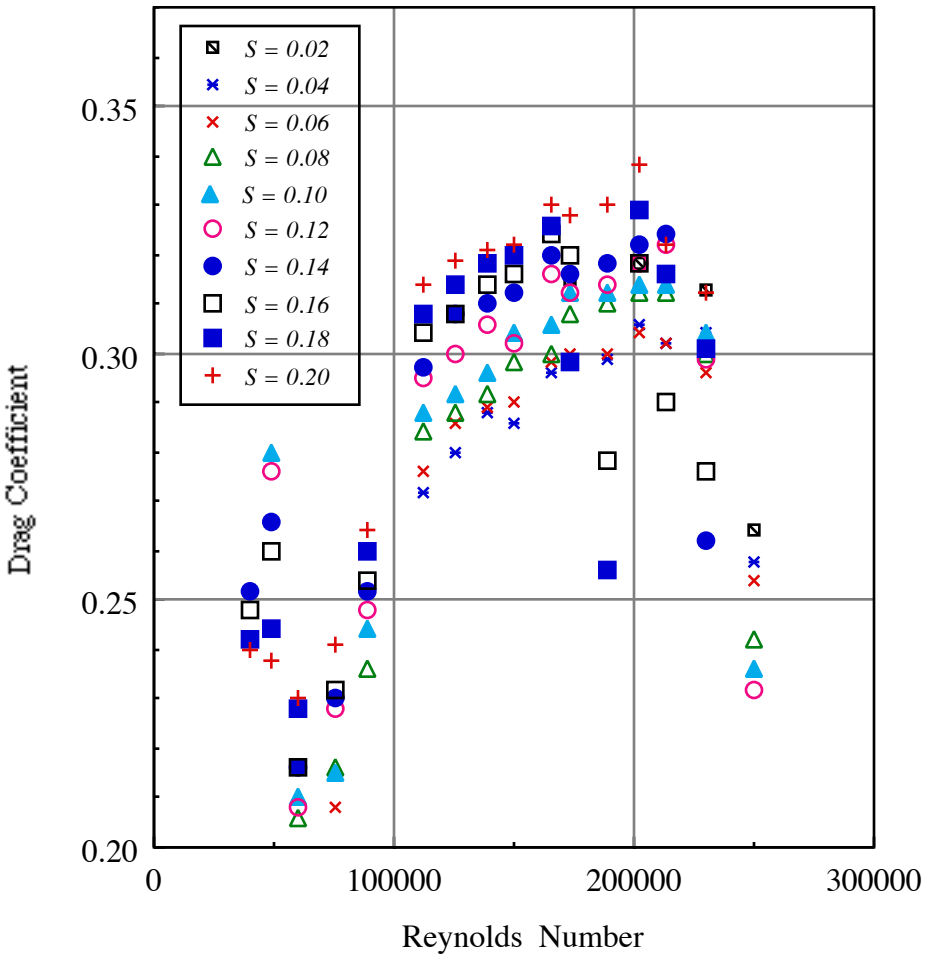

Figure 2–5: Drag coefficient versus Reynolds number for spinning golf balls (After Smits and Smith, 1994).

Figure 2–5 shows the drag coefficient versus Reynolds number from Smits and Smith (1994) golf-ball data for various values of spin parameter. Two interesting features

in figure 2–5 are the two sudden drops in drag coefficients at possible critical Reynolds numbers of 0.75×10^5 and 2.5×10^5. However, for $1.5 \times 10^5 < Re < 2.0 \times 10^5$ the coefficient of drag is consistently ranging from 0.27 to 0.33, bracketing the 0.31 value determined from the terminal velocity for the baseball.

The model used in this dissertation will be that of equation 2–13 though the drag coefficient will be estimated along with the initial conditions. The drag coefficient will be assumed to remain constant throughout the pitch and is expected to lie between 0.30 and 0.35. The rationale behind assuming a constant drag coefficient is that even if the drag coefficient was 0.47, the value for a non-spinning smooth sphere at $Re = 1.0 \times 10^5$, and integrating equation 2–13 over distance, the Reynolds number for any pitch traveling a distance 60.5 ft (18.44 m) would only decrease 14 percent and for a drag coefficient of 0.31 the decrease in *Re* is only 9.5 percent. Unless the pitch is released at exactly the critical *Re*, the magnitude of the drag coefficient will vary only slightly (less than 5 percent) throughout its half-second flight.

2.3.3 Cross-Force

In all previous studies on the aerodynamics of sport balls the aerodynamic force on the ball was defined as the sum of the drag and lift components as previously defined in equations 2–8 and 2–13. However, in most cases the lift reported was not the lift generated solely on the basis of the Magnus force but was the sum of all force components perpendicular to the drag. These studies assumed that, because of the symmetry of the ball in question, no other forces are present on the ball or the author simply ignores them. However, the baseball in most cases is released such that the stitch pattern on the ball is asymmetric in flight. In these cases an additional force component perpendicular to both the lift and drag, as shown in figure 2–1, most likely exists. This aerodynamic force component also will be considered in this dissertation and will be called the “cross-force”, **Y**, and will be characterized in terms of a dimensionless number, the cross-force coefficient, C_Y,

$$\mathbf{Y} = \tfrac{1}{2}\rho C_Y A V^2 \frac{\mathbf{L}\times\mathbf{D}}{|\mathbf{L}\times\mathbf{D}|}. \tag{2–14}$$

Since no information about this magnitude of this force component or coefficient is available, the magnitude of C_Y will be estimated as described in chapter 4.

2.4 Aerodynamic Moment

The lift, drag and cross-force are due to pressure and viscous shear forces that act on the ball while in flight. The shear forces can induce a moment on the ball that decreases the angular momentum and thus the spin rate. The moment on balls, nevertheless, is slight as noted by Maccoll (1928) and Selin (1957).

Smits and Smith (1994) measured the spin rate decay rate for golf-balls and determined an algebraic expression for spin rate decay as a function of spin parameter. The expression is valid for Reynolds numbers between 70,000 and 210,000 and spin parameter values between 0.08 and 0.20. Their equation is given by:

$$SRD = \left(\frac{d\omega}{dt}\right)\frac{r^2}{V^2} = -0.00002S \tag{2–15}$$

where; SRD is the spin rate decay, t is time and $S = r\omega/V$. Some interesting information is obtained by re-writing equation 2–15 as the following first order differential equation

$$\dot{\omega}\frac{r^2}{V^2} = -\alpha\frac{r\omega}{V} \tag{2–16}$$

where $\alpha = 0.00002$ and rearranging terms to put equation 2–16 in the following standard form of

$$\dot{\omega} + \frac{\omega}{\tau} = 0 \tag{2–17}$$

where $\tau = r/(\alpha V)$. The solution to equation 2–17 is easily obtained and is given by

$$\omega = \omega_0 e^{-t/\tau}. \tag{2–18}$$

For a 70 mph (31.29 m/s) curve rotating at 30 rps τ is 58.1 seconds. Applying equation 2–18 in the half-second it takes for the ball to reach home plate from release, the rotation rate decreases by only 0.86 percent.

Ranger (1996) showed that if one assumed that a rotating sphere experienced an exponential angular velocity decay in a viscous liquid no external moment was found acting on the sphere. For a 70 mph (31.29 m/s) curve rotating at 30 rps, in the half-second it takes for the ball to reach home-plate from release. Ranger's angular velocity equation predicts that the rotation rate decreases by 0.08 percent.

Since all previous work agrees that the aerodynamic moment on a spinning sphere is small, for this dissertation in cases where only trajectory data of the center of mass is known (i.e., no direct information about the spin rate) a constant angular velocity will be estimated and assumed to be in effect throughout the pitch. In cases where direct information about the spin rate is obtained, that spin value and any measurable spin decrease will be used. Note, that in making the assumption of constant angular velocity, the equations of motion now only consist of the translational equation 2–4 since the right hand side of equation 2–5 vanishes.

2.5 Coordinate Systems

Before the final form of the equations of motion can be derived, a local coordinate system must first be defined. Additionally, coordinate systems to define the orientation of markers on the ball and the orientation of the aerodynamic force with respect to the wind also are defined. The following sections describe these three coordinate systems.

2.5.1 Local Coordinate System

For the local coordinate system a Cartesian system will be used, with the *x*- and *y*-axes defining the horizontal plane with the *z*-axis mutually perpendicular and positive directed upwards. Figure 2–6 shows a planar view of a baseball infield with the coordinate frame origin located at the intersection of the first and third base lines at home-plate and the

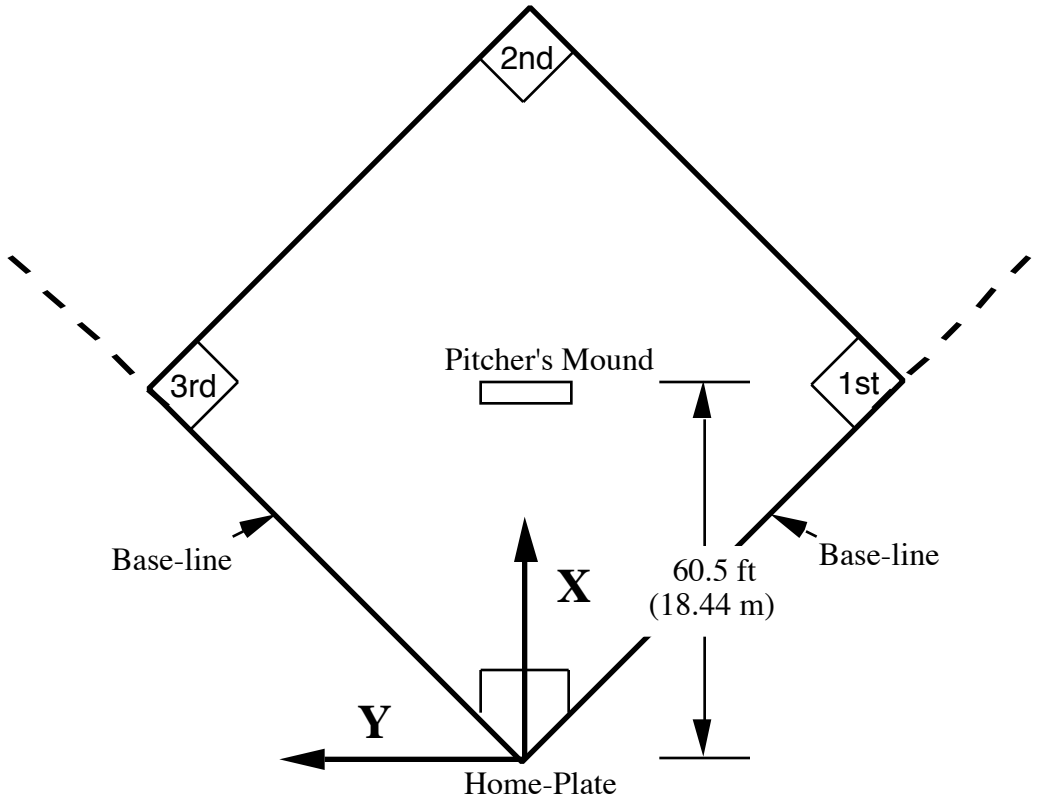

Figure 2–6: Local coordinate system. — The *x*- and *y*-axes define the horizontal plane, the *z*-axis is positive upwards and the origin is located at the intersection of the first and third base lines at home-plate.

positive *x*-axis pointed towards the mound. This results with the third-base side of the infield residing in the first quadrant. All calculations for this dissertation are based on this inertial coordinate system with all distances being represented in meters.

2.5.2 Ball Coordinate System

The ball coordinate system also will be a Cartesian system with the origin of the system located at the center of mass of the ball. The *x*- and *y*-axes are defined in such a way that a pure rotation about either of these axes will result with an ideal two-seam curve or fast-ball as shown in figure 2–7. The *z*-axis is mutually perpendicular to the *x*- and *y*-axes and a pure rotation about this axis will result in an ideal four-seam curve or fast-ball.

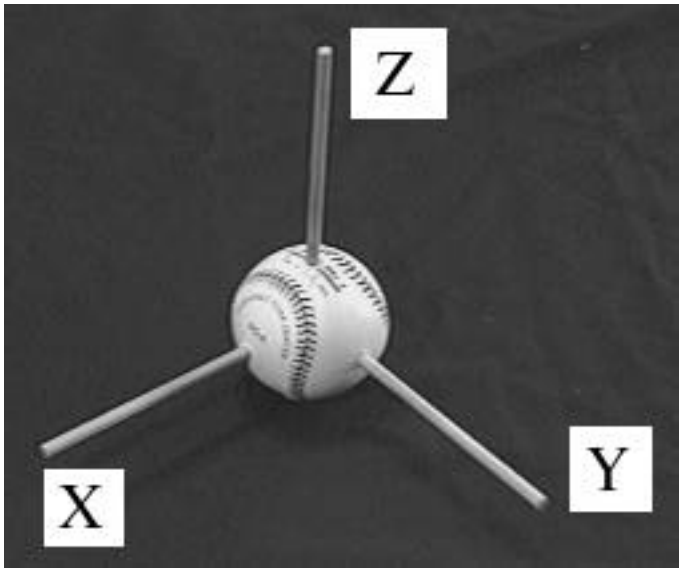

Figure 2–7: Ball coordinate system.

2.5.3 Wind Coordinate System

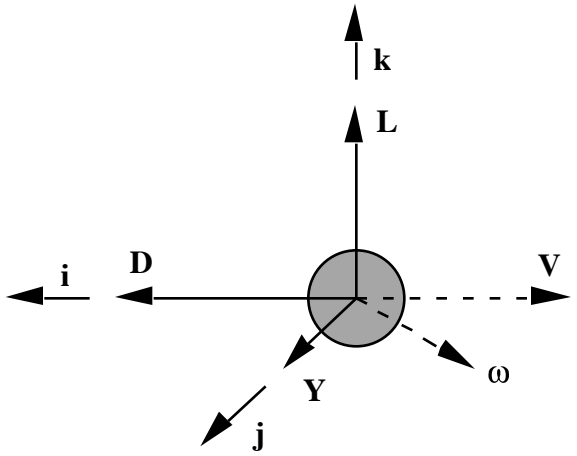

Figure 2–8: Wind coordinate system.

The wind coordinate system defines the direction of the lift, drag and cross-force components of the aerodynamic force with respect to the translational and angular velocity vectors of the ball as shown in figure 2–8. Notice that **D**, **V**, **Y** and ω all reside in the same plane. Based on figure 2–8 the total aerodynamic force equals

$$\mathbf{F}_A = D\mathbf{i} + Y\mathbf{j} + L\mathbf{k}\,. \tag{2–19}$$

2.6 Equations of Motion

Two types of trajectories are defined in the following sections. The first is for the center of mass of the ball and is entirely based on equation 2–4. The second is for trajectories of individual markers on the surface of the ball. These trajectories depend on the equations of motion for the center of mass (equation 2–4) and also include the angular velocity of the ball.

2.6.1 Center-of-Mass Trajectory

With the coordinate system established, equation 2–4 is re-written as the following expanded set of scalar differential equations,

$$m\dot{V}_x = D_x + L_x + Y_x, \tag{2–20}$$

$$m\dot{V}_y = D_y + L_y + Y_y, \tag{2–21}$$

and

$$m\dot{V}_z = D_z + L_z + Y_z + F_G. \tag{2–22}$$

Here, V_x, V_y and V_z are the x-, y-, and z-components of the velocity vector in the local coordinate frame. The lift, drag and cross-force also are transformed into their respective local coordinate frame components as follows. Equation 2–12 is first simplified by expanding the cross-product term that defines the lift component direction. This cross-product term has the component form of,

$$\omega \times \mathbf{V} = \begin{Bmatrix} V_z\omega_y - \omega_z V_y \\ V_x\omega_z - \omega_x V_z \\ V_y\omega_x - \omega_y V_x \end{Bmatrix} \tag{2–23}$$

where ω_x, ω_y and ω_z are the x-, y-, and z-components of the angular velocity vector in the local coordinate frame. Equation 2–12 is now easily expanded to[4],

$$L_x = \frac{\rho C_L A V\left(V_z\omega_y - \omega_z V_y\right)}{2\omega}, \tag{2–24}$$

---

[4] Note that V and ω without subscripts refers to the magnitude of $\mathbf{V}$ and ω, respectively.

$$L_y = \frac{\rho C_L A V (V_x \omega_z - \omega_x V_z)}{2\omega}, \tag{2–25}$$

and $$L_z = \frac{\rho C_L A V (V_y \omega_x - \omega_y V_x)}{2\omega} \tag{2–26}$$

Equation 2–13 is expanded into its respective components in the local coordinate frame as follows,

$$D_x = -\tfrac{1}{2}\rho C_D A V V_x, \tag{2–27}$$

$$D_y = -\tfrac{1}{2}\rho C_D A V V_y, \tag{2–28}$$

$$D_z = -\tfrac{1}{2}\rho C_D A V V_z \tag{2–29}$$

The cross-force direction in the local coordinate system is determined by expanding the cross product term of equation 2–14 and has the component form of,

$$\frac{\mathbf{L}\times\mathbf{D}}{|\mathbf{L}\times\mathbf{D}|} = \frac{1}{\omega V^2}\begin{Bmatrix} V_y^2\omega_x - V_x V_y \omega_y - V_x V_z \omega_z + V_z^2 \omega_x \\ V_z^2\omega_y - V_y V_z \omega_z - V_y V_x \omega_x + V_x^2 \omega_y \\ V_x^2\omega_z - V_z V_x \omega_x - V_z V_y \omega_y + V_y^2 \omega_z \end{Bmatrix}. \tag{2–30}$$

Equation 2–14 is now easily expanded to,

$$Y_x = \frac{\rho C_Y A}{2\omega}\left(V_y^2\omega_x - V_x V_y \omega_y - V_x V_z \omega_z + V_z^2 \omega_x\right), \tag{2–31}$$

$$Y_y = \frac{\rho C_Y A}{2\omega}\left(V_z^2\omega_y - V_y V_z \omega_z - V_y V_x \omega_x + V_x^2 \omega_y\right), \tag{2–32}$$

and $$Y_z = \frac{\rho C_Y A}{2\omega}\left(V_x^2\omega_z - V_z V_x \omega_x - V_z V_y \omega_y + V_y^2 \omega_z\right). \tag{2–33}$$

Combining the component-wise terms from the gravitational (equation 2–7), lift, drag and cross-force models, equation 2–4 is resolved into the following set of three first-order differential equations;

$$\dot{V}_x = \frac{\rho A V}{2m}\left[\frac{C_L}{\omega}\left(V_z\omega_y - \omega_z V_y\right) - C_D V_x + \frac{C_Y}{\omega V}\left(V_y^2\omega_x - V_x V_y \omega_y - V_x V_z \omega_z + V_z^2 \omega_x\right)\right], \tag{2–34}$$

$$\dot{V}_y = \frac{\rho A V}{2m}\left[\frac{C_L}{\omega}\left(V_x\omega_z - \omega_x V_z\right) - C_D V_y + \frac{C_Y}{\omega V}\left(V_z^2\omega_y - V_y V_z \omega_z - V_y V_x \omega_x + V_x^2 \omega_y\right)\right], \tag{2–35}$$

and

$$\dot{V}_z = \frac{\rho A V}{2m}\left[\frac{C_L}{\omega}\left(V_y\omega_x - \omega_y V_x\right) - C_D V_z + \frac{C_Y}{\omega V}\left(V_x^2\omega_z - V_z V_x\omega_x - V_z V_y\omega_y + V_y^2\omega_z\right)\right] - g\,. \quad (2\text{–}36)$$

To determine the position of the ball, the solutions to these three (Eqs. 2–34, 35, 36) first-order velocity differential equations will be integrated, implying that an additional set of three first-order kinematic differential equations are needed;

$$\dot{x} = V_x, \quad (2\text{–}37)$$

$$\dot{y} = V_y, \quad (2\text{–}38)$$

and $$\dot{z} = V_z. \quad (2\text{–}39)$$

Thus, in all, six first-order differential equations are used to model the trajectory of the center of mass of a baseball.

2.6.2 Marker Trajectories

In addition to knowing the position of the ball's center of mass, information about the ball's angular velocity is desired. This information is obtained by tracking markers on the ball's surface. The location of the markers must be modeled and this is accomplished by adding the surface rotation to the center-of-mass trajectory. In effect, the trajectories of markers on the ball are modeled by a translation of, and rotation about, the center of mass of the ball in flight. The method, therefore, to model these surface trajectories will consist of using the equations of motion derived in the previous section for the translation of the center of mass and then superimposing the rotational motion of individual markers located on the ball's surface.

This rotational motion is modeled with the following equation describing the motion of a point in a body due to a simple rotation of the body about an axis passing through the center of the body (Kane, Likins, and Levison, 1983),

$$\mathbf{a}^* = \mathbf{a}\cos(\psi) - \mathbf{a}\times\hat{\mathbf{c}}\sin(\psi) + \mathbf{a}\cdot\hat{\mathbf{c}}\cdot\hat{\mathbf{c}}(1-\cos(\psi)) \quad (2\text{–}40)$$

where here $\mathbf{a}$ is the initial (before rotation) vector to the marker being rotated, $\mathbf{a}^*$ is the vector to the final rotated position, $\hat{\mathbf{c}}$ is a unit vector defining the axis of rotation, and ψ is the rotation angle about $\hat{\mathbf{c}}$ as seen in figure 2–9. Note that vectors $\mathbf{a}$, $\mathbf{a}^*$ and $\hat{\mathbf{c}}$ are with respect to the ball-coordinate system. The marker trajectory is modeled on a frame-by-frame and marker-by-marker basis by assuming the marker location in the initial frame is given by $\mathbf{a}$, that $\hat{\mathbf{c}}$ is a unit vector parallel to the axis of rotation of the angular velocity vector, and ψ is the rotation experienced over a one-frame period by the ball. The position of $\mathbf{a}$ in the next frame is the value of $\mathbf{a}^*$ determined from equation 2–40 for the previous frame. This is repeated for each frame until the entire trajectory is determined for each marker. Once the rotational motion is determined for each marker it is superimposed onto the center-of-mass trajectory in the following manner,

$$\mathbf{p}_{ji} = \mathbf{p}_{Gi} + \mathbf{a}^*_{ji} \tag{2–41}$$

where $\mathbf{p}_{ji}$ is the position of the *j*th marker in the *i*th frame in the local coordinate system, $\mathbf{p}_{Gi}$ is the center of mass position in the *i*th frame, and $\mathbf{a}^*_{ji}$ is *j*th marker position in the *i*th frame in the ball-coordinate system. In effect, equation 2–40 is an algebraic vector equation that can be used to determine the location of the markers on the ball from frame-to-frame.

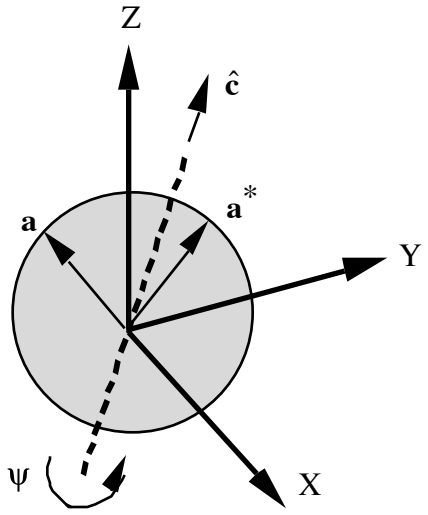

Figure 2–9: Definition of simple rotation.

In all, six first-order differential equations (equations 2–34 to 2–39) and one algebraic vector equation (equation 2–40) are used to model the trajectory of markers on the

surface of a baseball. These equations are the basis for the parameter estimation routine described in the chapter 4, and are the key to understanding how angular velocity affects the baseball trajectory.

CHAPTER 3 – DATA ACQUISITION

Using the models defined in chapter 2, theoretical trajectories of the center of mass and of markers on the ball can be determined. It will be shown in chapter 4 that using these predicted trajectories with accurately measured trajectories of the corresponding points on the ball, allows the initial conditions and other trajectory dependent parameters to be estimated. The success of this dissertation, therefore, relies in the definition of the models and the accurate acquisition of the trajectories of markers produced by a spinning thrown baseball.

In the previous studies on baseball trajectories by *Life*[1], *Look* (Cohane, 1949), Selin (1957), and Miller, Walton & Watts (Allman, 1982), high-speed or strobe photography was used to acquire images of the ball in flight. In the 1953 *Life*[2] investigation a half-white/half-black ball was used to determine a qualitative value for the spin rate. Selin and Alaways & Lightfoot (1998) obtained a qualitative assessment of spin by examining the seams on the ball from frame-to-frame. No previous work has been done to actually measure the position of markers on the ball while in flight. The following sections describe the video data acquisition system, its accuracy, and how the system was set-up to measure, as accurately as possible, the experimental data. Also included in the following sections is a description of the trials and data recorded during the experimental phase of this study.

3.1 Video Data Acquisition

The concept behind video data acquisition is that highly accurate three-dimensional positions of objects in motion can be determined in a non-invasive manner. This is achieved by using two or more high-speed high-resolution video cameras with over-

---

1 Baseball's Curve Balls: Are They Optical Illusions (1941); Camera and Science Settle the Old Rhubarb About Baseball's Curve Ball (1953)

2 Camera and Science Settle the Old Rhubarb About Baseball's Curve Ball (1953)

lapping fields-of-view. If high-contrasting markers are placed on the object, a video digitizer can automatically digitize the markers in question with very little human intervention. Software reconstructs the three-dimensional position of the markers from the two-dimensional images captured on each camera. The reconstruction is easily described as a simple triangulation of individual vectors originating from the two or more cameras and is known as the Direct Linear Transformation (DLT) (Abdel-Aziz and Karara, 1971).

The accuracy of such a system is dependent on many variables including lighting, marker size, fields-of-view, lens distortion and camera calibration. Here camera calibration means the determination of lens-specific parameters along with the camera's location and orientation with respect to the local coordinate frame using the inverse DLT. Camera calibration is a key factor in the ability to triangulate on a marker's position. It is because of the non-invasive nature of video data acquisition and the recent automation advances in the hardware and software, that this method was chosen for the experimental phase of this study.

3.2 Experimental Setup

The data-acquisition system was a ten-camera, high-speed, high-resolution MotionAnalysis system. The experiments were conducted at the MotionAnalysis Corporation indoor demonstration facilities in Santa Rosa, California. Two different experiments were conducted, the first with inexperienced and collegiate pitchers and the second using an Athletic Training Equipment Company (ATEC) pitching machine. The following sections describe and detail the layout of the experiments, explain the hardware and software used, outline the methods of calibration, and explain the locations of the markers on the balls.

3.2.1 Experiments

Two different tests were conducted, the first with pitchers and the second, in a more controlled setting, with a pitching machine. The second experiment was performed when it was determined that human pitchers were too random in their release position, that a mistake had occurred in the original camera calibration and that the marker arrangement used was too complicated to achieve the desired results. Note that because of these mistakes only center-of-mass trajectory data could be reconstructed in the first set of experiments.

3.2.1.1 Pitchers

In the first series of tests to measure spin and trajectory data, three pitchers threw the ball. The test subjects included[3], T, a Major League hopeful and former UC Davis pitcher, and two inexperienced throwers, M and S. A pitching mound, with Major League Baseball specifications was constructed and regulation 60.5 ft (18.44 m) pitches were thrown.

3.2.1.2 Pitching Machine

In the second series of tests, an ATEC pitching machine[4], seen in figure 3–1, was used to throw the ball. This pitching machine is designed with two variable-speed spinning wheels to introduce top- or back-spin on the ball in a direction roughly perpendicular to the velocity vector. The machine was set up 55 ft (16.73 m) from home-plate to simulate the release point of an actual pitcher and configured to throw only fast balls and curve balls (i.e., with the angular velocity vector directed towards the *y*-axis).

---

3 Trials, data and results in this study will be denoted by a pitch identification number based on the subjects first initial. For example, T7 will represent the seventh pitch by subject T.

4 The pitch identification number for pitching machine pitches will be based on the orientation of the ball's seams when fed into the machine. For example, P2S3 will denote the third pitch in the two-seam orientation for the pitch machine. Likewise, P4S5 will represent the fifth pitch in the four-seam orientation.

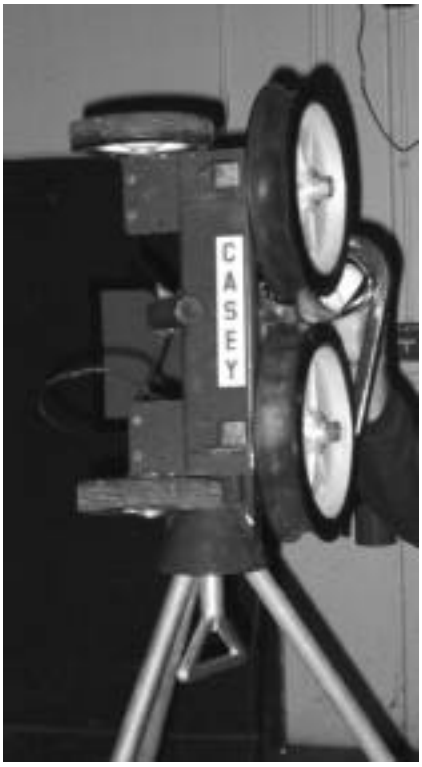

Figure 3–1: ATEC pitching machine.

3.2.2 Data-Acquisition Hardware

A MotionAnalysis ExpertVision 3D EVa HiRES system was used for the data acquisition. This system was based on ten 240-Hz MotionAnalysis FALCON cameras with red LED synchronized strobe lighting as seen in figure 3–2. Each camera has 648 (horizontal) × 240 (vertical) pixel resolution and were operated at shutter speeds of 1/2000 and 1/1000 sec for the pitchers and pitching machine trials, respectively. A MotionAnalysis video processor with internal digitizing resolution of 4096 × 4096 pixels digitized the raw data. The system was controlled with a SUN/SPARC workstation operating under the Solaris common desktop environment.

3.2.3 Data-Acquisition Software

The MotionAnalysis EVa software version 4.64 was used to synchronize the video cameras, and to perform calibration, tracking and editing of the acquired data sets. The EVa software transforms two-dimension camera data into three-dimension coordinate images via

dynamic ray tracking with proprietary “best fit” and per-camera noise rejection algorithms. MotionAnalysis 1997 specifications show that with the hardware described above and with their EVa software, static system accuracy is as high as 1/60,000 and dynamic accuracy is 1/35,000 of the field-of-view.

Figure 3–2: MotionAnalysis FALCON camera.

3.2.4 Camera Layout

As mentioned in section 3.2.2, ten cameras were utilized to acquire data. The basic concept behind three-dimensional track reconstruction is that at least two cameras view the object or marker in question at all times. Since synchronized spin and trajectory information from the same pitch is needed to verify the results, it was decided that six or seven cameras would track markers on the ball over the first four feet (1.22 m) of flight and the remaining cameras would track the ball’s trajectory as it passed over home plate. From the lessons learned from the pitcher experiments, a different camera layout was employed during the pitching machine tests. Both of these camera layouts are described in the following sections.

3.2.4.1 Pitchers

The top view of the camera layout for the pitcher tests is shown in figure 3–3 and a side view of the mound cameras only is shown in figure 3–4. The concept behind this camera layout was that by surrounding the calibrated control volume at the mound, all nine of circumferentially placed markers on the ball could be tracked immediately after the ball was released. The remaining four cameras were arranged to track the entire ball as a single object over the last 46 ft (14 m) of the trajectory.

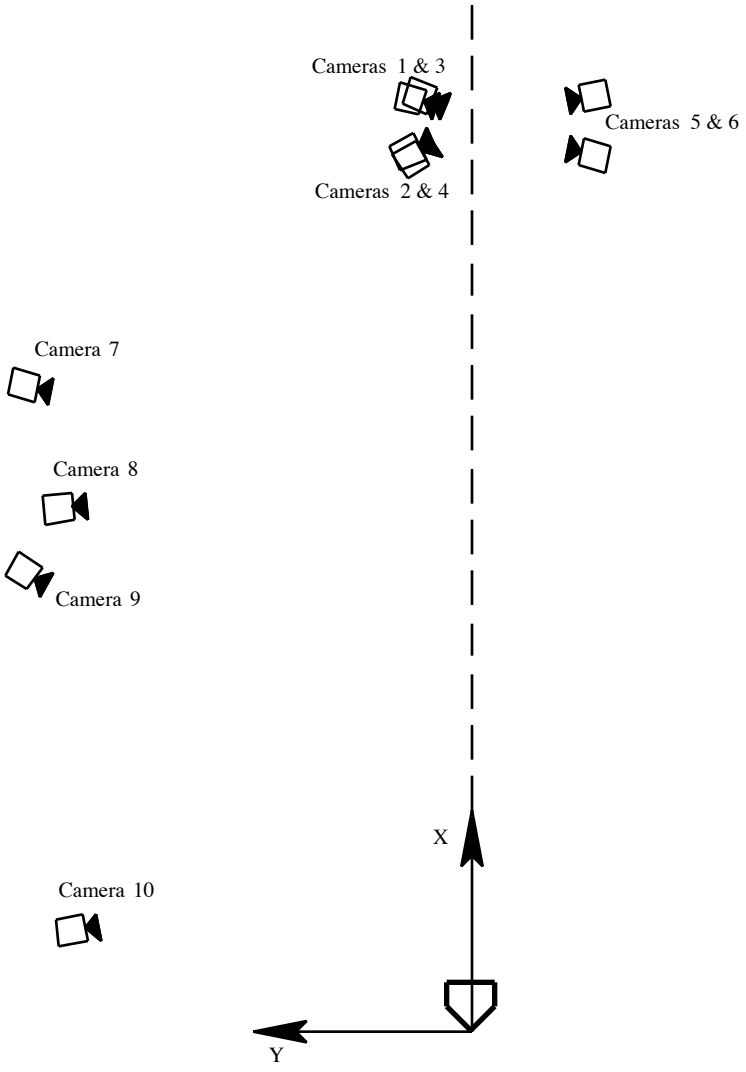

Figure 3–3: Top view of camera layout for the pitcher trials.

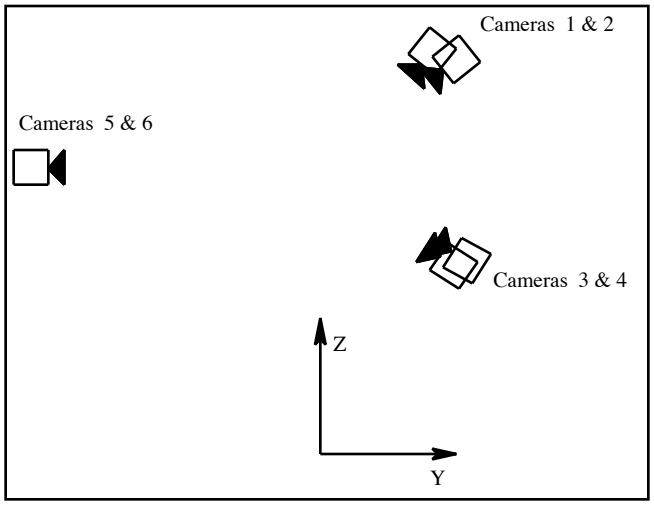

Figure 3–4: Side view of mound camera layout for the pitcher trials.

Table 3–1 lists the camera locations in the local coordinate frame (determined from the camera calibration described in section 3.2.5) and gives the associated lens type for each camera. Notice that the locations for camera 5 and 6 are estimates since calibration errors occurred with these cameras and their location is not precisely known (see section 3.2.5). Since the trajectory of the center of mass of the ball was of interest, additional 5000 Watt flood lamps, as shown in figure 3–5, were placed adjacent to cameras 7, 8, 9 and 10 to help with marker contrast.

Figure 3–5: Lighting arrangement used in center-of-mass trajectory measurements.

Table 3–1: Camera locations and lens type for the pitcher trials.
(The locations for cameras 5 and 6 are estimated.)

Camera	X – location; ft (m)	Y – location: ft (m)	Z – location; ft (m)	Lens – (mm)
1	55.64 (16.959)	2.40 (0.730)	9.48 (2.889)	8
2	52.53 (16.010)	2.94 (0.897)	9.28 (2.828)	6
3	55.53 (16.926)	2.86 (0.873)	4.76 (1.451)	6
4	52.86 (16.113)	3.15 (0.960)	4.87 (1.485)	6
5	52.5 (16.0)	-6.5 (-1.981)	7.0 (2.14)	12.5
6	55.75 (16.99)	-6.5 (-1.981)	7.0 (2.14)	12.5
7	38.39 (11.701)	26.01 (7.927)	3.10 (0.945)	6
8	31.29 (9.536)	23.81 (7.256)	6.17 (1.882)	8
9	27.07 (8.250)	26.18 (7.980)	9.99 (3.045)	8
10	6.07 (1.851)	23.19 (7.067)	5.65 (1.723)	6

3.2.4.2 Pitching Machine

After processing the data from the pitching tests it was determined that additional experiments were necessary. For these experiments a pitching machine threw the ball and only one hemisphere of the ball was marked and tracked (see section 3.2.6.2). The camera layout utilized seven cameras to track the markers on the ball at release and the remaining three cameras focused on the last 13 ft (3.96 m) of flight as shown in figure 3–6. Figure 3–7 shows a photo of the camera layout at the pitching mound and table 3–2 lists the locations and lens type of each camera in the local coordinate frame.

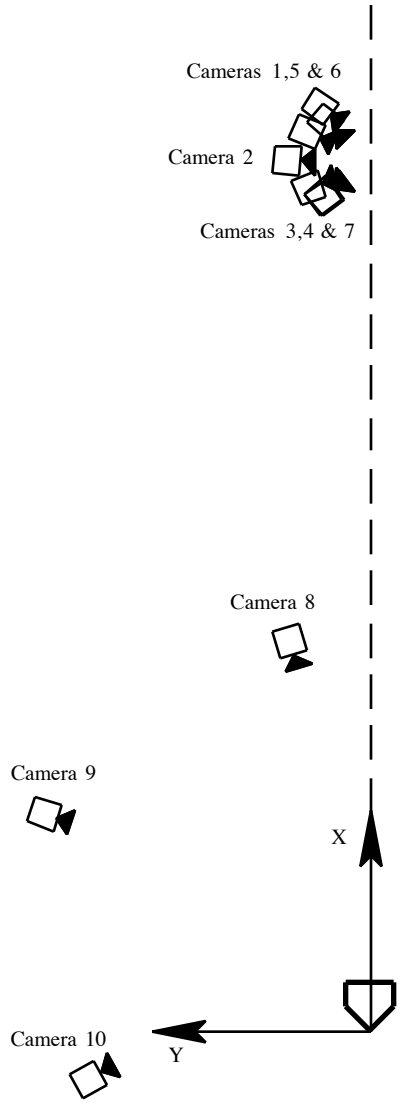

Figure 3–6: Top view of camera layout for the pitching machine trials.

Figure 3–7: Mound camera layout for pitching machine trials.

Table 3–2: Camera locations and lens type for pitching machine trials.

Camera	X – location; ft (m)	Y – location; ft (m)	Z – location; ft (m)	Lens – (mm)
1	53.49 (16.303)	2.98 (0.909)	6.65 (2.026)	6
2	52.09 (15.876)	4.15 (1.264)	6.57 (2.003)	6
3	50.70 (15.454)	2.89 (0.882)	6.54 (1.994)	6
4	50.46 (15.380)	2.23 (0.680)	4.08 (1.245)	6
5	53.84 (16.410)	2.06 (0.627)	4.17 (1.270)	6
6	54.69 (16.669)	2.37 (0.722)	9.16 (2.792)	6
7	50.33 (15.340)	2.10 (0.641)	9.04 (2.755)	6
8	22.50 (6.858)	4.51 (1.376)	4.88 (1.487)	12.5
9	12.73 (3.881)	18.76 (5.717)	3.35 (1.022)	8
10	-2.48 (-0.755)	16.14 (4.920)	5.15 (1.569)	8

3.2.5 Calibration

In order to reconstruct the three-dimensional position of an object from two-dimensional images captured with each camera, the location and orientation of each camera must be known. Additionally, for accurate reconstruction to be achieved a lens distortion map is needed for each lens. The determination of the locations, orientation and lens distortion maps are all accomplished using the following two-step procedure.

The first step in calibration is the determination of the six camera parameters that show the position and orientation angles of the camera in the local coordinate system. These camera parameters are determined from solving the inverse DLT problem of Abdel-Aziz and Karara (1971). In this method six or more non-coplanar control points are filmed and digitized by each camera. The inverse DLT is then solved for 11 parameters which contain the position and orientation of each camera. This procedure is called "cube calibration" in the MotionAnalysis ExpertVision software. The remaining five parameters determined by the inverse DLT are lens parameters which are improved upon by the second step in calibration, the "wand calibration."

Wand calibration produces a detailed lens distortion map for each lens/camera pair and updates all 11 DLT parameters determined in the cube calibration. Wand calibration is performed by passing a wand of known length through the control volume. The ExpertVision software then tracks three points on the wand and, using an iterative technique, creates the lens distortion map and updates the DLT parameters such that the wand has a constant three-dimensional length when reconstructed with three or more cameras. Great care must be taken to sweep the entire control volume in order to generate an accurate and complete distortion map, as an aid the EVa software displays the calibrated volume after the wand calibration is completed.

Because of the demand that synchronous spin and trajectory data be acquired for each pitch and the resulting unique camera layout, two distinct camera calibrations were conducted for each experiment. Different cubes and wands were used in each calibration to

maximize the accuracy of the data acquisition. The home plate calibration defined the local calibration system. In doing so great care was used to place the second "cube" at the mound to insure that its position and orientation were correct in the local coordinate system. The following sections describe the calibration methods for the pitcher and pitching machine experiments.

3.2.5.1 Cube Calibration

3.2.5.1.1 Home Plate

Pitchers

Figure 3–8 shows the cube calibration set-up for the home-plate portion of the pitcher trials. In this set-up a calibration cube supplied by MotionAnalysis with eight retro-reflective spherical control points was employed to define the local coordinate system origin location and axis directions; the cube is shown on the right in figure 3–8. The location of the eight control points are known to within 0.0264 in (0.0067 mm) as certified by the U.S. Bureau of Weights and Measures. Twelve additional control points were placed on both sides of the x-axis along the trajectory path to insure that at least six control points

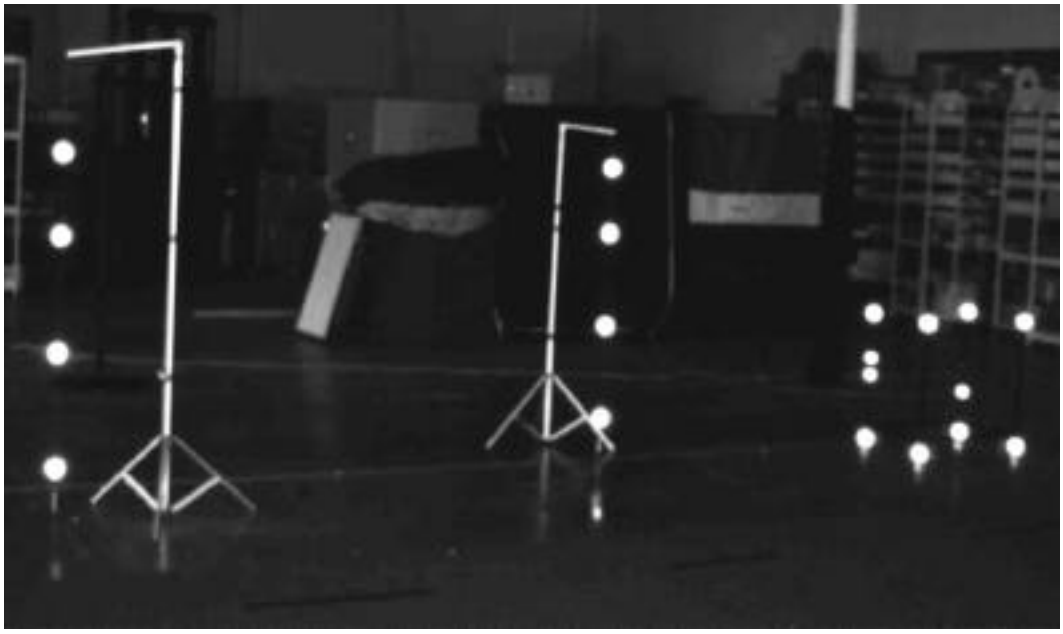

Figure 3–8: Cube calibration set-up for the home-plate portion of pitcher trials.

could be seen by all cameras. These control points were measured by hand to an accuracy of 0.125 ± 0.031 in (0.318 ± 0.079 cm) and eight control points are shown to the left in figure 3–8.

Pitching Machine

Figure 3–9 shows the calibration cube used for the home plate portion of the pitching machine trials. This cube was supplied by MotionAnalysis and uses eight retro-reflective spherical control points to define the local coordinate system origin and axis directions. The location of the eight control points are known to within 0.0264 inches (0.0067 mm) as certified by the U.S. Bureau of Weights and Measures.

Figure 3–9: Calibration cube for home-plate portion of pitching machine trials.

3.2.5.1.2 Mound

Figure 3–10 shows the "cube" calibration apparatus set-up for both the pitcher and pitching machine trials. This apparatus was constructed at UC Davis using 28 spherical control points. The center of each control point was determined to within 0.0012 inches (0.003 cm) using a Mitutoyo Bright 540 coordinate measuring machine. Selective spheres were coated with 3M retro-reflective tape to insure high contrasting control points. The apparatus was mounted on a four degree-of-freedom tripod and levels were attached to each end to insure proper pitch and roll. Two plumb bobs were hung from each end for yaw alignment.

Figure 3–10: Calibration apparatus for mound control volume.

In the pitcher experiments only nine markers were covered with the 3M retro-reflective tape. Because of this oversight, cameras 5 and 6 could only digitize six control points that were almost all in the same plane. This resulted in very poor results in the cube calibration and made cameras 5 and 6 useless in the data acquisition. However, this problem was not found until two weeks after the pitcher experiments were completed. It was corrected by coating an additional 10 control points with retro-reflective tape before the pitching machine trials were conducted.

3.2.5.2 Wand Calibration

3.2.5.2.1 Home Plate

Figure 3–11 shows the wand used in the wand calibration of the home plate control volume for the pitcher and pitching machine trials. This wand was supplied by Motion-

Figure 3–11: Calibration wand for home-plate control volume.

Analysis and had spherical control points placed on each end 59.05 inches (1.5 m) apart. The third control point between the two end spheres is used only to distinguish which end is which.

3.2.5.2.2 Mound

Figure 3–12 shows the wand used for to calibrate the control volume at the mound for all trials. This wand uses two spherical control points place on the ends of the wand 4.8 inches (0.122 m) apart. The third control point is used only to distinguish which end is which.

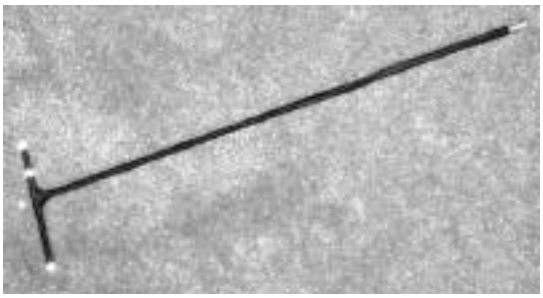

Figure 3–12: Calibration wand for mound control volume.

3.2.6 Ball Markers

The power of the MotionAnalysis system to handle ten cameras at 240-Hz lies in the video processor's ability to automatically threshold the image to a specific gray-scale. The basic concept of thresholding is fairly simple. Pixels that are black are given the value 0, white pixels are assigned 1023, and the various shades of gray lie in-between 0 and 1023. The user sets the value of threshold desired, for example 200, and then the video processor compares each pixel's gray-scale value with the threshold. If the pixel is darker than the threshold or less than 200, it is set to 0, if brighter or greater than 200, it is set to 1. With this in mind, it is easy to see that any marker or object that is in high contrast to the surrounding environment can, with the correct threshold, be automatically distinguished and digitized. In this case bright markers are ideal targets since the ball is already white and contrasts with the background.

The ball markers were made from 3M retro-reflective tape which reflects light back towards its source. Since each camera was equipped with ring lights, the signal back from the retro-reflective tape towards the camera is more intense than that from the ball or background. For the trajectory measurements, the background was covered with black cloth and additional lighting was supplied so that the ball itself would be significantly brighter than the surrounding environment. For each series of tests, different ball marker configurations were chosen and are presented below.

3.2.6.1 Pitchers

Figure 3–13 shows the configuration of the markers for the pitcher experiments. Eight 0.437 inch (1.11 cm) markers were placed circumferentially around the ball with an additional larger 1.0 inch (2.54 cm) marker placed 90 degrees out of plane with these markers. The larger marker was designed as an aid in helping to identify which side of the ball was being digitized.

Figure 3–13: Marker location for pitcher trials.

3.2.6.2 Pitching Machine

3.2.6.2.1 Two-Seam Trials

Figure 3–14: Marker locations for pitching machine tests. The ball on the right was used for the two-seam trials and the ball on left for the four-seam trials.

Figure 3–14 shows the marker configuration used for the two-seam pitching machine tests. Four 0.375 inch (0.953 cm) markers were placed in the shape of "λ" so that easy identification would be made possible. The marker positions were determined using a Mitutoyo Bright 540 coordinate measuring machine with a precision of 0.0394 inches (1 mm). Table 3–3 gives the azimuth and elevation angles of these markers in the ball coordinate frame. The definitions of the azimuth and elevation angles will be given in chapter 4.

Table 3–3: Marker azimuth and elevations angles for the two-seam pitching machine trials in the ball coordinate frame.

Marker Number	Azimuth – Deg	Elevation – Deg.
1	29.25	11.24
2	–33.82	11.49
3	–3.44	–7.89
4	26.62	–31.12

3.2.6.2.2 Four-Seam Trials

Figure 3–14 also shows the marker configuration for the four-seam pitching machine tests. Again, four 0.375 inch (0.953 cm) markers were used in the shape of "λ" so that easy identification would be made possible. The marker positions were then determined using a Mitutoyo Bright 504 coordinate measuring machine. Table 3–4 gives the azimuth and elevation angles of these markers in the ball coordinate frame.

Table 3–4: Marker azimuth and elevations angles for the four-seam pitching machine trials in the ball coordinate frame.

Marker Number	Azimuth – Deg	Elevation – Deg.
1	–59.12	61.00
2	63.13	63.05
3	–172.91	80.54
4	–137.05	48.16

3.3 Experimental Trials

All experimental trials were conducted at the MotionAnalysis indoor demonstration facility in Santa Rosa, California. This facility is located at latitude 38° 32' 42" North with a elevation of 50 ft (15.24 m). The ambient air temperature during both experiments was 50 ˚F (10 ˚C). This facility is completely enclosed and no noticeable air disturbances could be detected. The throwing phase of the experiments was conducted immediately after the cameras were calibrated to insure that no cameras were moved or changed in any way before data could be collected. During the pitching experiment, comments on the pitch were recorded for later comparison.

3.3.1 Pitchers

Three pitchers were used during the pitcher experiments. The first subject, T, was major league hopeful and former UC Davis standout, Tony Dellamano. The latter two subjects, M and S, were my inexperienced colleagues, Mike "Fast Ball" Hendry and Sean "Curve Ball" Mish. In all 47 pitch trajectories were acquired for pitcher T and his

comments were recorded as noted in table A–1 in Appendix A. Additionally 5 and 6 pitch trajectories were acquired for pitcher M and S, respectively, though no written comments were recorded.

3.3.2 Pitching Machine

Two series of trials were conducted during the pitching machine experiments. These trials were based on ball seam orientation and pitching machine speeds. Only two- and four-seam ball orientations were used (as mentioned in section 3.2.6). The pitching machine had individual speed control for each spinning wheel as shown in figure 3–15, and therefore only fast (back-spin), curve (top-spin) and knuckleball (no spin) data could be acquired without significant changes to the camera locations. Tables A–2 and A–3 in Appendix A lists the pitch numbers and wheel speeds for each pitching machine trial.

Figure 3–15: Pitching machine speed control.

3.4 Camera Images

Figure 3-16 shows an eight frame video sequence of a pitch, recorded on camera 2 in the pitching machine trials setup, using a 240 Hz VCR manufactured by MotionAnalysis. These images show an approximate 36 degree rotation of the ball per frame resulting in a spin rate of 24 rev/sec, and that the spin axis is directed away from camera 2 along the negative *y*-axis.

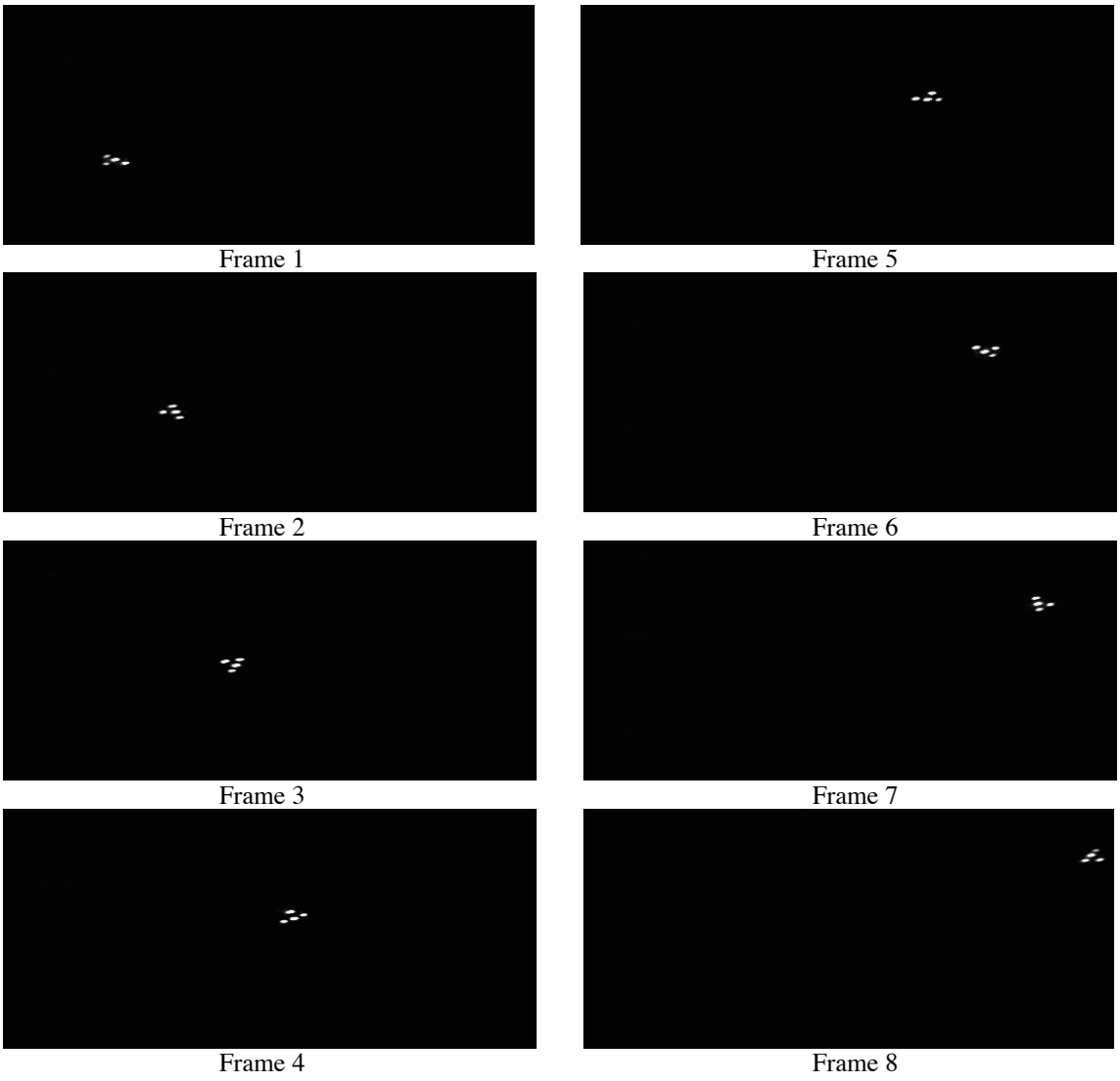

Figure 3–16: Representative frame-by-frame video images of a pitching machine trial.

CHAPTER 4 – PARAMETER ESTIMATION

The major objective of this study is the determination of the initial conditions and the corresponding outcome of a pitched baseball. This is accomplished by measuring the center of mass positions of the ball, individual marker locations on the ball, or both markers and center of mass positions. Once the position data is acquired and the best possible model is developed, the initial conditions and other non-coupled parameters can be estimated. This chapter details the parameter estimation procedure describes the parameters estimated, and gives an accuracy assessment of the estimated routine's robustness by means of testing with fictitious data. For a better understanding of the parameters the following definitions are presented here.

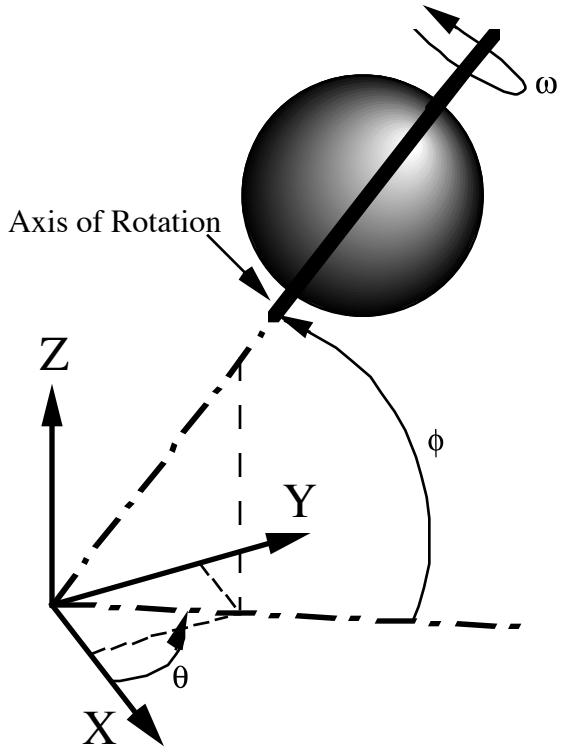

Figure 4–1: Definition of the angular velocity azimuth and elevation angles.

Angular Velocity Vector: The angular velocity vector is defined in terms of its direction and magnitude. The direction is given by the vector parallel to the axis of rotation originating from the local coordinate system origin and is defined in terms of its azimuth and elevation angles. The azimuth angle, θ, is measured from the x-axis to the projection of the axis of rotation onto the xy-plane and the elevation angle, ϕ, is

measured from the *xy*-plane projection to the axis of rotation as shown in figure 4–1. The magnitude of the angular velocity vector is the spin rate that is experienced by the ball about the axis of rotation.

Initial Orientation: The initial orientation describes how the ball's coordinate system at release is related to the local coordinate system. The orientation is the result of a simple rotation, in the local coordinate system, of the ball from a hypothetical unperturbed original state, in which the ball coordinate system and the local coordinate system are aligned so that corresponding axes are parallel. This simple rotation occurs about the *initial orientation direction*, characterized in the same manner as the angular velocity vector, but with α_0 and β_0 used to represent the azimuth and elevation angles, respectively. Instead of spin rate, the magnitude of the rotation is defined as the initial rotation, ψ_0, about the initial orientation direction.

Marker Position: Marker position defines the location on the surface of the ball where reflective markers are placed. These marker positions are defined by an azimuth and elevation angle, γ_j and λ_j, respectively for the *j*th marker, but in the ball coordinate system as shown in figure 4–2. The marker positions used for the pitching machine trials are given in tables 3–3 and 3–4.

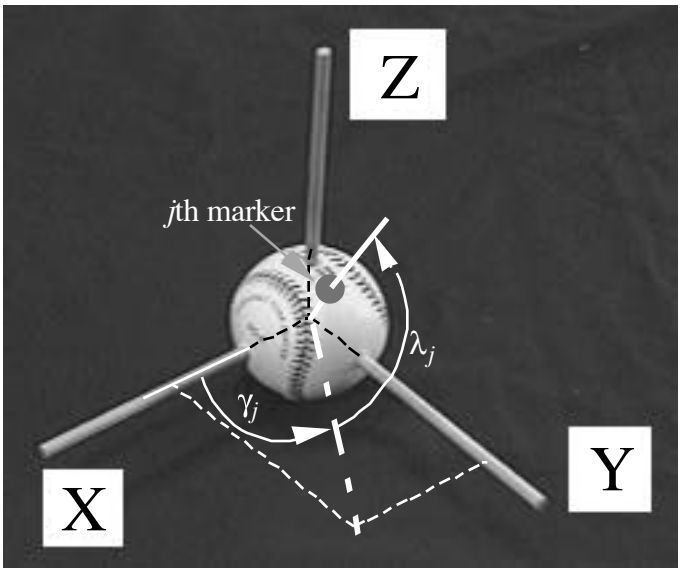

Figure 4–2: Definition of marker azimuth and elevation angles.

4.1 The Estimation Problem

As mentioned previously in chapter 2, there are two different types of trajectories that are of interest; the center-of-mass trajectory and the trajectories of markers on the ball's surface. If complete knowledge of the atmosphere is known, both of these trajectories depend uniquely on the position, translational velocity, angular velocity and orientation of the ball at the instant of release. Therefore the *i*th center of mass position of the ball can be written in a functional form as,

$$\left[x_i^{\mathrm{p}}, y_i^{\mathrm{p}}, z_i^{\mathrm{p}}\right] = \left[x_i^{\mathrm{p}}, y_i^{\mathrm{p}}, z_i^{\mathrm{p}}\right]\left(x_0, y_0, z_0, \dot{x}_0, \dot{y}_0, \dot{z}_0, \theta, \phi, \omega_0, \alpha_0, \beta_0, \psi_0\right) \tag{4–1}$$

where; x^{p}, y^{p}, and z^{p} are predicted values of x, y, and z using estimated initial conditions. , The trajectories of markers on the ball depend additionally on their position with respect to the ball's reference frame. Therefore, the *i*th position of the *j*th marker on the ball can be written in a functional form as,

$$\left[x_{ij}^{\mathrm{p}}, y_{ij}^{\mathrm{p}}, z_{ij}^{\mathrm{p}}\right] = \left[x_{ij}^{\mathrm{p}}, y_{ij}^{\mathrm{p}}, z_{ij}^{\mathrm{p}}\right]\left(x_0, y_0, z_0, \dot{x}_0, \dot{y}_0, \dot{z}_0, \theta, \phi, \omega_0, \alpha_0, \beta_0, \psi_0, \gamma_j, \lambda_j\right). \tag{4–2}$$

In either case the outputs of equations 4–1 and 4–2 are predicted values of x, y, and z using estimated initial conditions and these predicted values are the basis for estimating the initial conditions of a pitch.

In all estimation procedures a performance index indicating how well the estimated data corresponds to the measured data is needed. For this dissertation the performance index, R, is defined as the square root of the residual sum of squares of position uncertainties,

$$R = \sqrt{\frac{\left(\mathbf{x}^{\mathrm{p}} - \mathbf{x}^{\mathrm{m}}\right)^{\mathrm{T}}\left(\mathbf{x}^{\mathrm{p}} - \mathbf{x}^{\mathrm{m}}\right) + \left(\mathbf{y}^{\mathrm{p}} - \mathbf{y}^{\mathrm{m}}\right)^{\mathrm{T}}\left(\mathbf{y}^{\mathrm{p}} - \mathbf{y}^{\mathrm{m}}\right) + \left(\mathbf{z}^{\mathrm{p}} - \mathbf{z}^{\mathrm{m}}\right)^{\mathrm{T}}\left(\mathbf{z}^{\mathrm{p}} - \mathbf{z}^{\mathrm{m}}\right)}{3N}} \tag{4–3}$$

where; $\mathbf{x}^{\mathrm{p}}$, $\mathbf{y}^{\mathrm{p}}$ and $\mathbf{z}^{\mathrm{p}}$ are the N vectors of predicted values of x, y and z, respectively and $\mathbf{x}^{\mathrm{m}}$, $\mathbf{y}^{\mathrm{m}}$ and $\mathbf{z}^{\mathrm{m}}$ are the N vectors of measured values of x, y and z, respectively. Here N is the total number of frames in the acquired data set for the center-of-mass trajectory, for trajectories of markers on the ball, N is the product of the number of markers and the

number of frames acquired at release plus the number of center-of-mass frames as the ball passes over home-plate. Notice that R can be written as,

$$R = \sqrt{\frac{\sum_{i=1}^{3N} f_i^2}{3N}} \tag{4–4}$$

where $\mathbf{f}$, the error, or residuals, between the measured and estimated data, is the $3N$ vector defined by,

$$\mathbf{f} = \begin{Bmatrix} x_1^p - x_1^m \\ \cdots \\ \cdots \\ \cdots \\ x_N^p - x_N^m \\ \hline y_1^p - y_1^m \\ \cdots \\ \cdots \\ \cdots \\ y_N^p - y_N^m \\ \hline z_1^p - z_1^m \\ \cdots \\ \cdots \\ \cdots \\ z_N^p - z_N^m \end{Bmatrix}. \tag{4–5}$$

Using equation 4–4 as the performance index has the additional benefit that R is the standard deviation of $\mathbf{f}$ when the mean of $\mathbf{f}$ is zero.

The minimization of R through the choice of the initial conditions is the classical nonlinear least-squares estimation problem which will result in the estimation of the initial conditions and other aerodynamic parameters of the baseball. The estimation procedure to solve this problem is a modified version of the method presented for the estimating release conditions for the javelin throw by Hubbard and Alaways (1989) and is summarized in the following sections.

4.2 Parameter Lists

Since the primary goal of this study was to determine the initial conditions and key aerodynamic parameters associated with a pitch and, as mentioned in previous chapters, involves two different type of data sets, two sets of parameters will be estimated depending on which type of data is available. For example, when only center-of-mass trajectory data is measured, information about the initial ball orientation and angular velocity direction is not available and thus estimating these parameters is not feasible. Also depending on the data set certain assumptions are made concerning the characteristics of the pitch that are reflected in each parameter set. These assumptions and the resulting parameter lists are given below.

4.2.1 Center-of-Mass Trajectory

When only center-of-mass trajectory data is available for the estimation routine the following four assumptions are made:

1. The two extrapolated two- and four-seam lift coefficient lines in figure 2–4 are valid and the spin rate is such that the spin parameter is bounded by these lines.
2. The azimuth angle of the angular velocity vector is always perpendicular to the translational velocity vector.
3. The drag coefficient is constant.
4. Lift is defined as the total force component perpendicular to the drag component (i.e. lift is the vector sum of the lift and cross-force components defined in chapter 2.)

The desire to know the initial conditions of the pitch and the drag coefficient, compounded with the above assumptions results with the following set of parameters that will be estimated from the acquired center-of-mass trajectories:

x_0 – Initial x position.

y_0 – Initial y position.

z_0 – Initial z position.

$\dot{x}_0$ – Initial x velocity.

$\dot{y}_0$ – Initial y velocity.

$\dot{z}_0$ – Initial z velocity.

ϕ – Elevation angle of the angular velocity vector.

C_L – Lift coefficient.

C_D – Drag coefficient.

These initial conditions and C_D make up the parameter vector, **p**, used in the parameter estimation routine described in the following section and is given by,

$$\mathbf{p} = \{x_0, y_0, z_0, \dot{x}_0, \dot{y}_0, \dot{z}_0, \phi, C_L, C_D\}^{\mathrm{T}}, \tag{4–6}$$

where here the superscript T denotes vector transpose. In all nine parameters will be estimated for the center-of-mass trajectory trials.

4.2.2 Marker Trajectories

When data describing the trajectories of markers on the ball is available the following assumptions will be made in the estimation procedure:

1. The lift, drag and cross-force coefficients will remain constant throughout the pitch.
2. The angular velocity vector (magnitude and direction) will remain constant.

The set of parameters for this estimation will be based on those defined in equation 4–6 for the center-of-mass trajectory, but also will include the following parameters to account for ball seam and angular velocity orientations. Since the angular velocity vector is well defined the spin rate and cross-force are now also included as parameters. The additional parameters to equation 4–6 are given as follows:

θ – Azimuth angle of the angular velocity vector.

α_0 – Azimuth angle of the initial orientation vector.

β_0 – Elevation angle of the initial orientation vector.

ψ_0 – Initial rotation about initial orientation vector.

ω_0 – Initial angular velocity magnitude.

C_Y – Cross-force coefficient.

In this case the parameter vector is given by;

$$\mathbf{p} = \{x_0, y_0, z_0, \dot{x}_0, \dot{y}_0, \dot{z}_0, \theta, \phi, \omega_0, \alpha_0, \beta_0, \psi_0, C_D, C_L, C_Y\}^{\mathrm{T}}. \tag{4–7}$$

In all 15 parameters will be estimated for the marker trajectory trials.

4.3 Nonlinear Least-Squares Parameter Estimation

Although a complete dynamical model for the pitch is defined in chapter 2, it is difficult to use this model for the purpose for which it was intended because of uncertainties in both the model parameters and the initial conditions. Even if I was certain about the form of the model, the effects which are important and unimportant, and which factors should be included and which should be neglected, still it is necessary to know exact values for model parameters before the equations which embody the model can be used to extract information. In addition, it is desired to know the exact values of the initial conditions, which may therefore also be considered parameters as expressed in equations 4–6 and 4–7.

There is a way both to determine the set of parameters which can be as exact as possible in the sense that they predict the experimental data better than any other set of values of those same parameters, and to use the remaining residual difference between the predictions and the data as a measure of the measurement accuracy (see section 4–6). This is accomplished by the generation of an iterative set of parameter estimates which converges to an optimal set in the sense that they minimize the residuals. Such a technique was utilized by Hubbard and Alaways (1989) in the estimation of javelin release conditions. The approach taken here is similar.

First recall the definition of the residual vector **f** in equation 4–5 as being the differences between the predicted and measured positions. Further suppose that the predicted positions are functions of *M* parameters, arranged in the vector **p** as defined in equations 4–6 and 4–7, which is a combination of true parameters and initial conditions.

The parameter estimation problem can be formulated (Gelb, 1974) through the question "What are the values of the parameters which make the mean squared error between the predicted and measured positions a minimum?"

As shown in Hubbard and Alaways (1989) a solution to this problem is the limit of the converging iterative sequence

$$\mathbf{p}_{k+1} = \mathbf{p}_k + \delta\mathbf{p}_k \tag{4–8}$$

where the initial estimate $\mathbf{p}_0$ is simply a good initial guess (see section 4.5), and each correction $\delta\mathbf{p}_k$ is given by the solution to the linear equations

$$\mathbf{J}_k^T\mathbf{J}_k\delta\mathbf{p}_k = -\mathbf{J}_k^T\mathbf{f}_k \tag{4–9}$$

where the matrix $\mathbf{J}$ is the $M \times 3N$ Jacobian matrix of partial derivatives of R with respect to $\mathbf{p}$, and is computed numerically by perturbing each parameter in turn from its nominal value.

This method of non-linear least squares is called the Gauss-Newton method. One of its advantages is that it requires the evaluation of only the *first* derivatives of R though this method can achieve a quadratic rate of convergence. In addition, solving equation 4–9 using the singular-value decomposition (Gill, Murray, and Wright, 1981, p. 40), avoids any unnecessary exacerbation of the ill-conditioning, a common feature of nonlinear least-squares problems of this type.

For this work the Hubbard and Alaways' parameter estimation procedure was improved upon by implementing a univariate minimization of R in the $\delta\mathbf{p}_k$ direction. This minimization was performed using a modified Fibonacci search that not only returns the unimodal minimum over a search interval but also varies the search interval length to insure that the global minimum in the $\delta\mathbf{p}_k$ direction is found. The Fibonacci search is a well known univariate minimization technique and is outlined in most optimization textbooks, for example see (Gill, Murray, and Wright, 1981, p. 89).

4.4 Algorithmic Recipe

The estimation procedure is accomplished using an iterative comparison of the measured and predicted trajectories. This procedure can be broken down into the following five-step algorithm that will yield a "best" estimation of **p**:

1. Guess an initial parameter vector **p** and simulate.
2. Perturb, in turn, each entry of **p** holding the other components at their nominal values and simulate. This step will yield *M* simulations where *M* is the number of entries in **p** and allows calculation of the *M* rows of the Jacobian matrix.
3. Using the $M+1$ trajectory predictions created in steps 1 and 2 along with the measured trajectory, a Newton direction $\delta\mathbf{p}_k$ is calculated which best matches the measurements in the manner described in the estimation procedure.
4. Employing a univariate optimization technique (modified Fibonacci search), the optimal size of $\delta\mathbf{p}_k$ is determined to minimize the residual in the $\delta\mathbf{p}_k$ direction.
5. Repeat steps 2, 3 and 4 using the updated value of **p** until the RMS of the residual vector is minimized.

4.5 The Initial Guess

Because of the possibility of the existence of local or non-global minima, the accuracy of the initial guess is the key to global minimum convergence (Brender, 1995). An optimal initial guess can be found by exploiting the shape of the ball, the geometry of the marker locations and the fact that the linear and angular momentum vectors of the ball change only slightly in the first few feet of flight. The methods used to obtain the "best" initial guess of the 15 parameters in **p**, as defined in equation 4–7, are described in the following sections. Notice that the initial guess utilized for the nine parameters in equation 4–6 is not thoroughly detailed in this dissertation but is based on the following method.

4.5.1 Center-of-Mass Position

The best initial guess for the position of the center of mass at release is estimated by exploiting the facts that the shape of the ball is spherical and that the radius, r, is known. Using these facts the guess for the initial position is found by using the same parameter estimation procedure described in the previous sections. However, the performance index for this estimation is given by,

$$R = \frac{1}{2}\sum_{i=1}^{n}\left(r_i^{\mathrm{p}} - r\right)^2 \tag{4–10}$$

where r_i^{p} is the calculated distance from the estimated center of mass to the ith measured marker position and n is the number of markers on the ball. Only the initial frame of acquired data is used to determined the guess for the initial center of mass position. Even in this parameter estimation for the initial guess, an initial guess for the center of mass position is needed for rapid convergence. That guess is determined taking the algebraic mean of the measured marker positions in the first frame, then subtracting r from the y-coordinate. Subtracting r exploits the fact that during the pitching machine trials, all the markers were roughly $-r$ in the y-direction from the center of mass. The estimation results determined here serve as the initial guess for x_0, y_0, and z_0 in $\mathbf{p}$.

4.5.2 Translational Velocity Vector

The initial guess for the translational velocity vector is determined by noting a fact about the kinematics of the baseball's trajectory, that the translational momentum vector does not rapidly change in the first few feet of flight. With this information, an algebraic equation for the derivative is used in calculating the translational velocity vector. First, the center of mass position for the first four frames of data is determined using the technique outlined in section 4.5.1 on a frame-by-frame basis. Second, since the acceleration due to gravity is well known, the z- positions are altered to account for the gravitational force. Finally, the translational velocity vector is calculated for the first and second acquired frame

using the following forward difference equation; whose error term is of the form $O(h^2)$ (Burden, et al., 1981, pg. 128),

$$g_i'(t_0) = \frac{1}{2h}\left[-3g_i(t_0) + 4g_i(t_0 + h) - g_i(t_0 + 2h)\right] \text{ for } i = 1,2\,. \tag{4–11}$$

Here, $h = 1.0/f$ and f is the frequency of the acquired data. The accuracy of the translational velocity vector is improved from the second order by taking the vectorial average of the two calculated velocities, g_1 and g_2. The final result is used as the initial guess for $\dot{x}_0$, $\dot{y}_0$ and $\dot{z}_0$ in **p**.

4.5.3 Orientation

Like the center of mass position, the initial orientation of the ball is found by using the parameter estimation procedure described in section 4.3. The performance index is that given by equation 4–3, but here the measured positions are the measured marker positions in the first frame of the acquired data set. The corresponding predicted positions are calculated by rotating the markers from their unperturbed positions about the estimated orientation vector. To account for the non-zero center of mass position in the measured data the previously determined initial center of mass position from section 4.5.1 is added to the estimated marker positions. This estimation also needs an initial guess. In this case for ease in programming the guess was $\alpha_0 = \beta_0 = \psi_0 = 1.0$ rad. The results of the estimation are used for the initial guesses of α_0, β_0 and ψ_0 in **p**.

4.5.4 Angular Velocity Vector

Again, like the center of mass position and seam orientation, the initial angular velocity vector of the ball is determined using the parameter estimation procedure described in the previous sections. Once again, the cost function is equation 4–3 and the measured positions are the measured positions of the marker locations found in the second, third and fourth frame of the acquired data set and the predicted positions are described in Step 1

below. The estimation of the angular velocity vector is broken down into the following three steps.

Step 1 – Predicted Marker Positions

The predicted positions for the markers locations are found by using equation 2–40 to rotate the previously known unperturbed marker positions about the initial orientation vector determined in section 4.5.3. These new locations are again rotated, this time about the angular velocity vector through an angle ξ corresponding to the rotation angle that occurred between the first frame and the frame in question (i.e. $\xi = n\omega_0 / f$, where f is the frequency of the acquired data and n is the number of frames since the initial frame). Finally, the center of mass position, for the frame in question, determined using the method in section 4.5.1, is added to each marker location resulting in the final predicted marker positions.

Step 2 – Angular Velocity Direction

The angular velocity vector is found using the parameter estimation procedure outlined in section 4.3 with the predicted marker locations just determined for the second frame of data only. For ease in programming, the initial guess for the spin azimuth and elevation angles used in this estimation is 1.0 rad and the rotation angle ξ is $\pi/3$ rad. The angular velocity azimuth and elevation angles estimated are used as θ and ϕ for the $\mathbf{p}$ vector and the third parameter, ξ, is passed on to Step 3.

Step 3 – Angular Velocity Magnitude

The third parameter used to defining the angular velocity vector is the spin rate or magnitude. This parameter is found by repeating the parameter estimation, of Step 2, for the third and fourth frames of the data set, where in each case the total rotation angle from the first frame is determined. After all three estimations are completed, the magnitude of the angular velocity vector is determined using equation 4–11 to calculate the derivative of the rotation angle. This derivative is used as ω_0 in $\mathbf{p}$.

4.5.5 Aerodynamic Parameters

4.5.5.1 Drag Coefficient

The initial guess for C_D in $\mathbf{p}$ was set to 0.40. This value was chosen as a compromise between the drag coefficient for non-rotating spheres in figure 1–8 and the drag coefficient for spinning golf balls in figure 2–4 at $Re = 1.5 \times 10^5$.

4.5.5.2 Lift Coefficient

The initial guess for C_L in $\mathbf{p}$ was set to 0.35. This value was chosen as a expected upper bound for C_L.

4.5.5.3 Cross-Force Coefficient

Since the cross-force is associated with asymmetries in the ball and no previous information on the magnitude of this aerodynamic force component is available, the initial guess for C_Y was set to 0.0 in the initial parameter vector.

4.6 Estimation Accuracy

One of the important features of the estimation procedure presented in section 4.3 is that, although the entire problem is nonlinear, each (and therefore the last) iteration to find the refinement $\delta\mathbf{p}_k$ from equation 4–9 is a linear approximation. This allows the application of standard solution accuracy assessments which are available for linear least-squares problems. A method to determine this accuracy assessment was given in Hubbard and Alaways (1989) and is summarized here.

Consider equation 4–9 near the end of the iterative process. If the residual vector $\mathbf{f}_k$ were zero at the kth iteration (i.e. if the parameter vector $\mathbf{p}_k$ predicted all the observed motions exactly) then the kth refinement $\delta\mathbf{p}_k$ would be zero as well, $\mathbf{p}_{k+1} = \mathbf{p}_k$, and the algorithm would have converged. A much more typical situation is that $\mathbf{f}_k$ becomes very small, but never exactly zero, due to random errors associated with the measurements.

These measurement errors cause uncertainties in the parameter estimation $\mathbf{p}_k$, which can be calculated as follows.

Hubbard and Alaways (1989) showed that if the errors in the measurements of x^m, y^m and z^m are assumed to be non-correlated with variance

$$\sigma^2 = E[(x_{ij}^m - x_{ij})^2] = E[(y_{ij}^m - y_{ij})^2] = E[(z_{ij}^m - z_{ij})^2], \tag{4–12}$$

where E denotes the expected value operator, then the uncertainty in the solution of $\delta\mathbf{p}_k$ is given by its covariance

$$\mathbf{U} = \sigma^2\left(\mathbf{J}_k^T\mathbf{J}_k\right)^{-1}. \tag{4–13}$$

Because the approximated Jacobian matrix $\mathbf{J}$ is available at each iteration, equation 4–13 can be used to calculate the covariance of the estimate. The diagonal elements of the estimate covariance matrix $\mathbf{U}$ are interpreted as the mean square errors in the corresponding parameters.

4.7 Estimation Robustness[1]

To ensure that the estimation software was working accurately and to acquire some performance information on how robust the software is in handling measurement noise, a series of software validation trials were performed. The "measured" data in these tests was generated by simulation using the models described in chapter 2. The data was superimposed with random Gaussian noise to model the noise that is problematic of the data acquisition system. Test descriptions and results are presented in following sections.

4.7.1 Test Descriptions

Three different case studies were conducted to obtain performance information on the robustness of the estimation software. In all three case studies, six trials were conducted with a zero noise trial and with five trials with different levels (one standard

---

1 Throughout this dissertation the primary units used were based on the historical units of feet and mph. However, the following discussion utilizes the metric units of meters and m/s for convenience.

deviation) of random Gaussian noise superimposed (in all three directions) on the simulated data. In all trials, the simulated data was generated at 240 Hz in the two-seam orientation with the initial conditions and aerodynamic parameters given in table 4–1. This simulated data used the same marker locations as the two seam ball described in section 3.2.6.2. The

Table 4–1: Initial conditions used in testing.

Positions:	x_0 = 16.0 m	y_0 = 0.1 m	z_0 = 2.0 m
Linear Velocity:	$\dot{x}_0$ = –30.0 m/s	$\dot{y}_0$ = –0.1 m/s	$\dot{z}_0$ = 1.0 m/s
Orientation:	α_0 = 60.0 deg	β_0 = 30.0 deg	ψ_0 = 90 deg
Angular Velocity:	θ = –90.0 deg	ϕ = 1.0 deg	ω_0 = 30 rev/sec
Aerodynamics:	C_D = 0.45	C_L = 0.19	C_Y = 0.044

tests consisted of simulating acquired data in the same form as the experimental trials discussed in chapter 3. The simulated data sets consists of either four or eight frames of marker trajectory data at release and 15 or 30 frames of center-of-mass trajectory data as the ball crossed over home plate. Table 4–2 lists the "noise levels" (measurement uncertainty) and number of frames of simulated data used in each case study trial.

Table 4–2: Standard deviations and number of frames used for robustness studies.

Case	Frames at release	Frames at plate	"Noise" levels - mm
1	4	30	0, 1, 1.5, 2.5, 5 and 10
2	8	30	0, 1, 1.5, 2.5, 5 and 10
3	4	15	0, 1, 1.5, 2.5, 5 and 10

4.7.2 Test Results[2]

The estimation software converged for all 18 simulated data sets. The final results for each trial are given in table 4–3 and shows that with "noise levels" less than 5 mm the results, though not exact, describe the general nature of the pitch if enough data is acquired.

---

2 To get more statistical information on the robustness of the estimation routine the three cases studies were repeated using a different random number seed in the software. These additional case studies are identified as 1A, 2A and 3A in the following figures.

Table 4–3: Final parameter estimations of robustness studies.

Case 1									
Trial	Noise	x_0	y_0	z_0	$\dot{x}_0$	$\dot{y}_0$	$\dot{z}_0$	α_0	β_0
1	0.0	16.000	0.100	2.000	-30.00	-0.100	1.000	60.00	30.00
2	1.0	16.001	0.100	2.002	-30.01	-0.100	0.995	60.55	31.00
3	1.5	16.001	0.100	2.002	-30.01	-0.099	0.992	60.97	31.49
4	2.5	16.002	0.100	2.004	-30.02	-0.099	0.988	62.21	32.42
5	5.0	16.005	0.101	2.007	-30.03	-0.098	0.976	71.11	32.59
6	10.0	16.008	0.100	2.002	-30.05	-0.129	1.009	21.71	30.34
…	…	ψ_0	θ	ϕ	ω_0	C_D	C_L	C_Y	
1	0.0	90.00	-90.00	1.00	30.00	0.450	0.190	0.044	
2	1.0	90.52	-90.92	2.18	29.69	0.451	0.189	0.048	
3	1.5	90.81	-91.17	2.67	29.56	0.452	0.188	0.050	
4	2.5	91.50	-91.20	3.53	29.32	0.453	0.187	0.052	
5	5.0	96.60	-86.23	6.02	29.55	0.456	0.184	0.058	
6	10.0	80.90	-117.45	-2.43	23.33	0.459	0.220	0.043	
Case 2									
Trial	Noise	x_0	y_0	z_0	$\dot{x}_0$	$\dot{y}_0$	$\dot{z}_0$	α_0	β_0
1	0.0	16.000	0.100	2.000	-30.00	-0.100	1.000	60.00	30.00
2	1.0	16.002	0.101	2.001	-30.01	-0.097	1.000	63.75	28.94
3	1.5	16.003	0.101	2.002	-30.01	-0.097	1.000	65.46	28.35
4	2.5	16.002	0.101	2.000	-30.01	-0.088	1.001	62.18	31.62
5	5.0	16.005	0.106	2.005	-30.02	-0.109	1.011	73.46	23.99
6	10.0	16.013	0.108	1.995	-30.08	-0.134	1.087	59.57	37.96
…	…	ψ_0	θ	ϕ	ω_0	C_D	C_L	C_Y	
1	0.0	90.00	-90.00	1.00	30.00	0.450	0.190	0.044	
2	1.0	91.67	-87.49	3.86	30.57	0.451	0.189	0.052	
3	1.5	92.07	-86.55	5.28	30.79	0.452	0.188	0.055	
4	2.5	95.28	-84.99	0.61	30.90	0.452	0.191	0.039	
5	5.0	85.77	-86.52	13.93	31.13	0.452	0.181	0.083	
6	10.0	92.21	-81.09	-1.36	30.49	0.463	0.215	0.039	
Case 3									
Trial	Noise	x_0	y_0	z_0	$\dot{x}_0$	$\dot{y}_0$	$\dot{z}_0$	α_0	β_0
1	0.0	16.000	0.100	2.000	-30.00	-0.100	1.000	60.00	30.00
2	1.0	16.001	0.100	2.001	-30.02	-0.102	1.005	60.55	31.00
3	1.5	16.001	0.100	2.002	-30.04	-0.103	1.007	60.97	31.49
4	2.5	16.002	0.100	2.003	-30.06	-0.104	1.010	62.21	32.42
5	5.0	16.005	0.101	2.007	-30.12	-0.109	1.003	71.11	32.59
6	10.0	16.009	0.100	2.000	-30.19	-0.139	1.158	21.71	50.34
…	…	ψ_0	θ	ϕ	ω_0	C_D	C_L	C_Y	
1	0.0	90.00	-90.00	1.00	30.00	0.450	0.190	0.044	
2	1.0	90.52	-90.92	2.18	29.69	0.455	0.191	0.049	
3	1.5	90.81	-91.17	2.67	29.56	0.458	0.192	0.050	
4	2.5	91.50	-91.21	3.53	29.32	0.463	0.192	0.054	
5	5.0	96.60	-86.23	6.02	29.55	0.476	0.190	0.061	
6	10.0	80.98	-117.45	-2.43	23.33	0.490	0.262	0.044	

Besides the estimates of the 15 parameters in the parameter vector, the estimation software computes the standard deviation of the residual vector, **f**, and the parameter uncertainties. Figure 4–3 shows the residual standard deviations versus the noise level for all the robustness trials. The magnitude of the residual standard deviations are, in general, greater than the noise standard deviation for each case. The reason that the residual standard deviation is consistently greater is not fully understood. However, the trend in figure 4–3 that the higher noise levels in the data would result in higher noise levels in the residuals was expected. It is suspected that the nature of the problem, a "high level" of random noise when compared to the diameter of the ball in the four marker positions at release, results with larger residuals as the ball crosses over home plate. Note that since determining the trajectory of the ball is an initial value problem the "high level" of noise is magnified at the later stages of flight. Another possible source for the higher than expected residual standard deviation may be computational in natural and is not entirely understood.

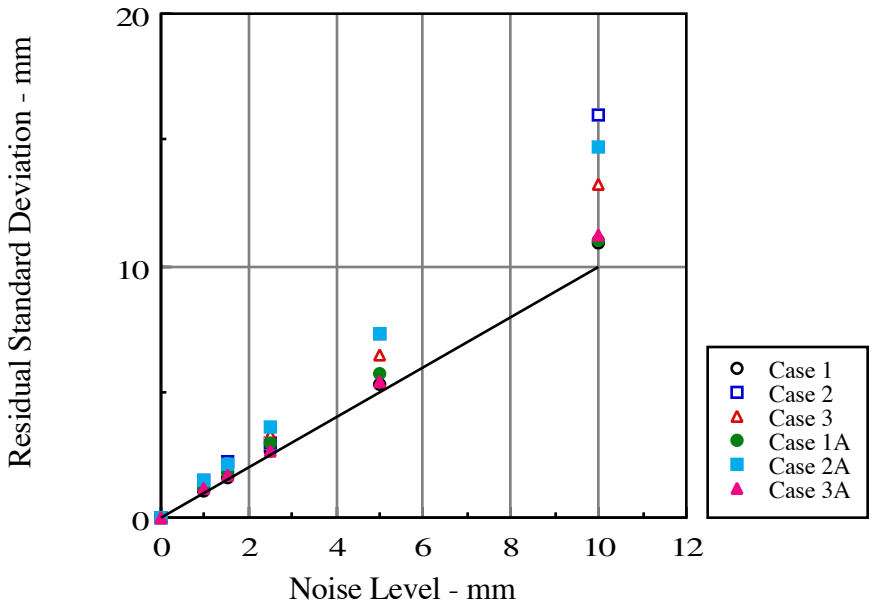

Figure 4–3: Residual standard deviation versus "noise level".

Figures 4–4 and 4–5 show the estimate of the lift coefficient and the lift coefficient uncertainties versus noise level, respectively, for all case studies. Figure 4–4 shows that the estimate for the lift coefficient is within 10 percent of its correct value of $C_L = 0.19$ for noise standard deviations up to 5 mm. Figure 4–5 shows that the lack of data at home plate, as in case 3 and 3A, is a leading contributor to larger parameter uncertainties in the lift coefficient as indicated by the larger slopes in these two cases.

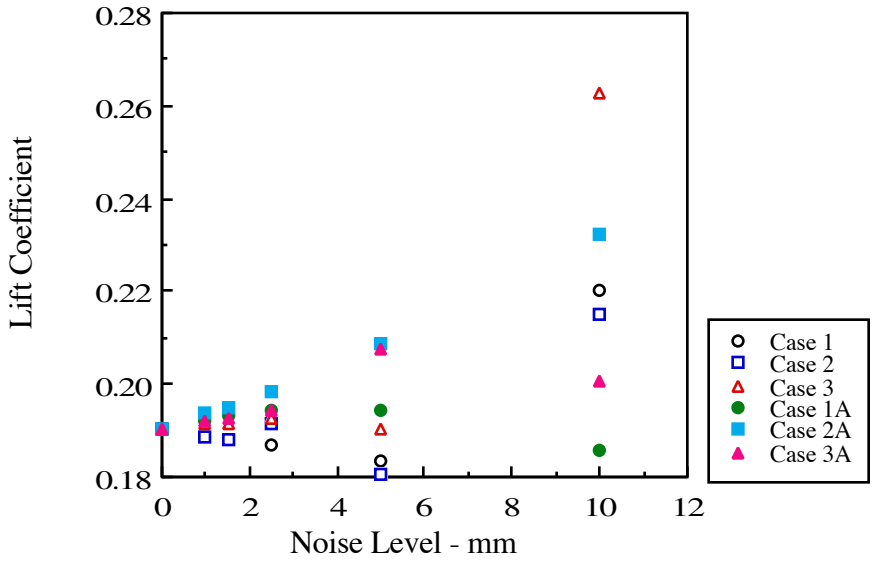

Figure 4–4: Estimated lift coefficients versus "noise level".

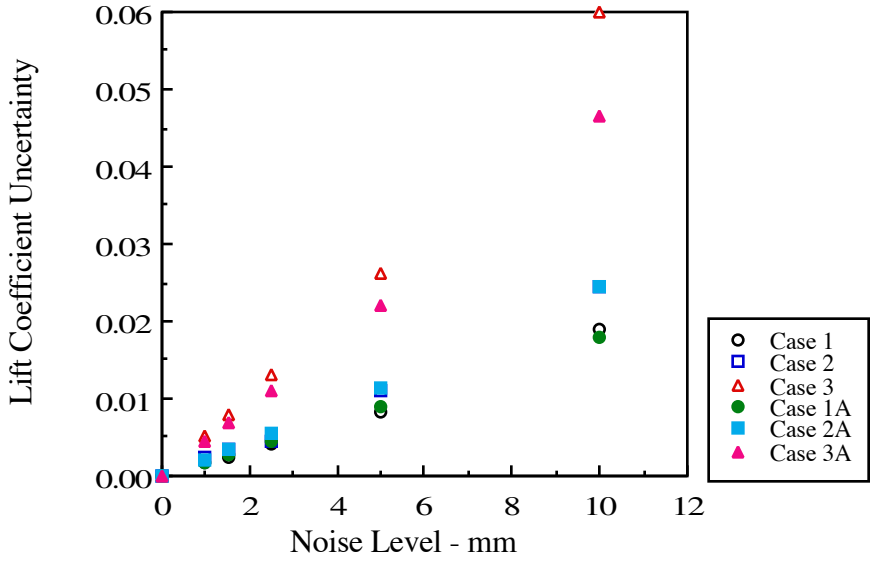

Figure 4–5: Lift coefficient uncertainty versus "noise level".

Figures 4–6 and 4–7 show the estimate and uncertainties in the spin rate, respectively, for all case studies. Figure 4–6 shows that in all cases, except case 3A, the estimate for the spin-rate was within 10 percent of the exact value ω_0 = 30 rev/sec for noise standard deviations less than 5 mm. Figure 4–7 shows that the smallest uncertainties in the spin-rate occurred for cases 2 and 2A with maximum uncertainties less than 14 percent of the exact value for noise levels up to 10 mm. Recall that for cases 2 and 2A eight frames of release data were used compared to four frames for the other cases, indicating that increasing the number of release frames will minimize the uncertainty in the spin-rate.

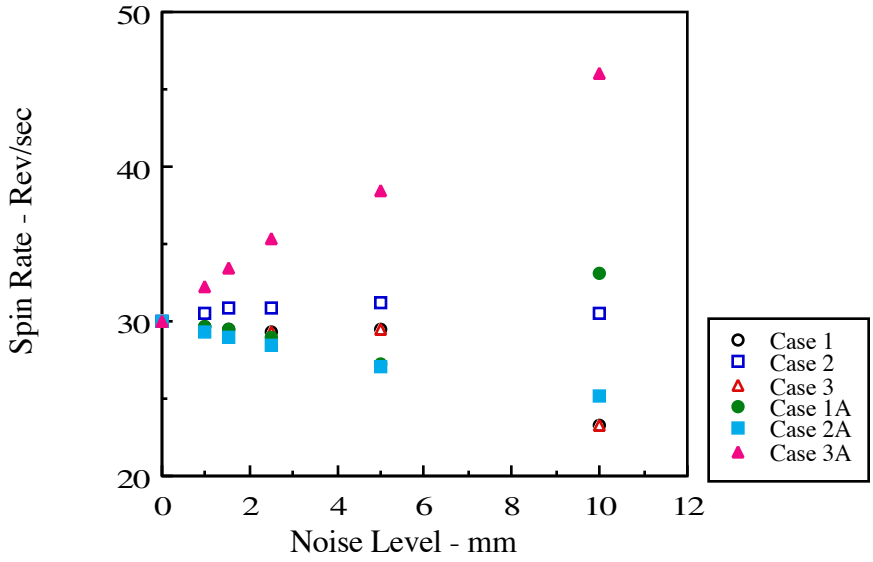

Figure 4–6: Spin-rate versus "noise level".

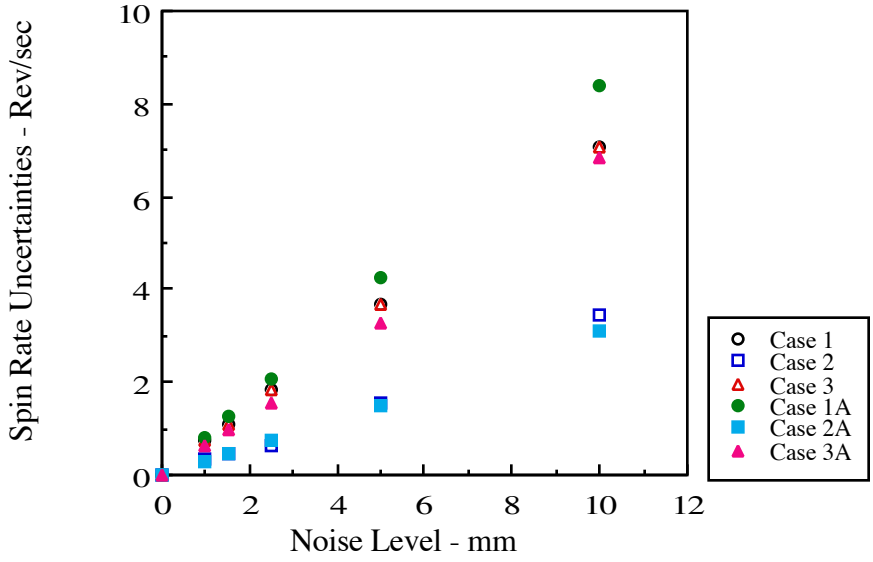

Figure 4–7: Spin-rate uncertainty versus "noise level".

Figures 4–8 and 4–9 show the estimated value and uncertainties for the drag coefficient, respectively, for all case studies. Figure 4–8 shows that in all cases, except case 3, the estimate for the drag coefficient $C_D = 0.45$ was within 3 percent of the exact value for noise levels up to 10 mm. Figure 4–9 shows that the highest uncertainties occurred in case 3 and 3A. Recall that these cases used half the number of center-of-mass trajectory frames as the other cases. This indicates that increasing the number of center-of-mass frames at the plate will decrease the uncertainty in the drag coefficient estimate.

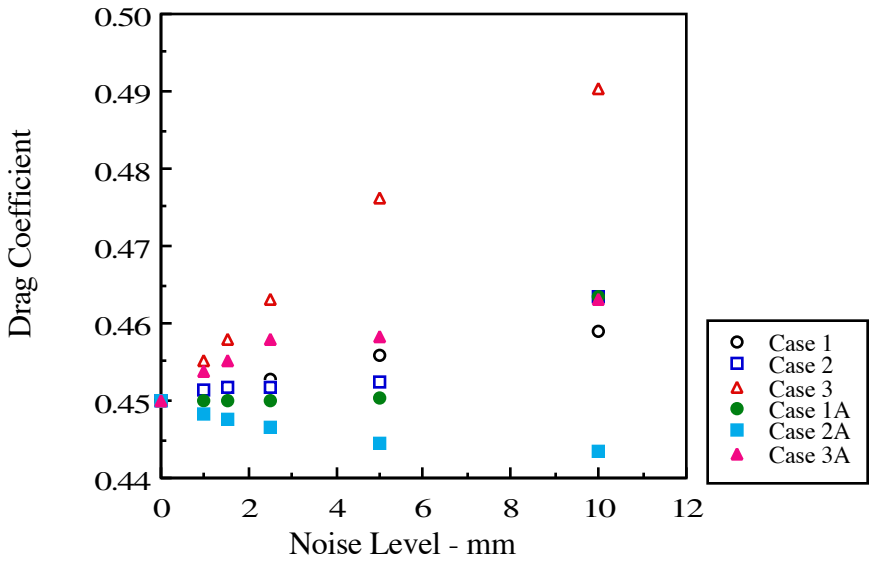

Figure 4–8: Drag coefficient versus "noise level".

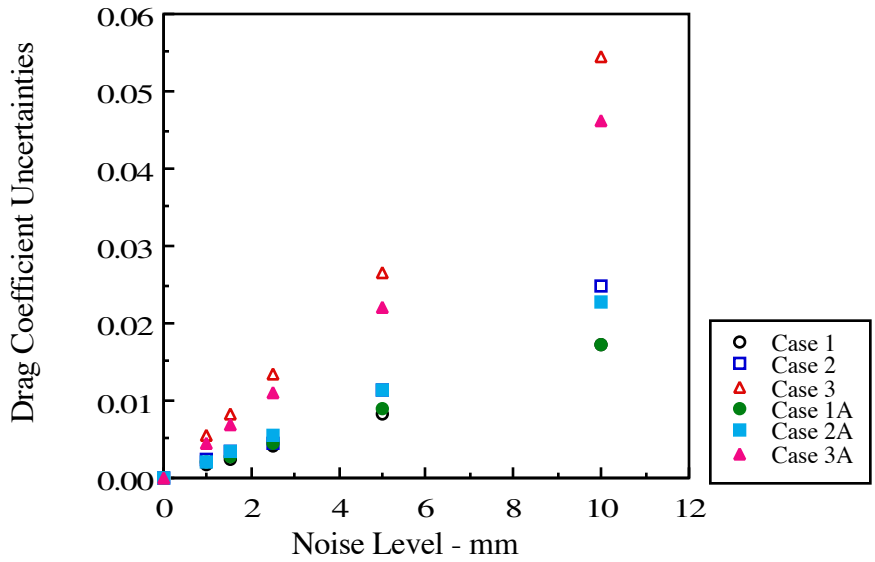

Figure 4–9: Drag coefficient uncertainties versus "noise level".

Figures 4–10 and 4–11 show representative parameter uncertainties for initial position and velocity estimates, respectively. Figure 4–10 shows that the initial position uncertainty is roughly 40 percent of the noise level, however, it is improved by increasing the number of frames in the data set. Figure 4–11 shows that increasing the number of frames in the data set decreases the uncertainty in the velocity estimate.

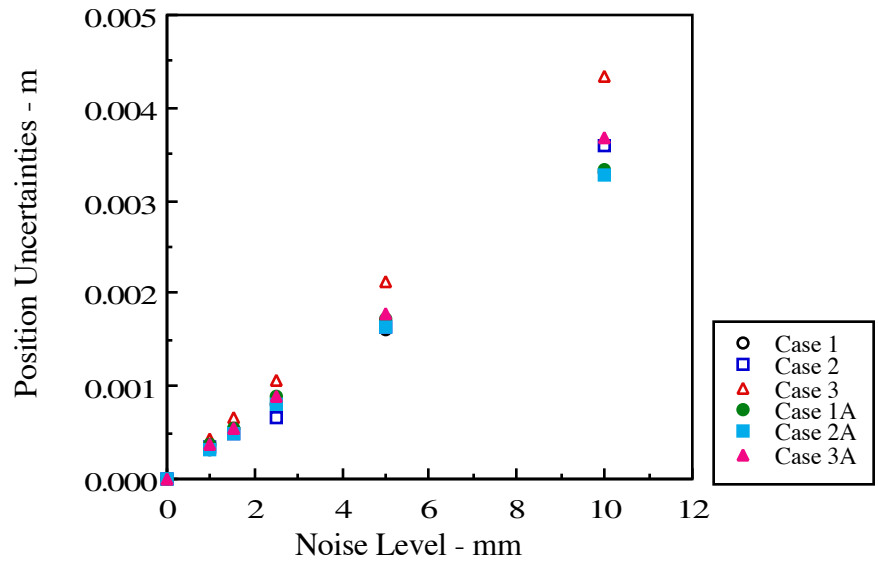

Figure 4–10: Position uncertainties versus “noise level”.

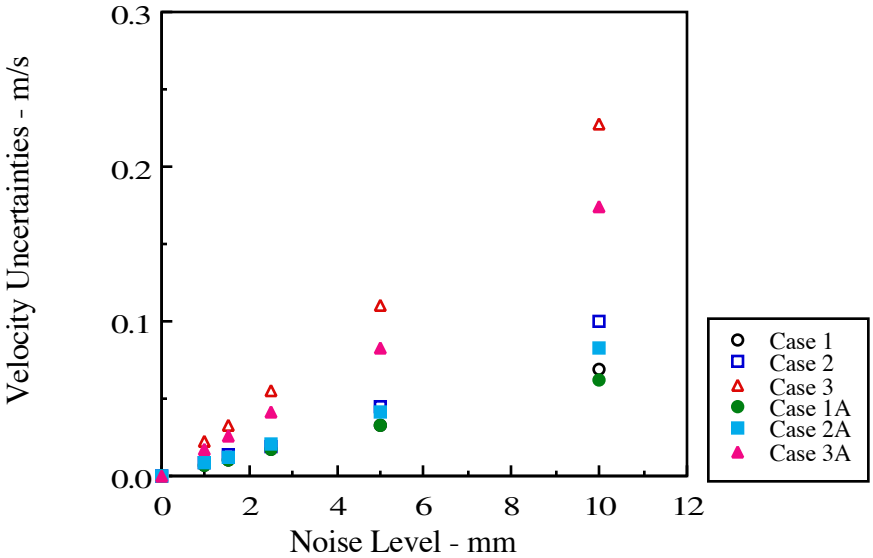

Figure 4–11: Velocity uncertainties versus “noise level”.

4.7.3 Robustness Conclusions

The estimation procedure converged for all 36 case studies at all levels of noise. In most cases the estimation results were reasonable. However, the robustness studies do show that estimate uncertainties decreased and overall accuracy improved in all cases with increasing numbers of frames. These studies show that with measurement uncertainties less than five millimeters the estimated results are within 10 percent of the exact values for all the parameters of interest when enough frames of data are acquired. However, when measurement uncertainties are greater than ten millimeters geometric and computational conditioning problems arise and the parameter estimation procedure is no longer robust.

CHAPTER 5 – RESULTS AND DISCUSSION[1]

5.1 General Comments

Using the data acquisition system previously described, 58 center-of-mass trajectories from the pitcher trials and 36 two-seam and 35 four-seam pitches from the pitching machine trials were acquired. All of these pitches from the pitcher trials and 20 selected pitching machine pitches were then processed using the parameter estimation procedure described in chapter 4. These results and comments concerning the findings are presented in the following sections, after a brief discussion on some of the key elements common to all the results.

5.1.1 Curve-ball

The strict 'baseball' definition for a curve-ball is, a ball released with top-spin resulting in a trajectory that lies below the normal gravitational arc. Figure 5–1 shows the simulated trajectories for a curve-ball, with the initial conditions given in table 5–1, and for a pitch with the same set of initial conditions except that the lift and cross-force components are set to zero in the aerodynamic force vector. Notice that the simulated trajectory has a total deviation from the drag only trajectory of 0.440 m (17.3 inches) and that the sideways deflection is caused by the cross-force component of the aerodynamic force.

Table 5–1: Initial conditions and aerodynamic parameters used for the simulated trajectory in figure 5–1.

Positions:	$x_0 = 16.0$ m	$y_0 = 0.1$ m	$z_0 = 2.0$ m
Linear Velocity:	$\dot{x}_0 = -30.0$ m/s	$\dot{y}_0 = -0.1$ m/s	$\dot{z}_0 = 1.0$ m/s
Orientation:	$\alpha_0 = 60.0$ deg	$\beta_0 = 30.0$ deg	$\psi_0 = 90$ deg
Angular Velocity:	$\theta = -90.0$ deg	$\phi = 1.0$ deg	$\omega_0 = 30$ rev/sec
Aerodynamics:	$C_D = 0.45$	$C_L = 0.19$	$C_Y = 0.044$

---

1 Throughout this study the primary units reported were based on the historical "baseball units" of ft and mph. However, the data acquisition system and the analysis software used metric units, therefore, metric units will be the primary units presented in this chapter and the remainder of this dissertation.

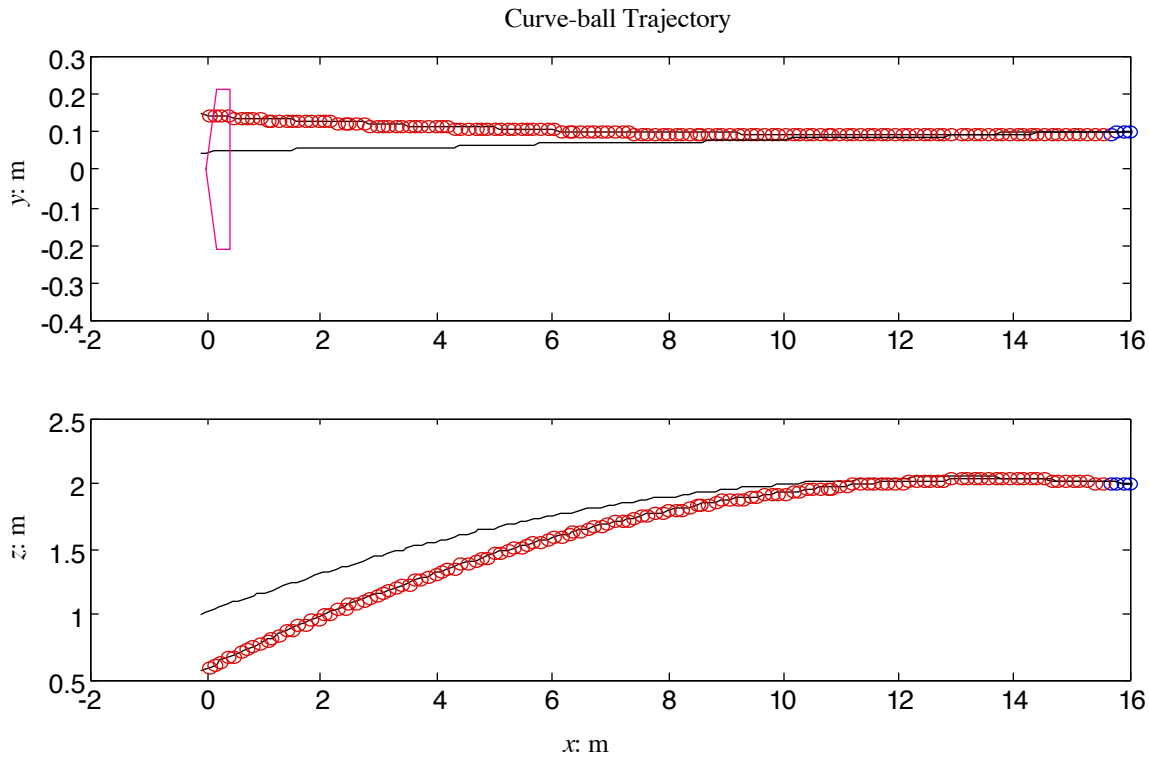

Figure 5–1: Simulated curve-ball trajectory. (The solid line represents the normal gravitational arc.)

5.1.2 Fastball

The strict 'baseball' definition for a fastball is, a ball released with back-spin resulting in a trajectory that lies above the normal gravitational arc. Figure 5–2 shows the simulated trajectories for a fastball, with the initial conditions given in table 5–2, and for a pitch with the same set of initial conditions except that the lift and cross-force components are set to zero in the aerodynamic force vector. Notice that the simulated trajectory has a total deviation from the drag only trajectory of 0.436 m (17.2 inches) and that the sideways deflection is caused by the cross-force component of the aerodynamic force.

Table 5–2: Initial conditions and aerodynamic parameters used for the simulated trajectory in figure 5–2.

Positions:	x_0 = 16.0 m	y_0 = 0.1 m	z_0 = 2.0 m
Linear Velocity:	$\dot{x}_0$ = –30.0 m/s	$\dot{y}_0$ = –0.1 m/s	$\dot{z}_0$ = 1.0 m/s
Orientation:	α_0 = 60.0 deg	β_0 = 30.0 deg	ψ_0 = 90 deg
Angular Velocity:	θ = –90.0 deg	ϕ = 1.0 deg	ω_0 = -30 rev/sec
Aerodynamics:	C_D = 0.45	C_L = 0.19	C_Y = 0.044

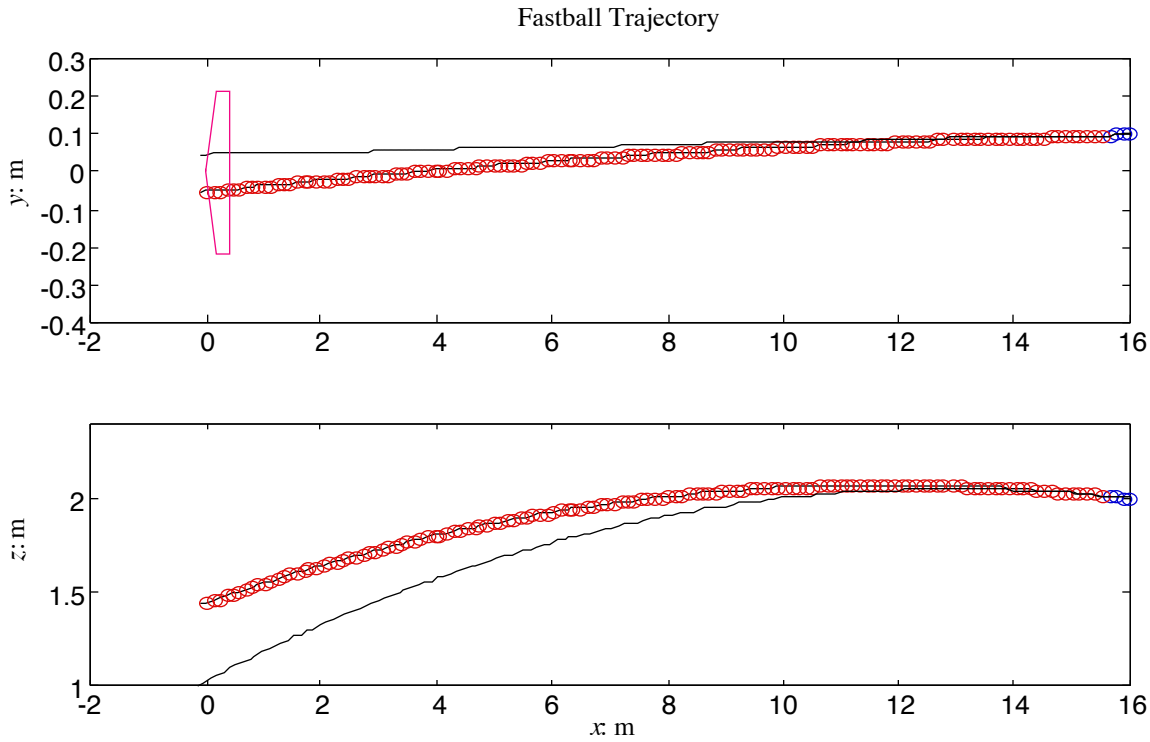

Figure 5–2: Simulated fastball trajectory. (The solid line represents the normal gravitational arc.)

5.1.3 Knuckleball

It was previously mentioned that the knuckleball was not of interest in this dissertation. However, three knuckleball trajectories were acquired during the pitching machine trials and the 15 parameters defined in section 4.2 were estimated. These results are presented and discussed in section 5.4.

5.1.4 Parameters and Parameter Uncertainties

In section 4.2 it was noted that up to 15 parameters would be estimated. Though all the parameters were estimated, only the aerodynamic and angular velocity parameters will be discussed in detail in this dissertation. However, to get an idea of how well the parameter estimation procedure converged a quick look at all the parameter uncertainties is given here.

The parameter uncertainties, in the pitching machine trials, for position varied from 0.28 to 1.61 mm, from 2.5 to 31.8 mm/s for translational velocity and from 0.36 to 2.36

degrees in ball and angular velocity orientation. For the pitcher trials, the position and velocity uncertainties ranged from 3.05 to 8.02 mm and 29.4 to 138.1 mm/s, respectively. The uncertainties in the lift, drag and cross-force coefficients ranged from 0.0004 to 0.0064 for the pitching machine trials and from 0.016 to 0.058 for the lift and drag coefficients in the pitcher trials. The maximum spin rate uncertainty was 0.47 rev/sec for the pitching machine trials.

Another indication of overall accuracy of the data acquisition method and parameter estimation procedure is indicated by the standard deviation of the residual vector as defined in equation 4–5. For the pitching machine trials and the pitcher trials the maximum standard deviation was 3.6 and 17.6 mm, respectively. It should be pointed out that the higher uncertainties and residual standard deviations in the pitcher data was due to a low threshold value and poor background in the pitcher trials. This resulted in tracking the nine reflective markers on the ball (see figure 3–13) as a single marker and assuming that this position was the actual center of mass of the ball, thus introducing measurement noise possibly as large as the radius of the ball (36.3 mm).

5.1.5 Residuals

Figures 5–3, 5–4 and 5–5 show typical estimation residuals determined during the data analysis. Recall that the residual vector, defined by equation 4–5, is the difference between the measured and estimated marker or center of mass positions. Figure 5–3 shows the residuals of equation 4–5 versus time for the marker locations of pitch P2S22 and indicates that the maximum marker position residual for this pitch is less than 4 mm in all three directions.

Ideally, the residual vector should look like white Gaussian noise when plotted if no systematic errors occurred while collecting or processing the data. Figure 5–4 shows the residuals of the center of mass positions, for pitch P2S22, as the ball crossed over home plate and shows a 55 Hz oscillation in the residuals. This frequency corresponds to the estimated spin rate for this pitch (54.74 Hz) and suggests that dirt, the seams, or other

thresholding problems occurred when the data was acquired. The oscillation suggests that the estimation procedure accurately predicted the spin rate of the ball.

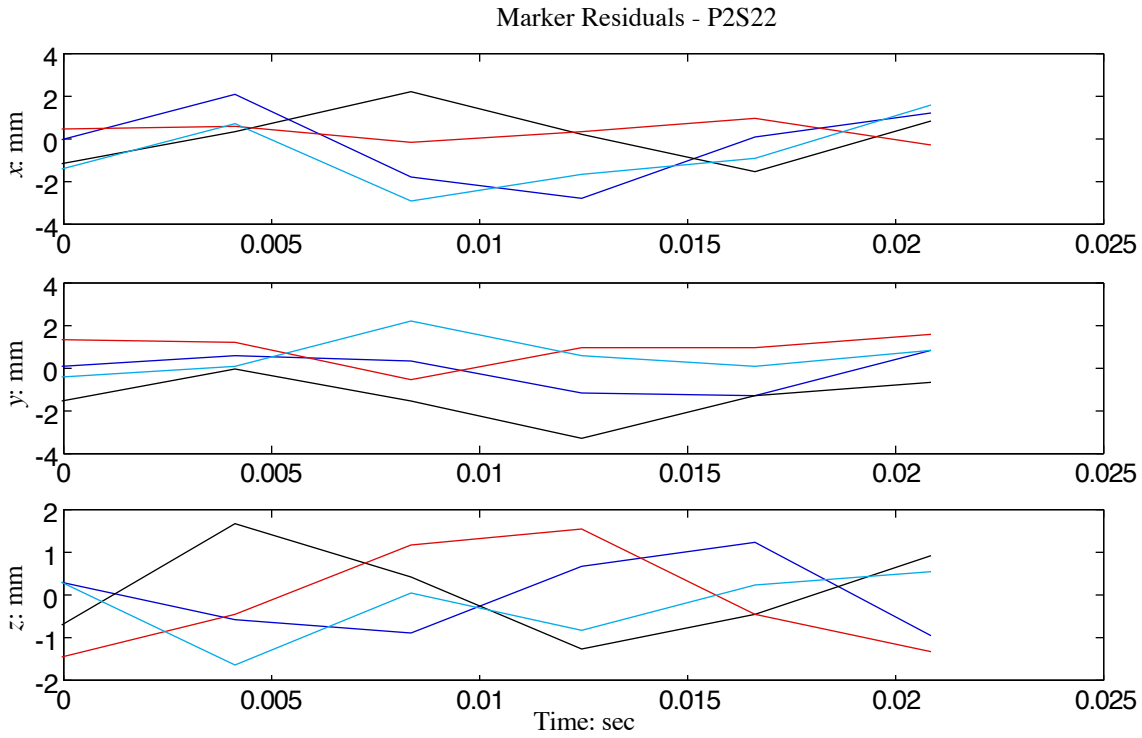

Figure 5–3: Marker residuals for pitch P2S22.

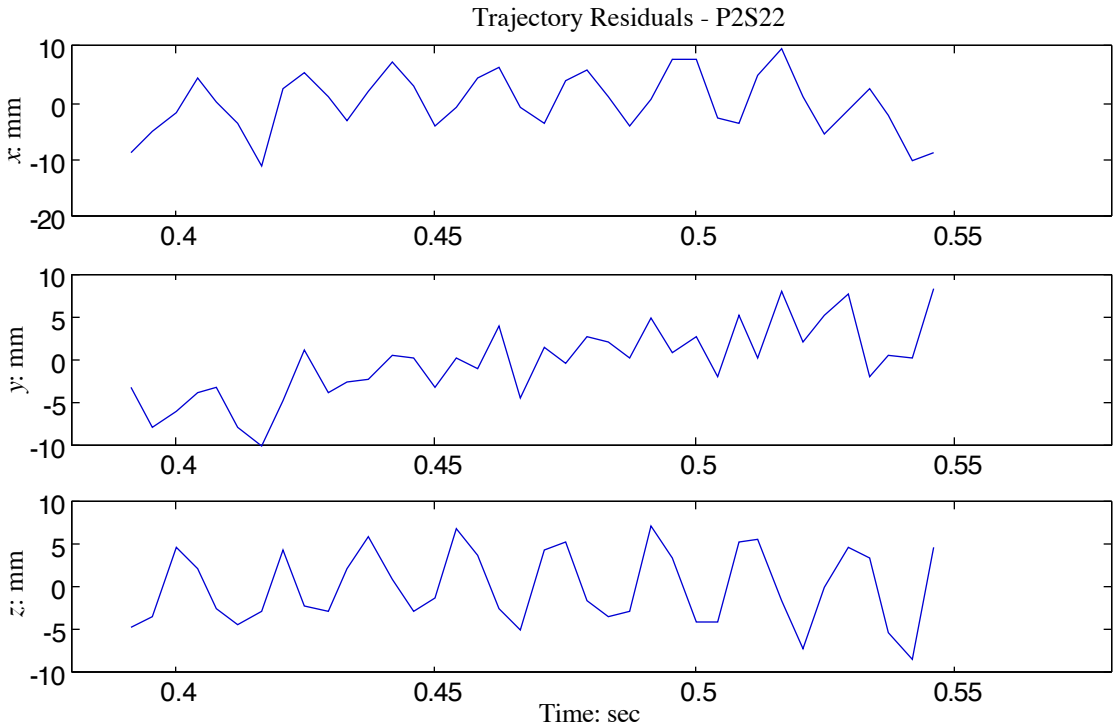

Figure 5–4: Trajectory residuals for pitch P2S22.

Figure 5–5 shows a typical trajectory residual from the pitcher trials, in this case pitch T6. Note that the zero values in the plot are due to missing frames in the data set.

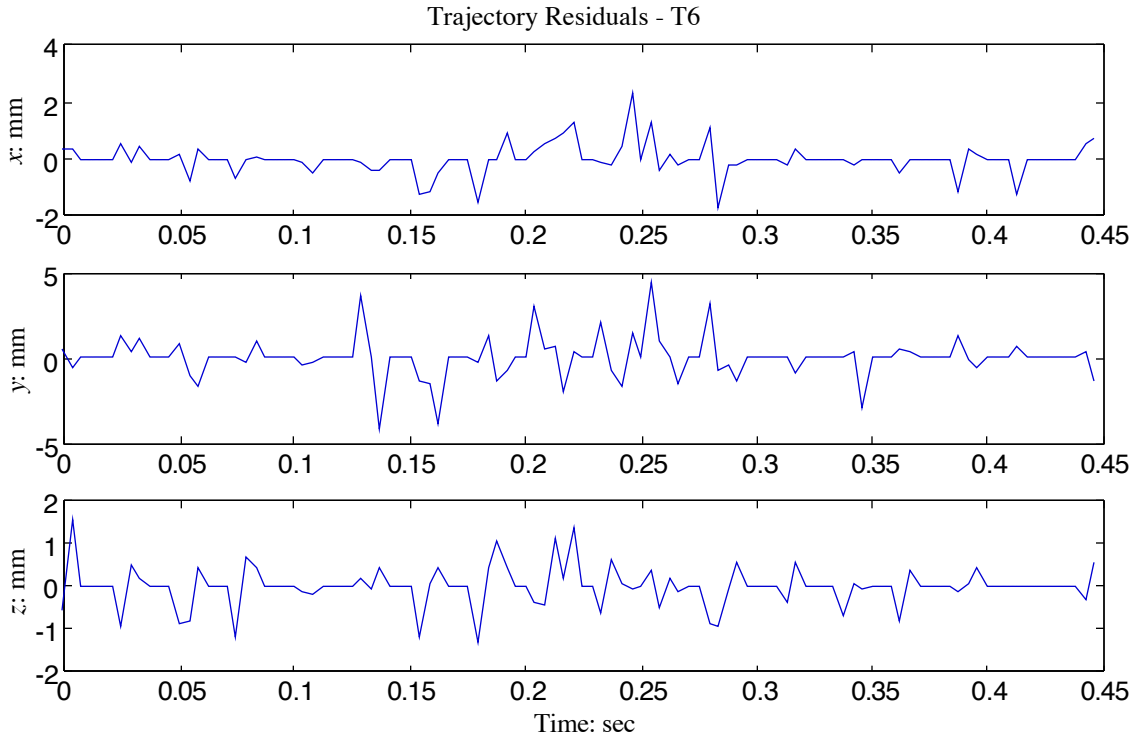

Figure 5–5: Trajectory residuals for pitch T6.

5.2 Pitchers

In all 58 pitches were acquired during the pitcher trials and processed using the parameter estimation software. Table 5–3 shows the range of translational and angular velocities estimated for these pitches. Since only center-of-mass trajectory data was acquired for the last 14 meters of flight, no clear determination of spin rate could be achieved. In all pitches, for subject T, the acquired trajectory matched the pitchers comments on the pitch as indicated in table A–1 of Appendix A.

Table 5–3: Estimated translational and angular velocities for the pitcher trials.

Pitcher	Translational Velocity	Two-Seam Spin Rate	Four-Seam Spin Rate
T	23.38 to 34.68 m/s	21.3 to 77.4 rev/sec	6.7 to 51.4 rev/sec
M	21.46 to 32.15 m/s	15.6 to 51.6 rev/sec	5.2 to 30.8 rev/sec
S	17.24 to 21.92 m/s	14.5 to 39.0 rev/sec	4.8 to 19.9 rev/sec

5.2.1 Center-of-Mass Trajectories

Figures 5–6 and 5–7 show a typical fast and curve balls, respectively, for subject T. The corresponding residuals plots for these pitches are respectively shown in figures 5–5 and 5–8. Note that the threshold setting and background during the pitcher trials were such that the center of mass of the ball was not directly acquired. Instead the nine reflective markers (see figure 3–13) were tracked as a single marker which introduced position errors in the data resulting in higher residuals. The markers did not envelope the ball, missing data occurred throughout the trajectory. Table 5–4 shows the estimated parameters for pitches T6 and T33. The raw trajectory data for pitches T6 and T33 is given in tables B–1 and B–2, respectively, in Appendix B.

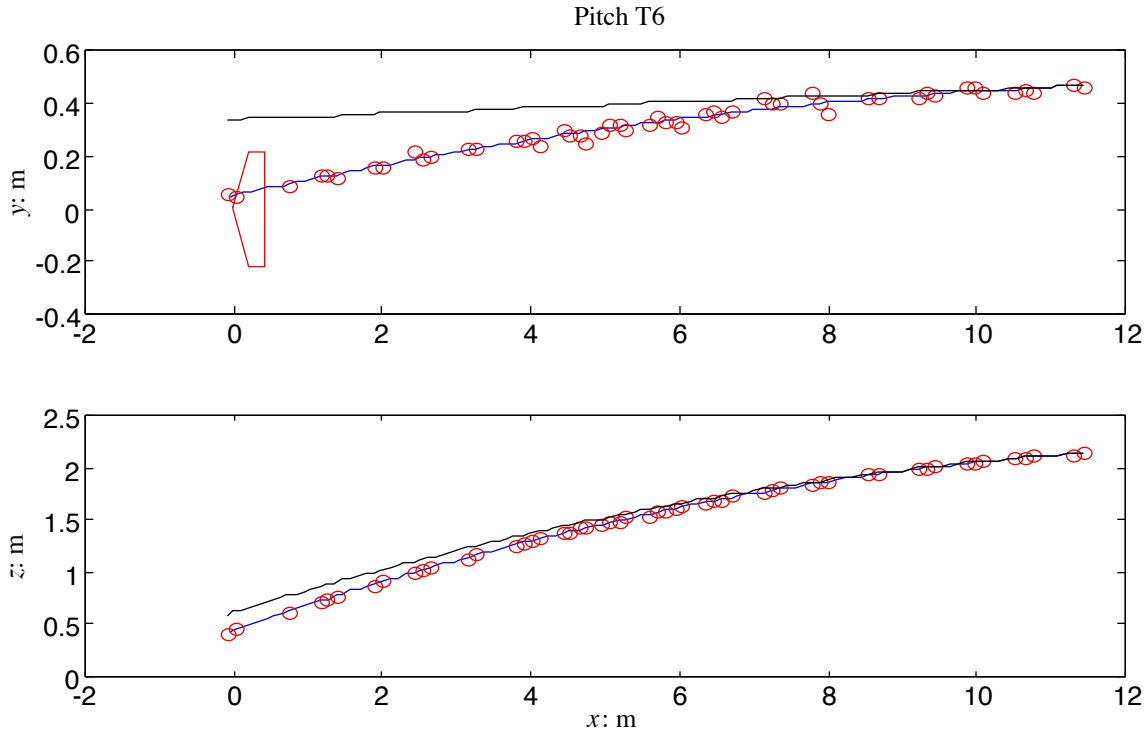

Figure 5–6: Pitch T6 trajectory. (The solid line represents the normal gravitational arc.)

Table 5–4: Estimated parameters for pitches T6 and T33.
(Units are either m, m/s or deg)

Pitch	x_0	y_0	z_0	$\dot{x}_0$	$\dot{y}_0$	$\dot{z}_0$	θ	ϕ	C_D	C_L
T6	11.44	0.47	2.13	-26.95	-0.30	-1.38	60.1	-77.9	0.412	0.295
T33	12.14	0.10	1.84	-33.84	-0.43	-2.36	-25.7	-56.3	0.376	0.243

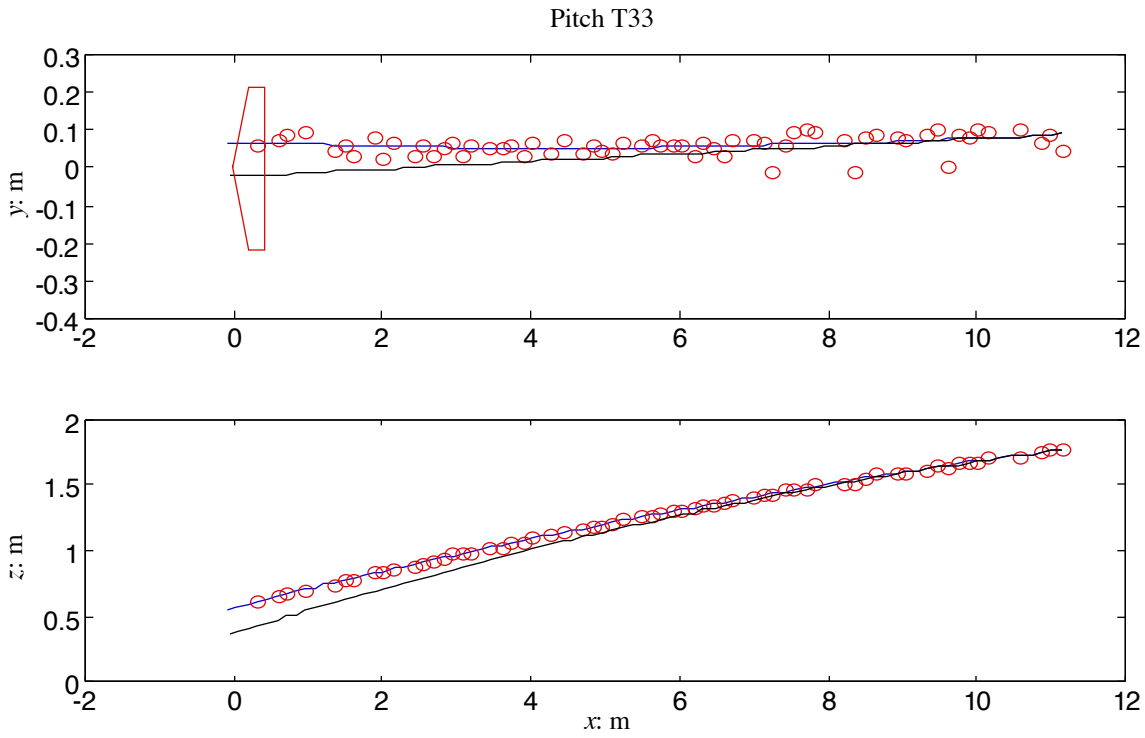

Figure 5–7: Pitch T33 trajectory. (The solid line represents the normal gravitational arc.)

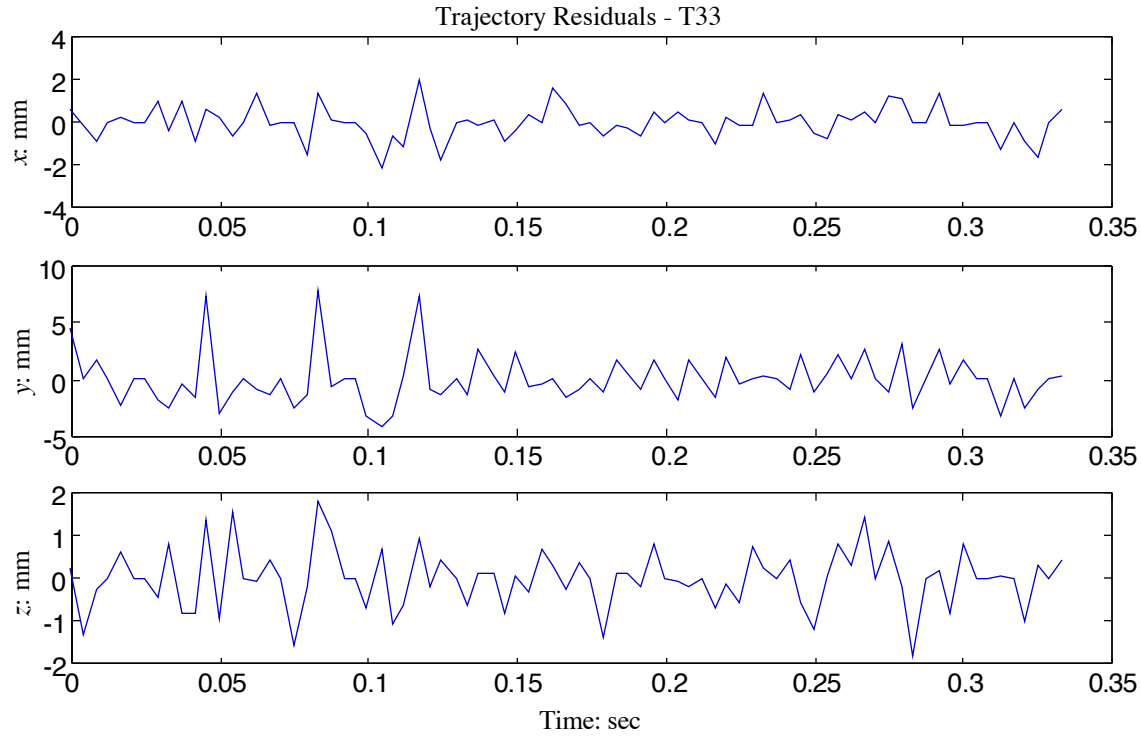

Figure 5–8: Trajectory residuals for pitch T33.

5.2.1.1 Lift Coefficients

Figure 5–9 shows the estimated lift coefficients versus Reynolds number for all three pitchers in the pitcher trials. Almost all of the lift coefficients are between the values determined by Sikorsky (Alaways & Lightfoot, 1998) and Watts & Ferrer (1987), but since the spin rate could not be determined little else can be learned from this plot. However, an upper and lower bound on S can be determined using the extrapolated lift coefficient lines of figure 2–4. For this data the spin parameter was in the range $0.05 < S < 0.68$.

An interesting but currently unexplainable feature of figure 5–9 is the obvious statistical significant families in subject T's data. Every means and test was performed using the comments of the pitcher noted in table A–1, but nothing could be found to satisfactory explain the significance seen in the data. Even possible significant sub-groups in the data could not be explained in terms of pitch type, spin rate or translational velocity.

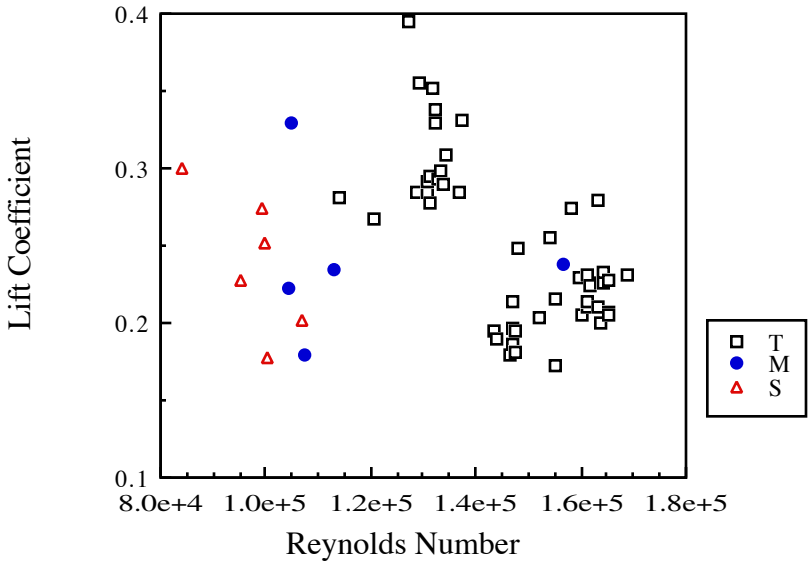

Figure 5–9: Lift coefficient versus Reynolds number for pitcher trials.

5.2.1.2 Drag Coefficients

Figure 5–10 shows the estimated drag coefficients versus Reynolds number for all three pitchers in the pitcher trials. The drag coefficient is consistently between 0.30 and

0.45 for the majority of the pitches; which is greater than the drag coefficient determined by Smits and Smith (1994) and less than the drag coefficients determined for the smooth non-rotating sphere previously shown in figure 1–8.

The difference in drag coefficients may suggest that the baseball's roughness ratio is less than that of a golf-ball. This can be expected since the stitching on the baseball is constrained to a specific pattern and therefore the roughness on baseballs is not as uniformly distributed as the dimples are on golf-balls and, probably more importantly, the ratio of dimple depth to radius is larger than that of seam height to radius. (This idea alone constitutes another doctorate dissertation and is out of the scope of this one).

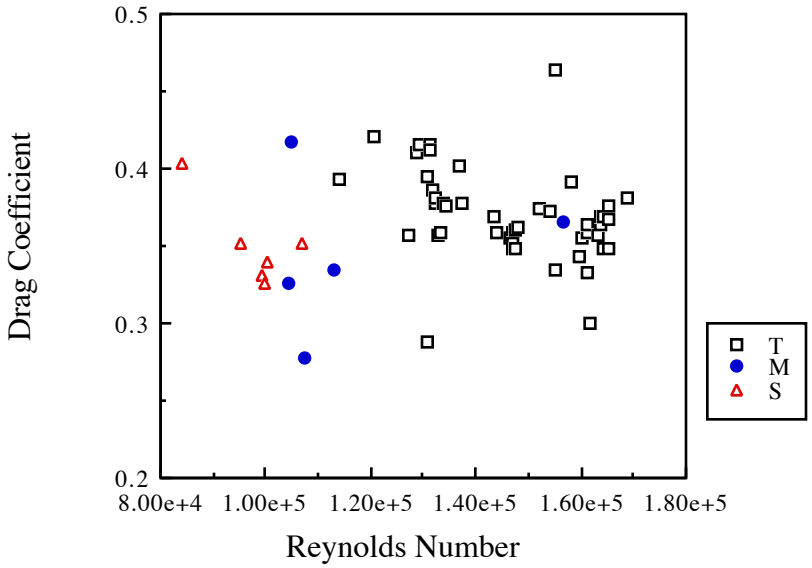

Figure 5–10: Drag coefficient versus Reynolds number for pitcher trials.

5.3 Pitching Machines

In all, 36 two-seam and 35 four-seam pitches were acquired during the pitcher trials. Of these 9 two-seam, 8 four-seam and 3 knuckleballs were successfully tracked, using the MotionAnalysis EVa software, and analyzed using the present parameter estimation software. The pitches analyzed are highlighted in boldface in tables A–2 and A–3 of Appendix A. Two different methods were used to estimate initial conditions and aerodynamic parameters for these 20 pitches. The first estimated all 15 parameters of

equation 4–7 using all the data available. The second estimated only the 9 parameters of equation 4–6 using only center of mass information and was conducted to compare the estimation results found using both methods. In both methods, the translational velocity at release was between 25.6 and 34.2 m/s. The spin rates varied between 16.6 to 64.5, 17.6 to 57.7, and 1.2 to 4.0 rev/sec for the two-seam, four-seam and knuckleball, respectively.

5.3.1 Marker Trajectories

The pitching machine trials were first analyzed by estimating all 15 parameters of equation 4–7. This was accomplished by first estimating the initial position, initial velocity vector, ball orientation vector and angular velocity vector using only the measured marker positions over the first four to eight frames of flight. Once these parameters were estimated the angular velocity vector was held constant and then the three aerodynamic parameters, along with the initial position, initial velocity and ball orientation vectors were again estimated but this time using all the available data.

5.3.1.1 Trajectories

Figures 5–11, 5–12 and 5–13 show the measured and estimated marker positions, over time, for the two-seam fastball trial, P2S22. The raw data for this pitch is given in table C–1 of Appendix C. All three figures show that the measured and estimated data has the same trends and shape as expected and each figure is representative of every pitch analyzed. The residual differences between the measured and estimated marker positions was previously shown in figure 5–3. Figure 5–14 shows the entire trajectory for pitch P2S22 along with the estimated trajectory when the lift and cross-force components of the aerodynamic force is set to zero. The residuals of the center-of-mass trajectory for pitch P2S22 is shown in figure 5–4. Table 5–5 gives the final estimated parameters for pitch P2S22 and for the four-seam curve-ball, P4S22, shown in figure 5–15. The raw data for pitch P4S22 is given in table C–2 of Appendix C. Figure 5–16 shows the trajectory

residuals for pitch P4S22, and, like the P2S22 residuals, an oscillation is seen in the residuals which corresponds to the estimated angular velocity.

Table 5–5: Estimated parameters for pitches P2S22 and P4S22.
(Units are in m, m/s, deg, rev/sec or N as variable indicates)

Pitch	x_0	y_0	z_0	$\dot{x}_0$	$\dot{y}_0$	$\dot{z}_0$	α_0	β_0
P2S22	16.147	-0.047	1.930	-32.37	-0.53	-1.10	42.1	3.6
P4S22	16.036	-0.040	2.033	-34.16	-0.11	1.45	174.1	2.0
⋯	ψ_0	θ	ϕ	ω_0	C_D	C_L	C_Y	
P2S22	178.6	87.0	-1.3	54.7	0.427	0.290	0.027	
P4S22	91.2	-83.8	1.5	22.8	0.413	0.232	-0.051	

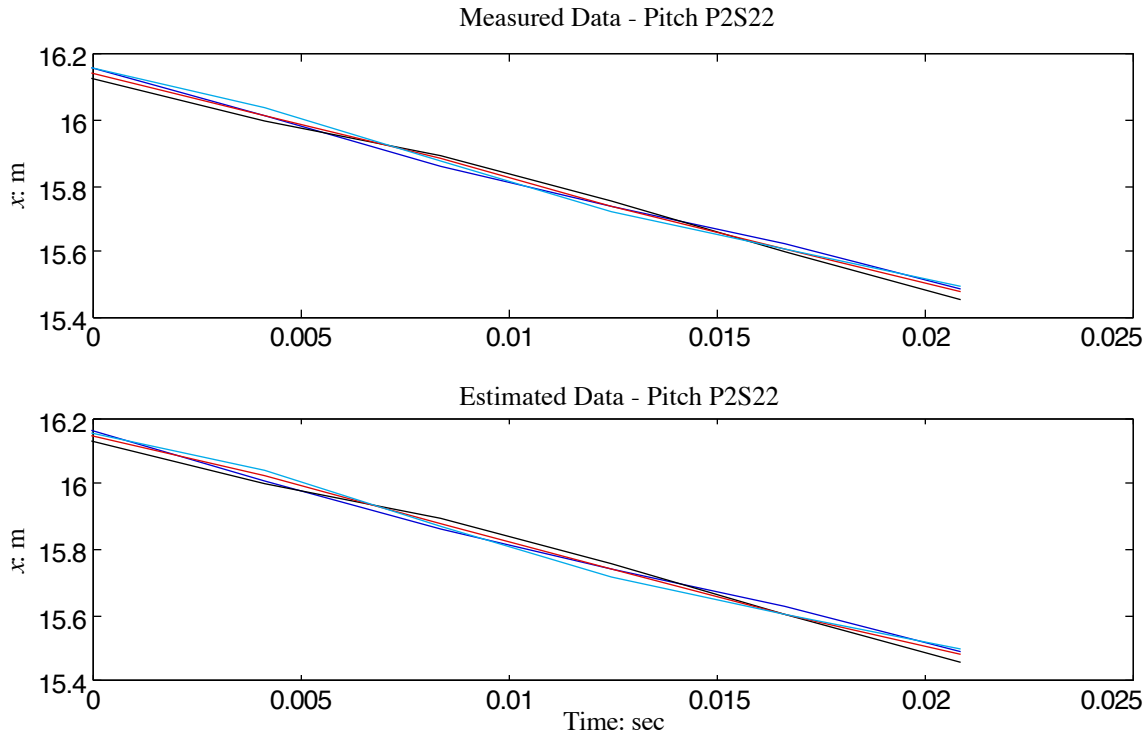

Figure 5–11: Measured and estimated x- marker positions for pitch P2S22.

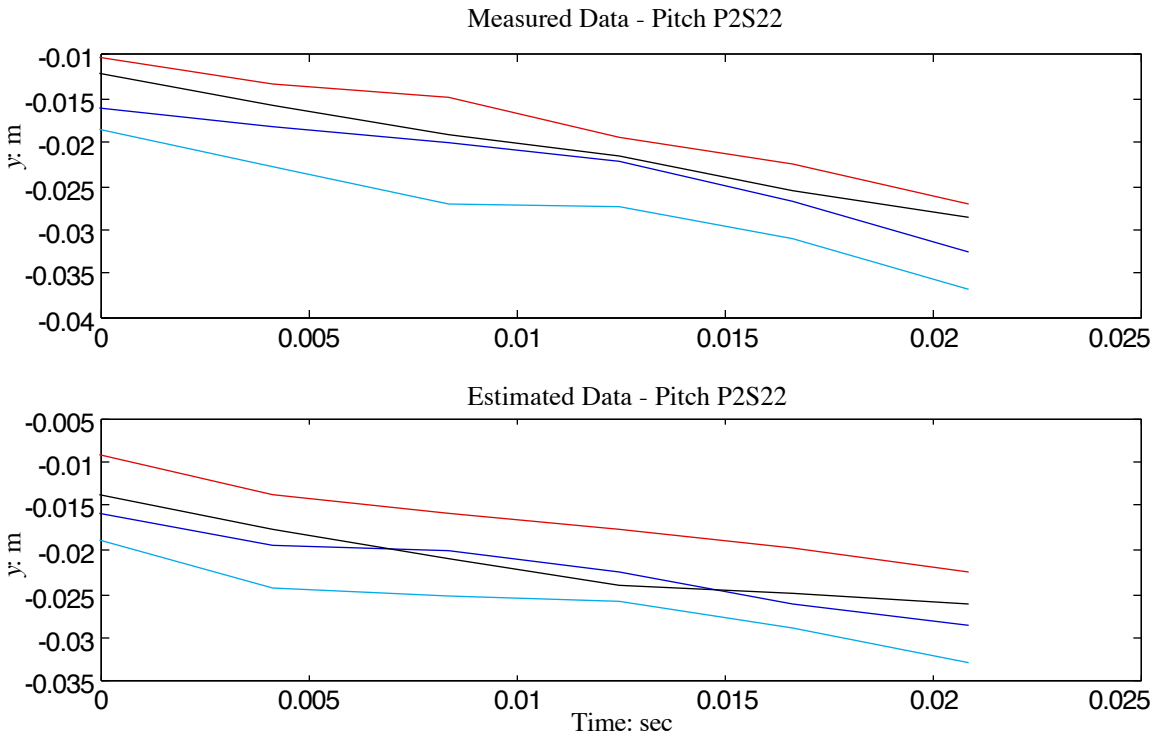

Figure 5–12: Measured and estimated *y*- marker positions for pitch P2S22.

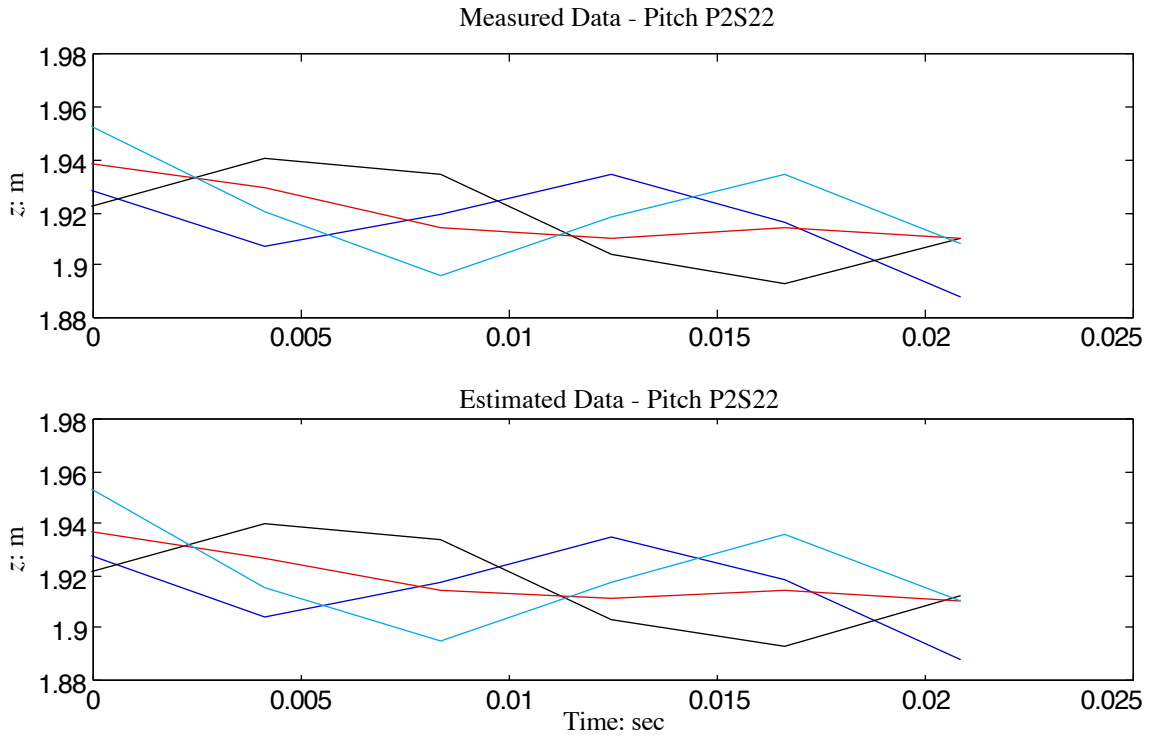

Figure 5–13: Measured and estimated *z*- marker positions for pitch P2S22.

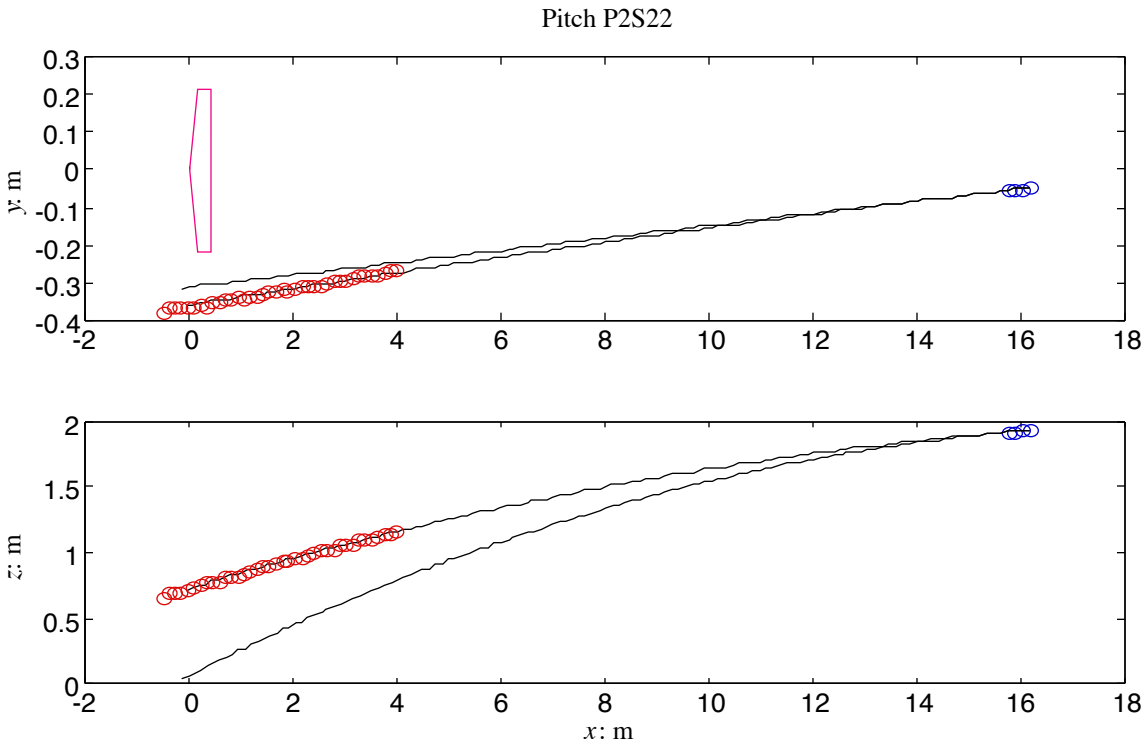

Figure 5–14: Pitch P2S22 trajectory. (The solid line represents the normal gravitational arc.)

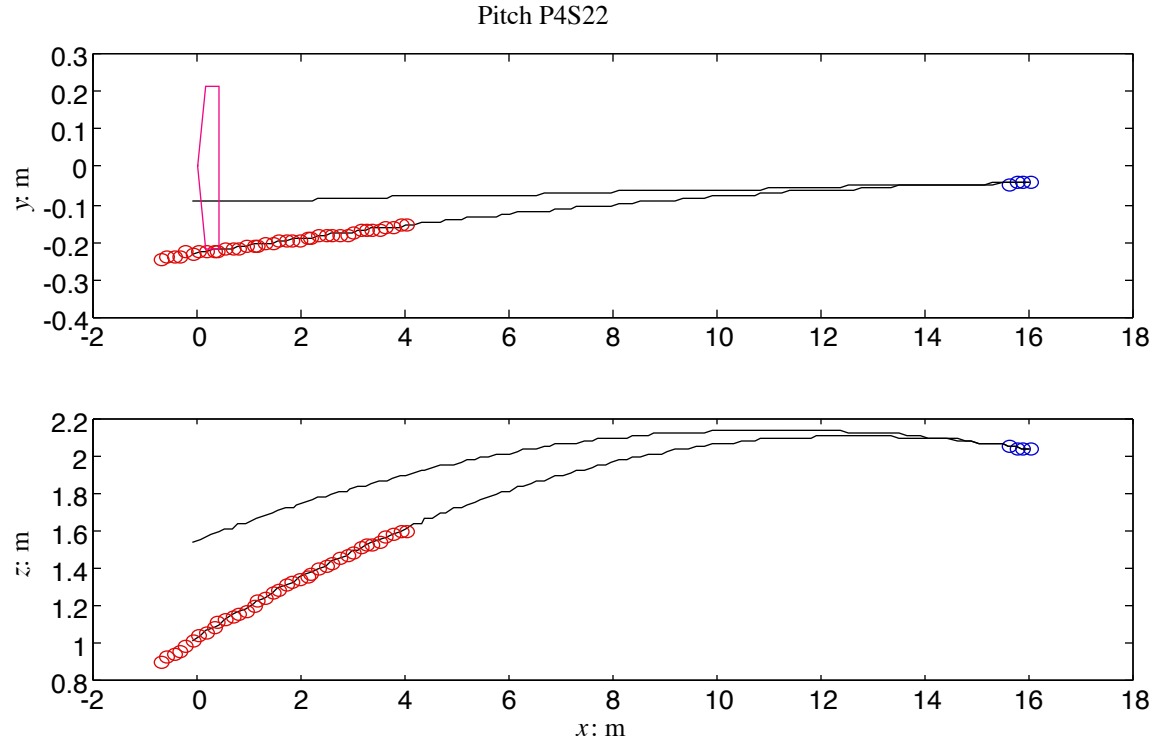

Figure 5–15: Pitch P4S22 trajectory. (The solid line represents the normal gravitational arc.)

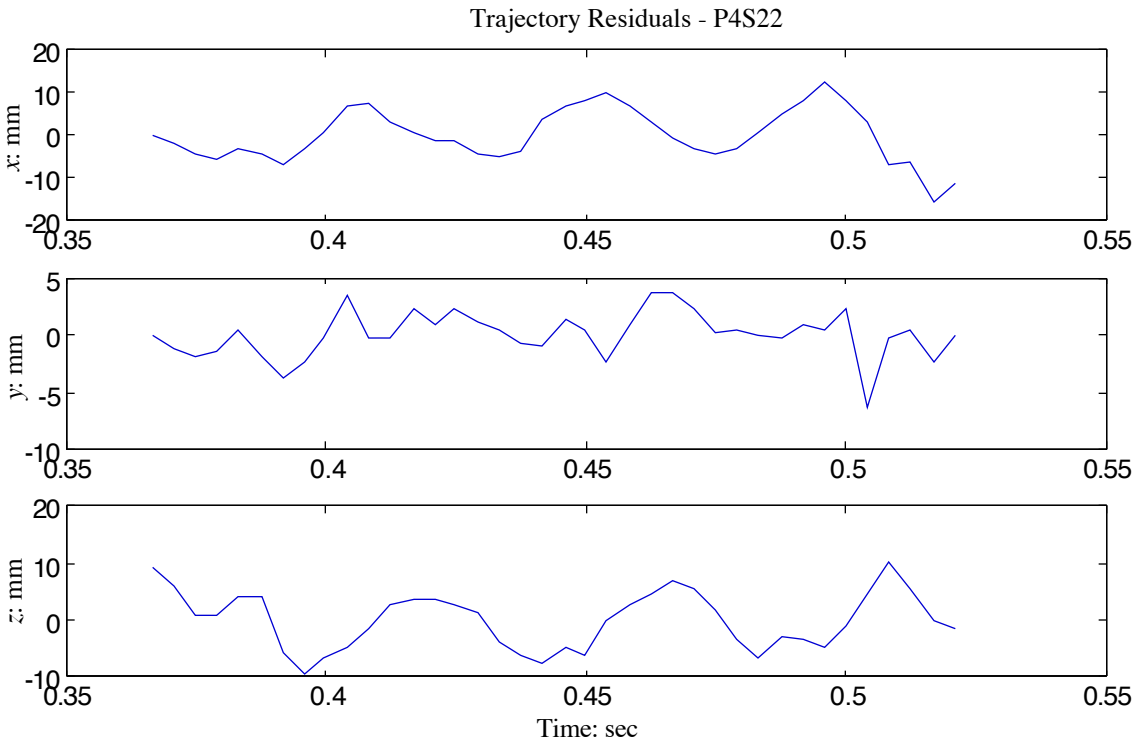

Figure 5–16: Trajectory residuals for pitch P4S22.

5.3.1.2 Lift Coefficients

Figure 5–17 shows the estimated lift coefficients versus spin parameter for the 17 two- and four-seam pitches analyzed from the pitching machine trials. The interesting feature of figure 5-17 is that there is a distinction between the two- and four-seam estimates. This is consistent with Sikorsky (Alaways & Lightfoot, 1998). However, as *S* increases the distinction is less noticeable which is consistent with the observation of Watts & Ferrer (1987). To ensure that the two sets of data in figure 5–17 were statistically significant (i.e. the two- and four-seam data did not belong to the same family) an analysis of covariance was performed on the data (see Neter, Wasserman & Kutner, 1990, p. 861). This analysis showed that the two- and four-seam data of figure 5–17 is very significant with a probability that the two sets belong to same family less than 0.01 percent.

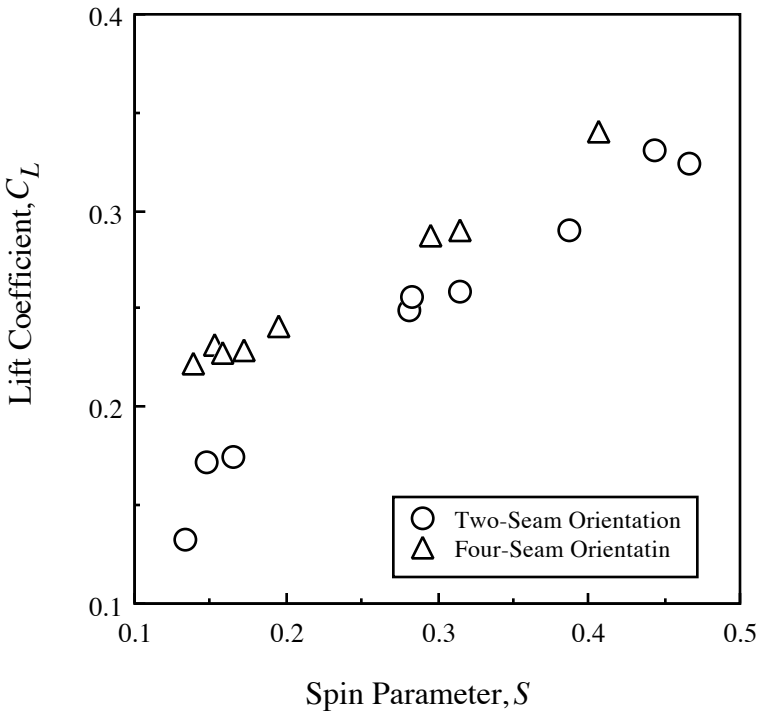

Figure 5–17: Estimated lift coefficients for the pitching machine trials.

Figure 5–18 shows the lift coefficients of figure 5–17 overlaid with the lift coefficients of Sikorsky, Watts & Ferrer and Briggs (1959). Figure 5–18 answers two questions about the previously reported lift-coefficient data. The first question concerns the Sikorsky four-seam data and the hypothesis made in chapter 2 that the decreasing slope of the four-seam lift coefficient plots seen at the spin parameter values near 0.1 is the beginning of the convergence of the two- and four-seam data. The results of this dissertation show that this hypothesis is correct and that the two- and four-seam lift coefficient results converge at higher values of S. This also explains why Watts and Ferrer could not detect any difference in lift coefficients while testing different seam orientations.

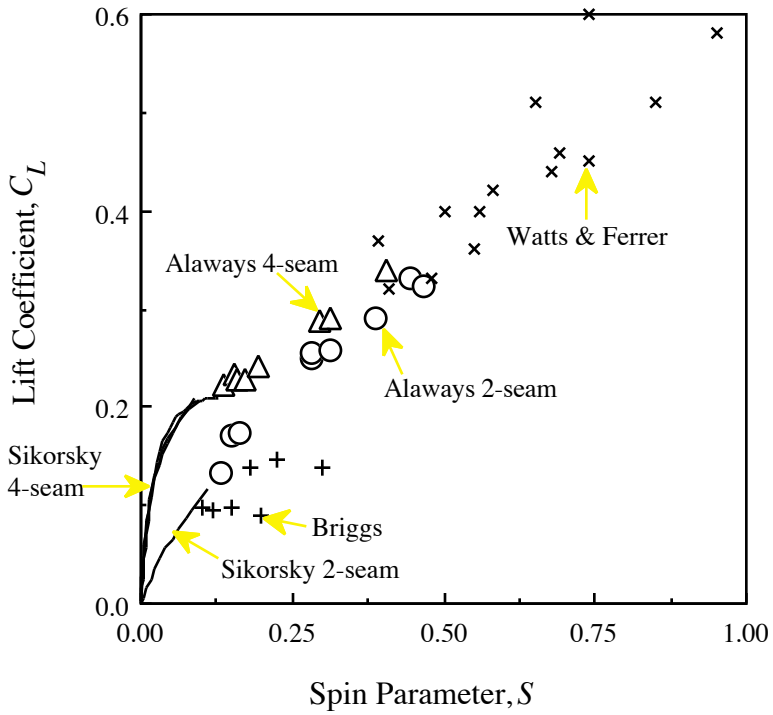

Figure 5–18: Comparison of baseball lift coefficients.

5.3.1.3 Drag Coefficients

Figure 5–19 shows the estimated drag coefficients versus Reynolds number for the 17 non-knuckleball pitches analyzed from the pitching machine trials. In general, the drag coefficients agree with those estimated from the pitcher trials.

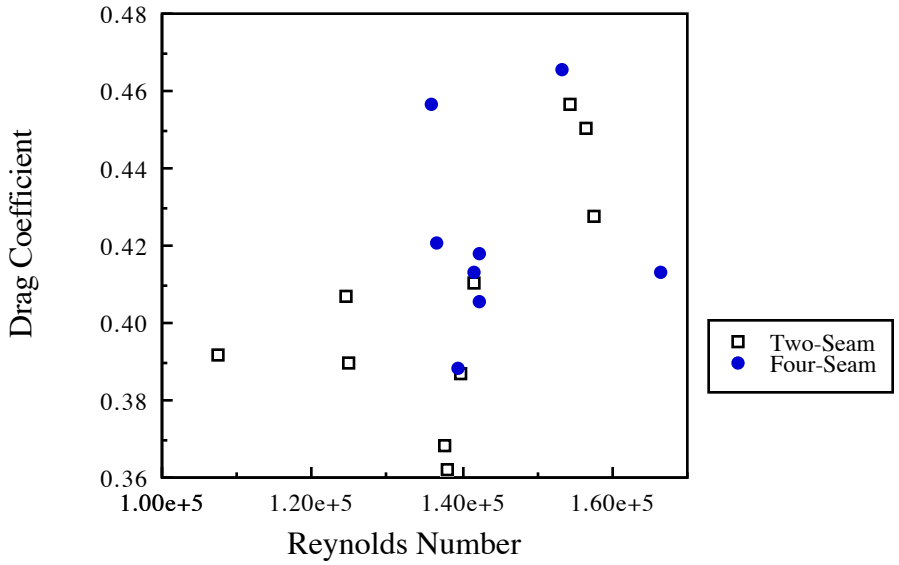

Figure 5–19: Drag coefficient versus Reynolds number for pitching machine trials.

5.3.1.4 Cross-Force

In general, due to the asymmetric design of the ball it is possible that a cross-force component in the aerodynamic force might exist as mentioned in chapter 2. The cross-force component, however, for the two- and four-seam orientations tested during the pitching machine trials is expected to be small due to symmetry in the stitching patterns in these orientations. This was found to be the case. Table 5–6 lists the cross-force, lift and drag magnitudes estimated for the non-knuckleball pitches analyzed from the pitching machine trials. Table 5–6 shows that there was only one pitch, P2S29, where the cross-force component was more than half of the lift component and in most cases the cross-force was less than 20 percent of the lift. This is not the case for the knuckleball; see section 5.4.

Table 5–6: Estimated cross-force, lift and drag magnitudes.
(For comparison, the gravitational force on the ball is 1.42 N).

Pitch	Cross-Force - N	Lift - N	Drag - N
P2S10	0.069 ± 0.007	0.680 ± 0.008	0.919 ± 0.009
P2S11	0.038 ± 0.001	0.646 ± 0.002	0.903 ± 0.002
P2S22	0.071 ± 0.001	0.612 ± 0.002	0.921 ± 0.002
P2S23	0.102 ± 0.006	0.450 ± 0.006	0.727 ± 0.006
P2S26	0.005 ± 0.006	0.293 ± 0.004	0.637 ± 0.007
P2S27	0.033 ± 0.003	0.229 ± 0.002	0.633 ± 0.004
P2S29	0.161 ± 0.010	0.307 ± 0.001	0.675 ± 0.018
P2S34	0.063 ± 0.005	0.346 ± 0.006	0.543 ± 0.006
P2S36	0.000 ± 0.007	0.343 ± 0.008	0.527 ± 0.008
P4S4	0.058 ± 0.004	0.401 ± 0.005	0.672 ± 0.005
P4S9	0.046 ± 0.011	0.454 ± 0.013	0.682 ± 0.013
P4S10	0.080 ± 0.005	0.449 ± 0.005	0.727 ± 0.005
P4S11	0.086 ± 0.004	0.653 ± 0.005	0.918 ± 0.005
P4S22	0.149 ± 0.006	0.546 ± 0.007	0.972 ± 0.007
P4S23	0.036 ± 0.004	0.424 ± 0.005	0.731 ± 0.005
P4S24	0.036 ± 0.004	0.394 ± 0.004	0.714 ± 0.004
P4S25	0.042 ± 0.004	0.390 ± 0.004	0.712 ± 0.004
MEAN	0.063 ± 0.005	0.448 ± 0.005	0.742 ± 0.006

5.3.2 Center-of-Mass Trajectories

A second analysis on the 17 non-knuckleball pitching machine pitches was conducted by estimating only the 9 parameters of equation 4–6. In this estimation the center of mass of the first four frames of data was first estimated using the method described in section 4.5.1. These estimates for the first four frames along with center-of-mass trajectory data at home plate was then used to estimate the parameters of equation 4–6. In all cases the estimate for position, velocity, lift coefficient, and drag coefficient agreed with the previous estimates when estimating all 15 parameters using the marker positions. The largest difference occurred in the azimuth and elevation angles of the spin vector, note the cross-force and lift components were combined to form a single "lift component" in the aerodynamic force.

5.3.2.1 Comparison of Results

Table 5–7 shows the estimated results for pitches P2S22 and P4S22 using both estimation procedures. Note that the trajectories and residual vectors were essentially the same for both estimations. The results for these two pitches show reasonable correlation

Table 5–7: Estimated parameters for pitches P2S22 and P4S22.
(Units are in m, m/s, deg, rev/sec or N as variable indicates)

Estimation Results for Center of Mass Trajectories									
Pitch	x_0	y_0	z_0	$\dot{x}_0$	$\dot{y}_0$	$\dot{z}_0$	ϕ	C_D	C_L
P2S22	16.147	-0.047	1.932	-32.38	-0.45	-1.11	8.1	0.427	0.294
P4S22	16.037	-0.039	2.034	-34.17	-0.11	1.44	15.3	0.414	0.238
Estimation Results for Marker Trajectories									
Pitch	x_0	y_0	z_0	$\dot{x}_0$	$\dot{y}_0$	$\dot{z}_0$	α_0	β_0	
P2S22	16.147	-0.047	1.930	-32.37	-0.53	-1.10	42.1	3.6	
P4S22	16.036	-0.040	2.033	-34.16	-0.11	1.45	174.1	2.0	
…	ψ_0	θ	ϕ	ω_0	C_D	C_L	C_Y		
P2S22	178.6	87.0	-1.3	54.7	0.427	0.290	0.027		
P4S22	91.2	-83.8	1.5	22.8	0.413	0.232	-0.051		

among all the parameters except, ϕ, the spin azimuth due to inclusion of the cross-force component in the marker trajectory estimation. Note that the cross-force in pitch P4S22 was a third of the lift, as seen in table 5–6, contributing to the 13.8 deg difference in spin azimuth.

5.3.2.2 Spin Estimates

Since the spin-rate could not be estimated directly when using the center of mass data, a range of possible spin rates were estimated from the extrapolated lift-coefficient curves in figure 2–4. Table 5–8 lists the spin-rate estimated from the marker trajectory and center-of-mass trajectory data sets, assuming that the trial was either an ideal two- or four-seam pitch. The spin-rate for the center-of-mass trajectory was determined by first

Table 5–8: Spin-rate estimates.

Pitch	Marker Estimate (rev/sec)	Two-Seam Estimate (rev/sec)	Four-Seam Estimate (rev/sec)	Percent Difference
P2S10	62.2	77.9		25.2
P2S11	64.5	75.4		16.9
P2S22	54.7	67.7		23.8
P2S23	39.9	53.7		34.6
P2S26	18.2	28.4		56.0
P2S27	16.6	18.6		12.0
P2S29	20.6	31.2		51.5
P2S34	31.6	45.6		44.3
P2S36	31.5	43.7		38.7
P4S4	21.5		17.8	–17.2
P4S9	36.1		30.7	–14.7
P4S10	38.2		31.8	–16.8
P4S11	55.7		48.4	–13.1
P4S22	22.8		22.3	–2.2
P4S23	24.9		20.8	–16.5
P4S24	20.0		17.0	–15.0
P4S25	17.6		15.7	–10.8

estimating the lift coefficient. Assuming that the pitch was either an ideal two- or four-seam pitch, the spin parameter was then determined from the extrapolated lift coefficient lines in figure 2–4. When comparing the two estimates of C_L in table 5–8 it is believed that the general shape of the two extrapolated C_L lines in figure 2–4 is correct and that the lines can be used as possible bounds in determining a range of spin-rates when only center-of-mass trajectory data is available.

5.4 Knuckleball

In addition to the 17 two- and four-seam pitches, 3 knuckleball trajectories were also acquired during the pitching machine trials. Figure 5–20 shows the trajectory of pitch P2S30 and figure 5–21 shows the residuals of the center of mass as the ball crossed over home plate. The trajectory data sets for pitches P2S30 and P4S1 are given in tables D–1 and D–2, respectively, in Appendix D.

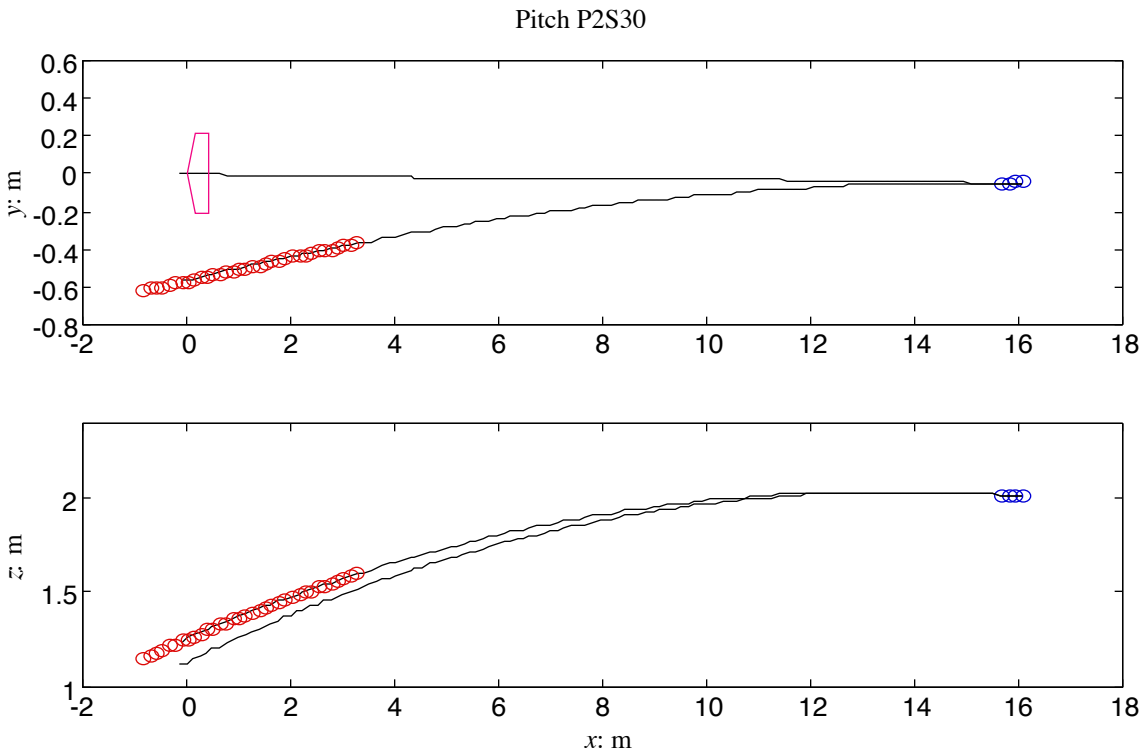

Figure 5–20: Pitch P2S30 trajectory. (The solid line represents the normal gravitational arc.)

The major difference between the knuckleballs and the other pitches analyzed was the lack of spin and high cross-force component of the aerodynamic force. The estimated

parameters for all three pitches is given in table 5–9. Notice that the spin rates were below 4.0 rev/sec and in two pitches the lift coefficient was negative.

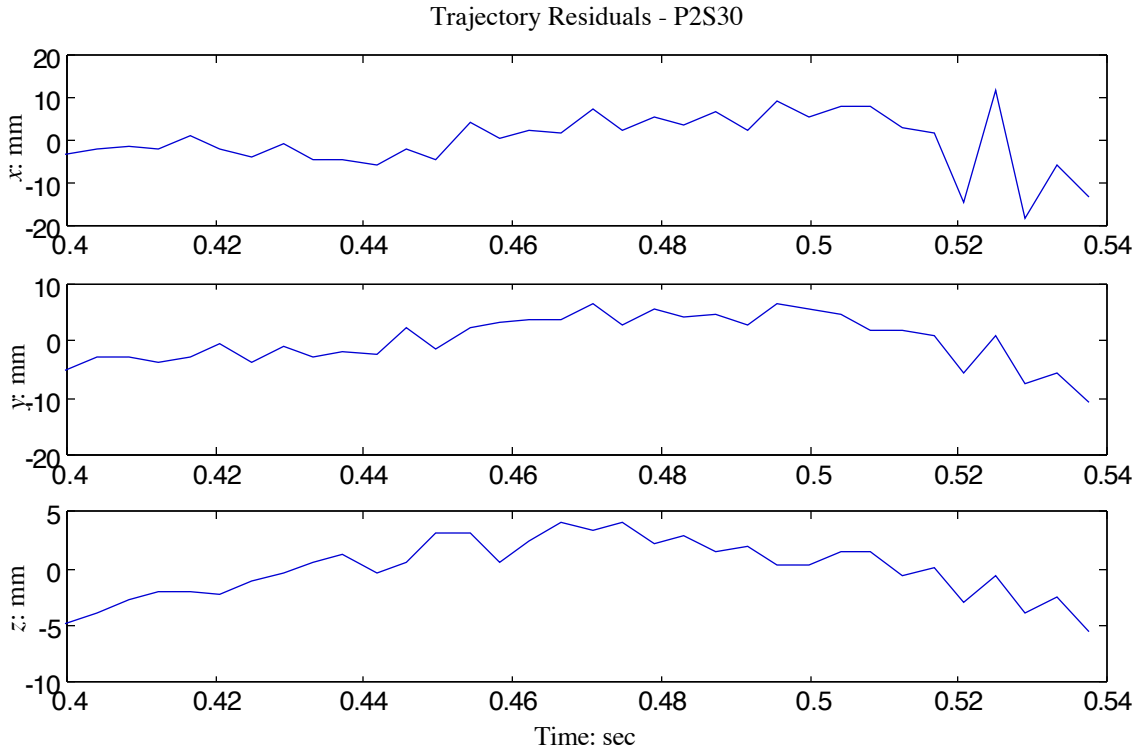

Figure 5–21: Trajectory residuals for pitch P2S30.

Table 5–9: Knuckleball estimated parameters.
(Units are in m, m/s, deg, rev/sec or N as variable indicates)

Pitch	x_0	y_0	z_0	$\dot{x}_0$	$\dot{y}_0$	$\dot{z}_0$	α_0	β_0
P2S30	16.074	-0.051	2.001	-33.61	0.09	0.70	37.3	-15.8
P2S31	15.997	-0.043	2.017	-33.47	0.22	0.06	32.64	9.3
P4S1	16.090	-0.039	2.004	-33.49	-0.54	1.49	123.9	24.5
$\cdots$	ψ_0	θ	ϕ	ω_0	C_D	C_L	C_Y	
P2S30	-166.7	173.4	-73.3	1.2	0.445	-0.261	-0.062	
P2S31	144.2	-88.5	-25.9	4.0	0.418	-0.200	-0.087	
P4S1	143.5	174.8	9.0	3.9	0.447	0.0	0.015	

Table 5–10 lists the magnitude of the cross-force, lift and drag components of the aerodynamic force for all three knuckleball pitches. For these pitches the cross-force component was 16 to 25 percent of the drag component for all three pitches and in one case the lift component was equal to zero. This shows that the asymmetric stitch configuration can play a significant role in the trajectory of the ball. Note that the cross-force component

of pitch P2S29, a two-seam curve, is nearly equal to the cross-force magnitudes estimated here and therefore, other asymmetries may also occur in baseball.

Table 5–10: Estimated cross-force, lift and drag magnitudes for knuckleball pitches. (For comparison, the gravitational force on the ball is 1.42 N).

Pitch	Cross-Force - N	Lift - N	Drag - N
P2S30	0.177 ± 0.011	0.531 ± 0.013	1.003 ± 0.014
P2S31	0.244 ± 0.007	0.451 ± 0.046	0.954 ± 0.006
P4S1	0.166 ± 0.012	0.000 ± 0.014	0.993 ± 0.007
MEAN	0.196 ± 0.010	0.327 ± 0.024	0.983 ± 0.009

5.5 Discussion

The present major findings are those involving the aerodynamic parameters of the ball in the flight and that the method to accurately measure the spin of the baseball was successful. The two most interesting findings concern the lift and drag coefficients for the baseball and are discussed here in more detail.

5.5.1 Lift Coefficients

The major contribution of this research was the finding that the lift coefficient is strongly dependent on the seam orientation at the lower values of the spin parameter as shown in figure 5–18. However, the convergence of the lift coefficients at higher spin parameters was not initially anticipated before this study. The correlation with the Sikorsky (Alaways & Lightfoot, 1998) and the Watts & Ferrer (1987) data validates the current results.

5.5.2 Drag Coefficients

Figure 5–22 is a comparison of all the drag coefficients versus Reynolds numbers determined. These estimates suggest that the roughness ratio of the baseball is not only less than that of the golf-ball but that the baseball should definitely not be considered smooth. One of the things to note is that no indication of the drag crisis occurred in this data but no data was acquired at the higher release velocities that occur in the Major League.

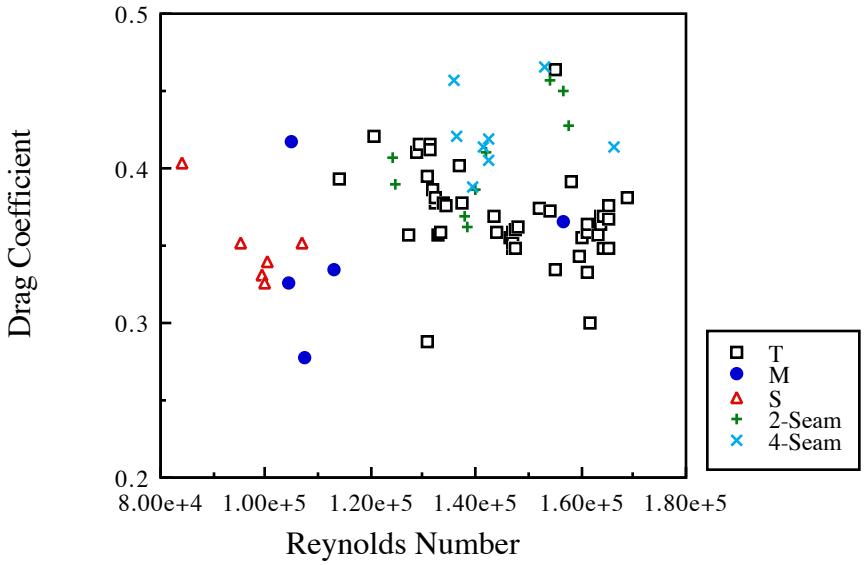

Figure 5–22: Estimated drag coefficients versus Reynolds number.

5.5.3 Rising Softballs

In baseball there is misnomer of the so called “rising fastball”. In table 5–6, the largest value of lift found in the pitching machine study was only 48 percent of the gravitational force acting on the ball. For pitch P2S22, for example, the lift to weight ratio was 0.43. It is of scientific curiosity to see what this ratio would be for a softball given the same initial conditions as pitch P2S22 (i.e. translational velocity and spin rate of 32.39 m/s and 54.7 rev/sec (343.69 rad/sec), respectively).

Let us assume that the lift coefficient results, shown in figure 5–18, are also valid for the softball. The diameter and mass of a softball are 3.8 in (9.7 cm) and 0.188 kg, respectively. For the initial conditions given above, the spin parameter is 0.51 corresponding to a lift coefficient of 0.35 from figure 5–18. Assuming an ambient air temperature of 70 ˚F and that ω and $\mathbf{V}$ are perpendicular, the lift component on the softball is equal to 1.63 N from equation 2–12 or a lift to weight ratio of 0.88, nearly twice as high as for the baseball. For a 100 mph (44.26 m/s) pitch with the same spin rate, the lift to weight ratio increases to 1.32 for a softball.

CHAPTER 6 – CONCLUSION

The objective was to show how spin influences the curve and to determine the aerodynamic parameters that influence the flight of pitched baseballs. This was achieved by measuring the position of markers on pitched baseballs, developing kinematic and aerodynamic models, and using parameter estimation to determine the initial conditions and other unknown aerodynamic parameters that influence the trajectory of the pitch.

Figure 6–1 shows the lift coefficient versus spin parameter determined for 17 pitches overlaid with results from the previous research of Sikorsky (Always and Lightfoot, 1998), Briggs (1959) and Watts & Ferrer (1987). The results from this dissertation correlate very well with the data of Sikorsky and Watts & Ferrer, showing that seam orientation does have strong influence on lift coefficient at lower values of spin parameter and that the seam orientation influence decreases with increasing spin parameter.

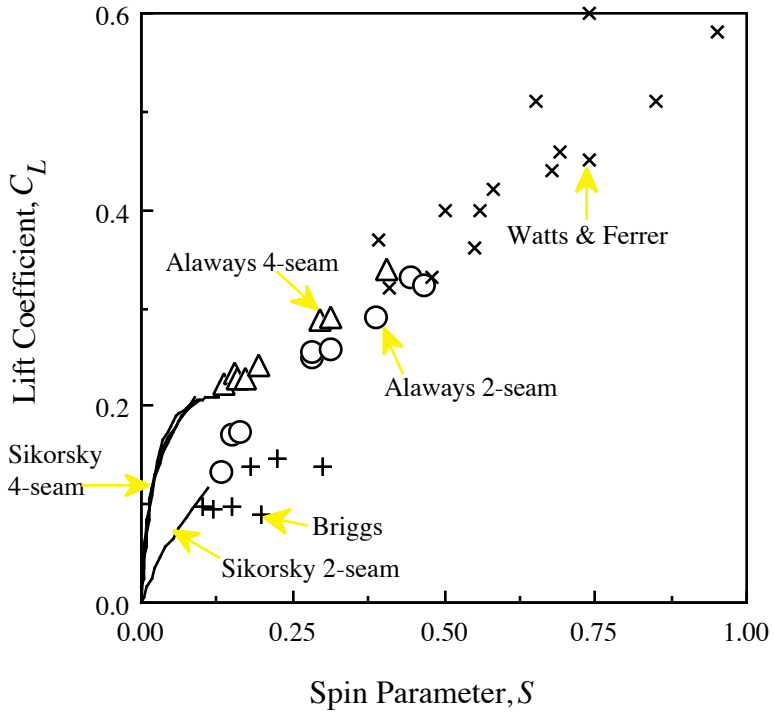

Figure 6–1: Comparison of baseball lift coefficients.

Figure 6–2 shows the estimated drag coefficients versus Reynolds number for all the baseball trials, the measured golf-ball drag coefficients of Smits and Smith (1994) and a straight line approximation of the smooth sphere curve of figure 1–8. These estimates indicate that the baseball is not a smooth sphere and that the baseball's roughness ratio is less than the golf-ball's.

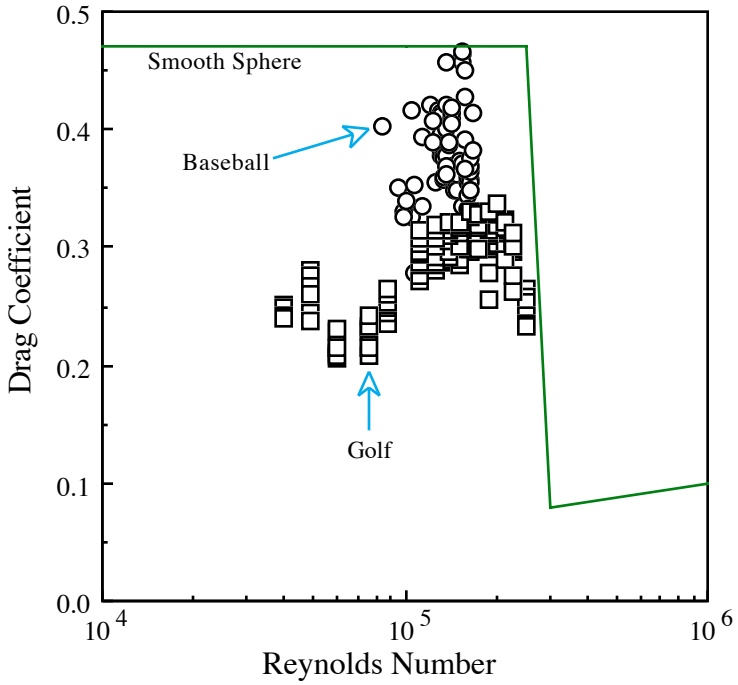

Figure 6–2: Baseball, golf-ball and smooth sphere drag coefficients versus Reynolds number.

The aerodynamic cross-force component was estimated and in the pure two- and four-seam pitch orientation the cross-force plays a minor role in the aerodynamic force. (However, for the knuckleball the cross-force component may play a major role).

Comparison between marker trajectory results and center of mass trajectory results show that additional information on the ball seam orientation is needed to determine the spin rate from the center-of-mass-only trajectory data. However, a range of spin rates and corresponding spin parameter can be determined and all other parameters (besides cross-force) accurately can be estimated. For the pitchers used for this dissertation the spin parameter was found to be in the range $0.05 < S < 0.68$.

In conclusion, key aerodynamic parameters along with the initial conditions of pitched baseballs were estimated using acquired center of mass and marker trajectory position data. The major results of this study are:

i). Seam orientation has a strong influence on the lift of the ball at lower values of spin parameter.

ii). Baseball drag coefficients lie between the smooth non-rotating sphere and golf-ball drag coefficients.

iii). An aerodynamic cross-force component does exist and, though it doesn't play a major role in the two- and four-seam spin orientations due to the symmetry of the ball, it could play a larger role than anticipated in pitches with random seam orientations and low spin parameter.

CHAPTER 7 – REFERENCES

Abdel-Aziz, Y.I. and H.M. Karara. 1971. Direct Linear Transformation from Comparator Coordinates into Object Space Coordinates in Close-Range Photogrammetry. In ASP Symposium on Close Range Photogrammetry. Falls Church, VA.: American Society of Photogrammetry.

Achenbach, E. 1974. The Effects of Surface Roughness and Tunnel Bloackage on the Flow Past Spheres. Journal of Fluid Mechanics 65 (part 1): 113–125.

Adair, R.K. 1990. The Physics of Baseball. New York: Harper and Row.

Alaways, L.W., M. Hubbard, T.M. Conlan, and J.A. Miles. 1996. Static and Dynamic Accuracy Determination of a Three-Dimensional Motion Analysis System. In 1st International Conference on the Engineering of Sport, ed. Steve Haake. Sheffield, United Kingdom: A.A. Balkema.

Alaways, L.W. and R.B. Lightfoot. 1998. Aerodynamics of a Curveball: The Sikorsky Lift Data. Sports Engineering Submitted November 1998.

Allman, W.F. 1981. Dance of the Curve. Science81, October, 90-91.

Allman, W.F. 1982. Pitching Rainbows: The Untold Physics of the Curve Ball. Science82, October, 32-39.

Barkla, H.M. and L.J. Auchterlonie. 1971. The Magnus or Robins Effect on Rotating Spheres. Journal of Fluid Mechanics 47 (3): 437-447.

Baseball's Curve Balls: Are They Optical Illusions. 1941. Life 11 (11): 83-89.

Bearman, P.W. and J.K. Harvey. 1976. Golf Ball Aerodynamics. Aeronaut. Q. 27: 112-122.

Brancazio, P.J. 1997. The Physics of a Curveball. Popular Mechanics 174 (10): 56-57.

Brender, M.Y. 1995. A Bobsled Dynamic Model and Its Experimental Validation. Master's Thesis, University of California, Davis.

Briggs, L.J. 1959. Effect of Spin and Speed on the Lateral Deflection (Curve) of a Baseball; and the Magnus Effect for Smooth Spheres". Am. J. Phys. 27: 589-596.

Burden, R.L., J.D. Faires, and A.C. Reynolds. 1981. Numerical Analysis. Boston, MA: Prindle, Weber & Schmidt.

Camera and Science Settle the Old Rhubarb About Baseball's Curve Ball. 1953. Life 35 (4): 104-107.

Cohane, T. 1949. Visual Proof that a Baseball Curves. Look, July 19, 74-77.

Cole, G.H.A. 1962. Fluid Dynamics. New York: John Wiley & Sons Inc.

Cummings, W.A. *n.d.* (ca. 1900) How I Pitched the First Curve. Baseball Magazine: (Archived at the National Baseball Hall of Fame) : 21-22.

Davies, J.M. 1949. The Aerodynamics of Golf Balls. Journal of Applied Physics 20: 821-828.

de Mestre, N. 1990. The Mathematics of Projectiles in Sport. Australian Mathematical Society Lecture Series. Cambridge: Cambridge University Press.

Drury Jr., J.F. 1953. The *Hell* It Don't Curve! The American Mercury, May, 101-106.

Frohlich, C. 1984. Aerodynamic Drag Crisis and its Possible Effect on the Flight of Baseballs. Am. J. Phys. 52 (4): 325-334.

Gelb, A. 1974. Applied Optimal Estimation. Cambridge, MA: MIT Press.

Gill, P.E., W. Murray, and M.H. Wright. 1981. Practical Optimization. New York: Academic Press.

Gutman, D. 1995. Banana Bats and Ding-Dong Balls. New York: Macmillan.

Hoerner, S.F. 1965. Fluid-Dynamic Drag. Midland Park, NJ.: by the author.

Hollenberg, J.W. 1986. Secrets of the Knuckleball. The Bent of Tau Beta Pi (Fall): 26-30.

Houghton, E.L. and N.B. Carruthers. 1982. Aerodynamics for Engineering Students. London: Edward Arnold.

Houston, N. 1941. Department of Amplification: Letter to the Editor. The New Yorker, July 5, 48.

Hubbard, M. and L.W. Alaways. 1989. Rapid and Accurate Estimation of Release Conditions in the Javelin Throw. Journal of Biomechanics 22 (6/7): 583-595.

Kaat, J. 1997. The Mechanics of a Breaking Pitch. Popular Mechanic 174 (10): 52-57.

Kane, T.R., P.W. Likins, and D.A. Levison. 1983. Spacecraft Dynamics. New York: McGraw-Hill Book Co.

Kaufman, W. 1963. Fluid Mechanics. Translated by E.G. Chilton. New York: McGraw–Hill Book Company, Inc.

Kinst, E.,"Ball Bat," Patent No. 430,388, Patented June 17, 1890, U.S. Patent and Trademark Office.

Koff, D.G. 1990. Accuracy and Precision of the *ExpertVision* 3-D Motion Analysis System. Unpublished Report, Motion Analysis Corporation.

Maccoll, J.W. 1928. Aerodynamics of a Spinning Sphere. The Journal of the Royal Aeronautical Society 28: 777-798.

Madden, R.W. 1941. Our Skeptical Correspondents: Letter to the Editor. The New Yorker, May 24, 61-67.

McKenna, J.E. and A.M. Baker,"Base Ball Curver," Patent No. 385,816, Patented July 10, 1888, U.S. Patent and Trademark Office.

Mehta, R.D. 1985. Aerodynamics of Sports Balls. Annual Review of Fluid Mechanics 17: 151-189.

Mercurio, J.A. 1990. Record Profiles of Baseball's Hall of Famers. New York: Harper & Row, Publishers, Inc.

Mozley, A.V., R.B. Haas, and F. Forster-Hahn. 1972. Eadweard Muybridge: The Stanford Years, 1872-1882. Stanford, CA.: Department of Art, Stanford University.

Neter, J., W. Wasserman, and M.H. Kutner. 1990. Applied Linear Statistical Models: Regression, Analysis of Variance and Experimental Designs. 3rd ed., Burr Ridge, Illinois: Richard D. Irwin, Inc.

Newton, I. 1671. New Theory about Light and Colors. Philosophical Transactions of the Royal Society 6: 3078.

Prindle, E.J. 1888. The Art of Curve Pitching. Philadelphia: A.J. Reach Co.

Quigley, M. 1984. The Crooked Pitch: The Curveball in American Baseball History. Chapel Hill, NC: Algonquin Books.

Ranger, K.B. 1996. Time-Dependent Decay of the Motion of a Sphere Translating and Rotating in a Viscous Liquid. Quarterly Journal of Mechanics and Applied Mathematics 49 (4): 621-633.

Lord Rayleigh. 1877. On the Irregular Flight of a Tennis Ball. Messenger of Mathematics 7: 14-16.

Resnick, R. and D. Halliday. 1977. Physics. New York: John Wiley & Sons.

Roberson, J.A. and C.T. Crowe. 1980. Engineering Fluid Mechanics. Boston: Houghton Mifflin Company.

Rubinow, S.I. and J.B. Keller. 1961. The Transverse Force on a Spinning Sphere Moving in a Viscous Fluid. Journal of Fluid Mechanics 11 (part 3): 447-459.

Selin, C.W. 1957. An Analysis of the Aerodynamics of Pitched Baseballs. Doctoral Dissertation, State University of Iowa.

Smits, A.J. and D.R. Smith. 1994. A New Aerodynamic Model of a Golf Ball in Flight. In The 1994 World Scientific Congress of Golf, ed. A J Cochran and M R Farrally:340-347. St. Andrews, UK: E & FN Spon.

Spalding, A.G. 1992. America's National Game. Lincoln and London: University of Nebraska Press. Original edition, New York: American Sports Pub. Co., 1911.

Tait, P.G. 1896. On the Path of a Rotating Spherical Projectile. Trans. R. Soc. Edinburgh 39 Part 2 (16): 491-506.

Verwiebe, F.L. 1942. Does a Baseball Curve? Am. J. Phys. 10 (2): 119-120.

Walton, J.S. 1981. Close-Range Cine-Photogrammetry: A Generalized Technique for Quantifying Gross Human Motion. Doctoral Dissertation, Pennsylvania State University.

Walton, J.S. 1994. Imaged-Based Motion Measurement: New Technology, New Applications. In 21st International Congress on High-Speed Photography and Photonics, 2513:862-880. Taejon, Korea: Society of Photo-Optical Instrumentation Engineers (SPIE).

Watts, R.G. and A.T. Bahill. 1990. Keep Your Eye On The Ball. New York: W.H. Freeman and Company.

Watts, R.G. and R. Ferrer. 1987. The Lateral Force on a Spinning Sphere: Aerodynamics of a Curveball. Am. J. Phys. 55 (1): 40-44.

Weast, R.C., ed. 1982. CRC Handbook of Chemistry and Physics. Boca Raton, Florida: CRC Press, Inc.

APPENDIX A – PITCH IDENTIFICATION

In table A–1, "outside" is in the positive *y* direction, and the code letters, C, CU, FB, 2S and 4S are abbreviations for curve, change-up, fastball, two-seam, and four-seam, respectively.

Table A–1: Pitch type and comments for pitcher, T.

Pitch #	Pitch Type	Comments/Outcome	Pitch #	Pitch Type	Comments/Outcome
T1	—	Low, Outside	T25	FB – 4S	Tail to right
T2	—	Outside	T26	CU	Bad
T3	—	—	T27	CU	Good Downward
T4	—	Outside	T28	FB – 2S	—
T5	—	—	T29	FB – 2S	Average
T6	C	Low, Good	T30	CU	Good
T7	—	—	T31	FB – 4S	Fast
T8	FB – 2S	Low, Outside	T32	FB – 4S	Normal
T9	CU	—	T33	FB – 2S	Good Tail In
T10	C	Low	T34	FB – 2S	—
T11	C	Slow	T35	C	Down
T12	C	Average	T36	C	Bad, Outside
T13	C	Low	T37	C	—
T14	FB – 4S	—	T38	C	Good
T15	CU	Good Movement	T39	—	—
T16	FB – 2S	Good Movement	T40	C	Average
T17	CU	Average	T41	FB	—
T18	CU	Outside	T42	FB	—
T19	C	Lazy	T43	CU	—
T20	C	A bit better than T19	T44	FB – 2S	Good
T21	CU	Good	T45	FB – 2S	Normal
T22	FB - 2S	Average	T46	FB – 2S	Normal
T23	C	Slow	T47	C	Average
T24	C	Average			

Table A–2: Pitch number, wheel speeds and pitch type for two-seam pitching machine trials. (Bold face indicates pitches that were analyzed)

Pitch #	Top Wheel Speed Setting	Bottom Wheel Speed Setting	Pitch Type
P2S1	10	3	Curve
P2S2	10	3	Curve
P2S3	10	3	Curve
P2S4	10	3	Curve
P2S5	10	3	Curve
P2S6	10	3	Curve
P2S7	10	3	Curve
P2S8	10	3	Curve
P2S9	10	3	Curve
P2S10	**10**	**4**	**Curve**
P2S11	**10**	**4**	**Curve**
P2S12	10	5	Curve
P2S13	10	6	Curve
P2S14	10	7	Curve
P2S15	10	10	Knuckle
P2S16	10	10	Knuckle
P2S17	8	10	Fast
P2S18	8	10	Fast
P2S19	8	10	Fast
P2S20	6	10	Fast
P2S21	4	10	Fast
P2S22	**4**	**10**	**Fast**
P2S23	**4**	**8**	**Fast**
P2S24	4	8	Fast
P2S25	4	6	Fast
P2S26	**5**	**7**	**Fast**
P2S27	**5**	**7**	**Fast**
P2S28	7	5	Curve
P2S29	**7**	**5**	**Curve**
P2S30	**7**	**7**	**Knuckle**
P2S31	**7**	**7**	**Knuckle**
P2S32	4	6	Fast
P2S33	4	6	Fast
P2S34	**4**	**7**	**Fast**
P2S35	**4**	**7**	**Fast**
P2S36	4	7	Fast

Table A–3: Pitch number, wheel speeds and pitch type for four-seam pitching machine trials. (Bold face indicates pitches that were analyzed)

Pitch #	Top Wheel Speed Setting	Bottom Wheel Speed Setting	Pitch Type
P4S1	**7**	**7**	**Knuckle**
P4S2	7	7	Knuckle
P4S3	7	5	Curve
P4S4	**7**	**5**	**Curve**
P4S5	5	7	Fast
P4S6	5	7	Fast
P4S7	5	7	Fast
P4S8	4	6	Fast
P2S9	4	8	Fast
P4S10	**4**	**8**	**Fast**
P4S11	**4**	**10**	**Fast**
P4S12	4	10	Fast
P4S13	6	10	Fast
P4S14	6	10	Fast
P4S15	8	10	Fast
P4S16	8	10	Fast
P4S17	10	10	Knuckle
P4S18	10	8	Curve
P4S19	10	8	Curve
P4S20	10	6	Curve
P4S21	10	6	Curve
P4S22	**8**	**6**	**Curve**
P4S23	**7**	**5**	**Curve**
P4S24	**7**	**5**	**Curve**
P4S25	**7**	**5**	**Curve**
P4S26	8	6	Curve
P4S27	8	6	Curve
P4S28	8	5	Curve
P4S29	8	5	Curve
P4S30	8	5	Curve
P4S31	6	4	Curve
P4S32	6	4	Curve
P4S33	4	6	Fast
P4S34	4	6	Fast
P4S35	4	6	Fast

APPENDIX B – PITCHER DATA

Table B–1: Center-of-mass trajectory data for pitch T6.
(Missing data is assigned the value of -99.9)

Frame	Time	X	Y	Z
140	0.579	11.43397	0.46076	2.13829
141	0.583	11.32138	0.47059	2.11146
142	0.588	-99.9	-99.9	-99.9
143	0.592	-99.9	-99.9	-99.9
144	0.596	-99.9	-99.9	-99.9
145	0.600	-99.9	-99.9	-99.9
146	0.604	10.76018	0.44514	2.10417
147	0.608	10.65487	0.45248	2.08305
148	0.613	10.53763	0.44326	2.07864
149	0.617	-99.9	-99.9	-99.9
150	0.621	-99.9	-99.9	-99.9
151	0.625	-99.9	-99.9	-99.9
152	0.629	10.09500	0.43881	2.05873
153	0.633	9.99345	0.45553	2.04970
154	0.638	9.87141	0.46063	2.02945
155	0.642	-99.9	-99.9	-99.9
156	0.646	-99.9	-99.9	-99.9
157	0.650	-99.9	-99.9	-99.9
158	0.654	9.43763	0.43375	2.00967
159	0.658	9.32054	0.43483	1.98180
160	0.663	9.20898	0.42112	1.97490
161	0.667	-99.9	-99.9	-99.9
162	0.671	-99.9	-99.9	-99.9
163	0.675	-99.9	-99.9	-99.9
164	0.679	-99.9	-99.9	-99.9
165	0.683	8.65972	0.42256	1.92976
166	0.688	8.55395	0.41766	1.91960
167	0.692	-99.9	-99.9	-99.9
168	0.696	-99.9	-99.9	-99.9
169	0.700	-99.9	-99.9	-99.9
170	0.704	-99.9	-99.9	-99.9
171	0.708	8.00128	0.36507	1.85974
172	0.713	7.89465	0.39832	1.85036
173	0.717	7.78559	0.43686	1.83334
174	0.721	-99.9	-99.9	-99.9
175	0.725	-99.9	-99.9	-99.9
176	0.729	-99.9	-99.9	-99.9
177	0.733	7.35727	0.39645	1.79918
178	0.738	7.24725	0.39468	1.77392
179	0.742	7.13244	0.41443	1.75750
180	0.746	-99.9	-99.9	-99.9
181	0.750	-99.9	-99.9	-99.9
182	0.754	-99.9	-99.9	-99.9
183	0.758	6.70849	0.36691	1.71986
184	0.763	6.58461	0.34793	1.68808
185	0.767	6.47634	0.36888	1.66785
186	0.771	6.35959	0.36043	1.65970
187	0.775	-99.9	-99.9	-99.9
188	0.779	-99.9	-99.9	-99.9
189	0.783	6.04199	0.31122	1.62331
190	0.788	5.93141	0.33227	1.60832
191	0.792	5.82119	0.32651	1.57724
192	0.796	5.71251	0.34856	1.57152
193	0.800	5.60029	0.32185	1.54345
194	0.804	-99.9	-99.9	-99.9
195	0.808	-99.9	-99.9	-99.9

Table B–1 (Continued): Center-of-mass trajectory data for pitch T6.
(Missing data is assigned the value of -99.9)

Frame	Time	X	Y	Z
196	0.813	5.29315	0.29371	1.51512
197	0.817	5.18673	0.31750	1.48592
198	0.821	5.07296	0.32132	1.47502
199	0.825	4.94695	0.28664	1.45946
200	0.829	-99.9	-99.9	-99.9
201	0.833	4.74401	0.24784	1.42017
202	0.838	4.65413	0.27959	1.41151
203	0.842	4.54213	0.28378	1.38671
204	0.846	4.43878	0.29441	1.37220
205	0.850	-99.9	-99.9	-99.9
206	0.854	-99.9	-99.9	-99.9
207	0.858	4.10680	0.23371	1.32503
208	0.863	4.02890	0.26828	1.30735
209	0.867	3.90705	0.26044	1.27986
210	0.871	3.80154	0.26474	1.25432
211	0.875	-99.9	-99.9	-99.9
212	0.879	-99.9	-99.9	-99.9
213	0.883	-99.9	-99.9	-99.9
214	0.888	-99.9	-99.9	-99.9
215	0.892	3.27295	0.22616	1.16621
216	0.896	3.16200	0.23090	1.13631
217	0.900	-99.9	-99.9	-99.9
218	0.904	-99.9	-99.9	-99.9
219	0.908	-99.9	-99.9	-99.9
220	0.913	-99.9	-99.9	-99.9
221	0.917	2.63959	0.19538	1.04587
222	0.921	2.53622	0.18849	1.01722
223	0.925	2.42952	0.21507	0.99764
224	0.929	-99.9	-99.9	-99.9
225	0.933	-99.9	-99.9	-99.9
226	0.938	-99.9	-99.9	-99.9
227	0.942	2.01539	0.15949	0.91790
228	0.946	1.90658	0.15611	0.88336
229	0.950	-99.9	-99.9	-99.9
230	0.954	-99.9	-99.9	-99.9
231	0.958	-99.9	-99.9	-99.9
232	0.963	-99.9	-99.9	-99.9
233	0.967	1.39658	0.11799	0.77455
234	0.971	1.27844	0.12536	0.74894
235	0.975	1.17597	0.12374	0.72148
236	0.979	-99.9	-99.9	-99.9
237	0.983	-99.9	-99.9	-99.9
238	0.988	-99.9	-99.9	-99.9
239	0.992	0.77587	0.08862	0.63035
240	0.996	-99.9	-99.9	-99.9
241	1.000	-99.9	-99.9	-99.9
242	1.004	-99.9	-99.9	-99.9
243	1.008	-99.9	-99.9	-99.9
244	1.013	-99.9	-99.9	-99.9
245	1.017	-99.9	-99.9	-99.9
246	1.021	0.03605	0.04820	0.45839
247	1.025	-0.06872	0.05759	0.42401

Table B–2: Center-of-mass trajectory data for pitch T33.
(Missing data is assigned the value of -99.9)

Frame	Time	X	Y	Z
126	0.521	11.14356	0.04624	1.76444
127	0.525	11.00963	0.08762	1.76964
128	0.529	10.87838	0.07057	1.74844
129	0.533	-99.9	-99.9	-99.9
130	0.538	10.58719	0.10652	1.71844
131	0.542	-99.9	-99.9	-99.9
132	0.546	-99.9	-99.9	-99.9
133	0.550	10.16236	0.09748	1.69604
134	0.554	10.03625	0.10448	1.67254
135	0.558	9.88410	0.08090	1.67721
136	0.563	9.76390	0.09200	1.66582
137	0.567	9.60961	0.00207	1.63236
138	0.571	9.47486	0.10509	1.64410
139	0.575	9.34457	0.08558	1.60729
140	0.579	-99.9	-99.9	-99.9
141	0.583	9.04884	0.07964	1.60011
142	0.588	8.92496	0.08318	1.58286
143	0.592	-99.9	-99.9	-99.9
144	0.596	8.64787	0.09402	1.57869
145	0.600	8.52574	0.08225	1.55241
146	0.604	8.35946	-0.00934	1.51989
147	0.608	8.23434	0.07295	1.51467
148	0.613	-99.9	-99.9	-99.9
149	0.617	-99.9	-99.9	-99.9
150	0.621	7.82848	0.09528	1.49445
151	0.625	7.70670	0.10369	1.46820
152	0.629	7.55570	0.09524	1.47240
153	0.633	7.42322	0.05953	1.45509
154	0.638	7.25519	-0.01130	1.42635
155	0.642	7.14136	0.06983	1.42440
156	0.646	7.01942	0.07293	1.40472
157	0.650	-99.9	-99.9	-99.9
158	0.654	6.72757	0.07328	1.38787
159	0.658	6.59414	0.03382	1.36667
160	0.663	6.45605	0.05596	1.35290
161	0.667	6.32967	0.06872	1.34840
162	0.671	6.18842	0.03477	1.32547
163	0.675	6.04587	0.06414	1.31534
164	0.679	5.91374	0.06135	1.29082
165	0.683	5.76208	0.05705	1.28028
166	0.688	5.63456	0.07246	1.27175
167	0.692	5.50832	0.06470	1.25115
168	0.696	-99.9	-99.9	-99.9
169	0.700	5.24348	0.06669	1.23902
170	0.704	5.10340	0.03959	1.20926
171	0.708	4.96984	0.05077	1.19438
172	0.713	4.83811	0.06520	1.18256
173	0.717	4.69311	0.03763	1.15770
174	0.721	-99.9	-99.9	-99.9
175	0.725	4.42437	0.07173	1.13589
176	0.729	4.29308	0.03993	1.12169
177	0.733	-99.9	-99.9	-99.9
178	0.738	4.03669	0.07010	1.09504
179	0.742	3.88991	0.03603	1.07408
180	0.746	3.75929	0.05967	1.06284
181	0.750	3.62632	0.05456	1.03330
182	0.754	3.47659	0.05179	1.02228
183	0.758	-99.9	-99.9	-99.9
184	0.763	3.22319	0.06502	0.98813
185	0.767	3.08628	0.03496	0.98214

Table B–2 (Continued): Center-of-mass trajectory data for pitch T33.
(Missing data is assigned the value of -99.9)

Frame	Time	X	Y	Z
186	0.771	2.96219	0.06738	0.97153
187	0.775	2.83223	0.05209	0.94216
188	0.779	2.68789	0.03574	0.91821
189	0.783	2.55784	0.05698	0.90694
190	0.788	2.42080	0.03307	0.87824
191	0.792	-99.9	-99.9	-99.9
192	0.796	2.14770	0.06975	0.85002
193	0.800	2.01635	0.02759	0.84362
194	0.804	1.89552	0.08351	0.84247
195	0.808	-99.9	-99.9	-99.9
196	0.813	1.61684	0.03541	0.78826
197	0.817	1.50067	0.06486	0.78014
198	0.821	1.36774	0.04621	0.74604
199	0.825	-99.9	-99.9	-99.9
200	0.829	-99.9	-99.9	-99.9
201	0.833	0.98422	0.09478	0.69996
202	0.838	-99.9	-99.9	-99.9
203	0.842	0.71822	0.08901	0.67468
204	0.846	0.59449	0.07347	0.64346
205	0.850	-99.9	-99.9	-99.9
206	0.854	0.30920	0.06383	0.60501

APPENDIX C – PITCHING MACHINE DATA

Table C–1: Trajectory data for pitch P2S22.
(Missing data is assigned the value of -99.99)

Time	X1	Y1	Z1	X2	Y2	Z2	X3	Y3	Z3	X4	Y4	Z4
0.663	16.16470	-0.01600	1.92787	16.12902	-0.01219	1.92248	16.14334	-0.01049	1.93836	16.15797	-0.01847	1.95281
0.667	16.01075	-0.01839	1.90710	16.00111	-0.01586	1.94049	16.01844	-0.01328	1.92903	16.03545	-0.02275	1.91955
0.671	15.86032	-0.02000	1.91917	15.89002	-0.01913	1.93401	15.88173	-0.01495	1.91416	15.87549	-0.02709	1.89655
0.675	15.74142	-0.02219	1.93380	15.75902	-0.02151	1.90450	15.73884	-0.01932	1.90980	15.72040	-0.02729	1.91816
0.679	15.62785	-0.02692	1.91596	15.60148	-0.02569	1.89291	15.60468	-0.02256	1.91409	15.60897	-0.03084	1.93413
0.683	15.48450	-0.03251	1.88713	15.45672	-0.02862	1.90967	15.47977	-0.02707	1.90943	15.49821	-0.03680	1.90769
0.688	-99.99	-99.99	-99.99									
0.692	-99.99	-99.99	-99.99									
0.696	-99.99	-99.99	-99.99									
0.700	-99.99	-99.99	-99.99									
0.704	-99.99	-99.99	-99.99									
.												
.												
.												
1.033	-99.99	-99.99	-99.99									
1.038	-99.99	-99.99	-99.99									
1.042	-99.99	-99.99	-99.99									
1.046	-99.99	-99.99	-99.99									
1.050	-99.99	-99.99	-99.99									
1.054	4.01704	-0.26939	1.16320									
1.058	3.88961	-0.26748	1.15033									
1.063	3.76278	-0.27198	1.12980									
1.067	3.63319	-0.27680	1.12052									
1.071	3.51406	-0.27996	1.11272									
1.075	3.39466	-0.27784	1.10233									
1.079	3.27905	-0.27843	1.08834									
1.083	3.14222	-0.28613	1.06876									
1.088	3.01639	-0.29461	1.06269									
1.092	2.89783	-0.29226	1.05085									
1.096	2.77940	-0.29608	1.03315									
1.100	2.65131	-0.29918	1.01664									
1.104	2.52365	-0.30449	1.00849									
1.108	2.40524	-0.30673	0.99927									
1.113	2.29012	-0.30626	0.98462									
1.117	2.16497	-0.31237	0.96343									
1.121	2.03736	-0.31375	0.95333									
1.125	1.91359	-0.32104	0.94636									
1.129	1.79894	-0.31552	0.93545									
1.133	1.67939	-0.32389	0.91257									
1.138	1.55038	-0.32469	0.89807									
1.142	1.42686	-0.33051	0.89122									
1.146	1.31038	-0.33254	0.87944									
1.150	1.19392	-0.33328	0.86523									
1.154	1.06782	-0.34091	0.84116									
1.158	0.93953	-0.33967	0.83108									
1.163	0.81869	-0.34415	0.82453									
1.167	0.70789	-0.34207	0.81036									
1.171	0.58762	-0.35211	0.78676									
1.175	0.45859	-0.34954	0.77216									
1.179	0.33349	-0.36013	0.76480									
1.183	0.22143	-0.35709	0.75623									
1.188	0.10718	-0.36285	0.73435									
1.192	-0.01756	-0.36782	0.71517									
1.196	-0.14134	-0.36106	0.70153									
1.200	-0.25711	-0.36629	0.69572									
1.204	-0.36893	-0.36857	0.68365									
1.208	-0.49065	-0.37932	0.65589									

(Center-of-mass trajectory data nearing home-plate.)

Table C–2: Trajectory data for pitch P4S22.
(Missing data is assigned the value of -99.99)

Time	X1	Y1	Z1	X2	Y2	Z2	X3	Y3	Z3	X4	Y4	Z4
1.042	16.05337	-0.00357	2.05170	16.04903	-0.00388	2.02271	16.03932	-0.00096	2.04152	16.02736	-0.00706	2.05702
1.046	15.89644	-0.00767	2.06344	15.90943	-0.00514	2.03564	15.89080	-0.00158	2.04535	15.87334	-0.00924	2.05304
1.050	15.74072	-0.01115	2.06550	15.76583	-0.00878	2.04964	15.74427	-0.00350	2.04713	15.72405	-0.01088	2.04308
1.054	15.58972	-0.01697	2.05948	15.61686	-0.01175	2.06075	15.60221	-0.00824	2.04697	15.58885	-0.01650	2.03491
1.058	-99.99	-99.99	-99.99	15.46998	-0.01374	2.06630	15.46513	-0.01129	2.04605	15.46262	-0.01700	2.02793
1.063	-99.99	-99.99	-99.99									
1.067	-99.99	-99.99	-99.99									
1.071	-99.99	-99.99	-99.99									
1.075	-99.99	-99.99	-99.99									
1.079	-99.99	-99.99	-99.99									
.												
.												
.												
1.388	-99.99	-99.99	-99.99									
1.392	-99.99	-99.99	-99.99									
1.396	-99.99	-99.99	-99.99									
1.400	-99.99	-99.99	-99.99									
1.404	-99.99	-99.99	-99.99									
1.408	4.04321	-0.15429	1.60483									
1.413	3.91503	-0.15517	1.59322									
1.417	3.78689	-0.15663	1.58315									
1.421	3.65787	-0.15927	1.56737									
1.425	3.52558	-0.16323	1.54821									
1.429	3.39722	-0.16305	1.53214									
1.433	3.27031	-0.16337	1.52557									
1.438	3.13697	-0.16691	1.51292									
1.442	3.00374	-0.17117	1.49358									
1.446	2.86785	-0.17721	1.47426									
1.450	2.73840	-0.17573	1.45401									
1.454	2.61323	-0.17787	1.43250									
1.458	2.48716	-0.18269	1.41368									
1.463	2.36032	-0.18377	1.39575									
1.467	2.23161	-0.18735	1.37897									
1.471	2.10664	-0.18859	1.36197									
1.475	1.97850	-0.19001	1.34892									
1.479	1.84897	-0.19126	1.33231									
1.483	1.71341	-0.19348	1.31443									
1.488	1.58232	-0.19818	1.29300									
1.492	1.45326	-0.19969	1.27478									
1.496	1.32352	-0.19919	1.24932									
1.500	1.19948	-0.20487	1.22623									
1.504	1.07576	-0.21016	1.20425									
1.508	0.95176	-0.21272	1.18184									
1.513	0.82682	-0.21374	1.16265									
1.517	0.70113	-0.21415	1.14603									
1.521	0.57307	-0.21681	1.13020									
1.525	0.44235	-0.21909	1.11219									
1.529	0.31120	-0.22124	1.08746									
1.533	0.18159	-0.22499	1.06609									
1.538	0.05075	-0.22714	1.04574									
1.542	-0.07114	-0.23152	1.02008									
1.546	-0.19242	-0.22562	0.99218									
1.550	-0.30864	-0.23425	0.96439									
1.554	-0.43482	-0.23750	0.94620									
1.558	-0.55152	-0.23731	0.92898									
1.563	-0.68132	-0.24257	0.90761									

(Center-of-mass trajectory data nearing home-plate.)

APPENDIX D – KNUCKLE BALL DATA

Table D–1: Trajectory data for pitch P2S30.
(Missing data is assigned the value of -99.99)

Time	X1	Y1	Z1	X2	Y2	Z2	X3	Y3	Z3	X4	Y4	Z4
0.658	16.08972	-0.02038	1.98527	16.06097	-0.01043	2.00247	16.08219	-0.00972	2.00450	16.10170	-0.01898	2.00943
0.663	15.95060	-0.02280	1.98786	15.92171	-0.01205	2.00510	15.94249	-0.01018	2.00629	15.96166	-0.02261	2.01120
0.667	15.81098	-0.02632	1.98913	15.78440	-0.01570	2.00794	15.80487	-0.01347	2.00901	15.82353	-0.02380	2.01421
0.671	15.67261	-0.03100	1.99238	15.64475	-0.01734	2.00985	15.66469	-0.01629	2.01042	15.68215	-0.03052	2.01549
0.675	15.53321	-0.03547	1.99397	15.50535	-0.02132	2.01193	15.52615	-0.02251	2.01295	15.54458	-0.03316	2.01808
0.679	-99.99	-99.99	-99.99									
0.683	-99.99	-99.99	-99.99									
0.688	-99.99	-99.99	-99.99									
0.692	-99.99	-99.99	-99.99									
0.696	-99.99	-99.99	-99.99									
.												
.												
.												
1.038	-99.99	-99.99	-99.99									
1.042	-99.99	-99.99	-99.99									
1.046	-99.99	-99.99	-99.99									
1.050	-99.99	-99.99	-99.99									
1.054	-99.99	-99.99	-99.99									
1.058	3.29086	-0.36803	1.60144									
1.063	3.16266	-0.37700	1.58922									
1.067	3.03597	-0.38411	1.57649									
1.071	2.91047	-0.38969	1.56417									
1.075	2.78067	-0.39810	1.55237									
1.079	2.65778	-0.40708	1.54076									
1.083	2.53339	-0.41086	1.52747									
1.088	2.40432	-0.42078	1.51452									
1.092	2.28269	-0.42643	1.50140									
1.096	2.15672	-0.43423	1.48811									
1.100	2.03233	-0.44118	1.47728									
1.104	1.90289	-0.45324	1.46340									
1.108	1.78079	-0.45688	1.44801									
1.113	1.64662	-0.46804	1.43505									
1.117	1.52531	-0.47656	1.42448									
1.121	1.39833	-0.48490	1.40935									
1.125	1.27412	-0.49208	1.39408									
1.129	1.14405	-0.50271	1.38132									
1.133	1.02447	-0.50701	1.36678									
1.138	0.89701	-0.51734	1.35475									
1.142	0.77410	-0.52409	1.34021									
1.146	0.64718	-0.53259	1.32721									
1.150	0.52724	-0.53853	1.31268									
1.154	0.39628	-0.55014	1.29975									
1.158	0.27647	-0.55763	1.28520									
1.163	0.15009	-0.56519	1.26948									
1.167	0.02642	-0.57032	1.25440									
1.171	-0.09209	-0.57857	1.24159									
1.175	-0.21356	-0.58579	1.22587									
1.179	-0.32057	-0.58797	1.21357									
1.183	-0.46990	-0.60300	1.19592									
1.188	-0.56360	-0.60320	1.18359									
1.192	-0.69856	-0.61335	1.16655									
1.196	-0.81363	-0.61739	1.15365									

(Center-of-mass trajectory data nearing home-plate.)

Table D–2: Trajectory data for pitch P4S1.
(Missing data is assigned the value of -99.99)

Time	X1	Y1	Z1	X2	Y2	Z2	X3	Y3	Z3	X4	Y4	Z4
0.408	16.10104	-0.02052	1.98081	16.07115	-0.01313	1.98867	16.09053	-0.00668	1.99353	16.10815	-0.01326	2.00231
0.413	15.96074	-0.02397	1.98341	15.93394	-0.01586	1.99187	15.95338	-0.01058	1.99603	15.97021	-0.01448	2.00409
0.417	15.82370	-0.02793	1.98573	15.79771	-0.02087	1.99322	15.81516	-0.01326	1.99717	15.83224	-0.01599	2.00666
0.421	15.68330	-0.03734	1.98820	15.65875	-0.02482	1.99615	15.67647	-0.01800	1.99876	15.69466	-0.01982	2.00826
0.425	15.55018	-0.03903	1.99109	15.52007	-0.02926	1.99712	15.53788	-0.02363	2.00022	15.55577	-0.02301	2.00893
0.429	-99.99	-99.99	-99.99									
0.433	-99.99	-99.99	-99.99									
0.438	-99.99	-99.99	-99.99									
0.442	-99.99	-99.99	-99.99									
0.446	-99.99	-99.99	-99.99									
.												
.												
.												
0.813	-99.99	-99.99	-99.99									
0.817	-99.99	-99.99	-99.99									
0.821	-99.99	-99.99	-99.99									
0.825	-99.99	-99.99	-99.99									
0.829	-99.99	-99.99	-99.99									
0.833	2.57444	-0.30899	1.65879	(Center-of-mass trajectory data nearing home-plate.)								
0.838	2.45344	-0.31693	1.65120									
0.842	2.32674	-0.32049	1.63965									
0.846	2.19824	-0.32449	1.63004									
0.850	2.07230	-0.32710	1.61686									
0.854	1.94917	-0.32926	1.60468									
0.858	1.82136	-0.33315	1.59006									
0.863	1.70274	-0.33300	1.57767									
0.867	1.57519	-0.33757	1.56457									
0.871	1.44861	-0.34184	1.55093									
0.875	1.32489	-0.34240	1.53676									
0.879	1.19880	-0.34673	1.52117									
0.883	1.07316	-0.34856	1.50577									
0.888	0.95089	-0.35328	1.49197									
0.892	0.82659	-0.35553	1.47595									
0.896	0.70158	-0.35900	1.46130									
0.900	0.57774	-0.36205	1.44492									
0.904	0.45387	-0.36474	1.42796									
0.908	0.32857	-0.36905	1.41326									
0.913	0.20705	-0.37256	1.39603									
0.917	0.07967	-0.37597	1.37885									
0.921	-0.03500	-0.37672	1.36260									
0.925	-0.15824	-0.37902	1.34593									
0.929	-0.28536	-0.38410	1.32766									
0.933	-0.40480	-0.38799	1.31146									
0.938	-0.53263	-0.39257	1.29592									
0.942	-0.65013	-0.39436	1.27726									
0.946	-0.76543	-0.39760	1.26099									